

การผลิตแก๊สไฮโดรเจนเข้มข้นจากโฟโรไลซิส-แกซิฟิเคชันของชีวมวลด้วยตัวเร่งปฏิกิริยาร่วมกับตัวดูดซับ



นายธีระยุทธ บุญมา

บทคัดย่อและแฟ้มข้อมูลฉบับเต็มของวิทยานิพนธ์ตั้งแต่ปีการศึกษา 2554 ที่ให้บริการในคลังปัญญาจุฬาฯ (CUIR) เป็นแฟ้มข้อมูลของนิสิตเจ้าของวิทยานิพนธ์ ที่ส่งผ่านทางบัณฑิตวิทยาลัย

The abstract and full text of theses from the academic year 2011 in Chulalongkorn University Intellectual Repository (CUIR) are the thesis authors' files submitted through the University Graduate School.

วิทยานิพนธ์นี้เป็นส่วนหนึ่งของการศึกษาตามหลักสูตรปริญญาวิทยาศาสตรดุษฎีบัณฑิต

สาขาวิชาเคมีเทคนิค ภาควิชาเคมีเทคนิค

คณะวิทยาศาสตร์ จุฬาลงกรณ์มหาวิทยาลัย

ปีการศึกษา 2560

ลิขสิทธิ์ของจุฬาลงกรณ์มหาวิทยาลัย

HYDROGEN RICH GAS PRODUCTION FROM PYROLYSIS-GASIFICATION OF BIOMASS WITH
COMBINED CATALYST AND SORBENT



A Dissertation Submitted in Partial Fulfillment of the Requirements
for the Degree of Doctor of Philosophy Program in Chemical Technology

Department of Chemical Technology

Faculty of Science

Chulalongkorn University

Academic Year 2017

Copyright of Chulalongkorn University

ธีระยุทธ บุญมา : การผลิตแก๊สไฮโดรเจนเข้มข้นจากไพโรไลซิส-แกซิฟิเคชันของชีวมวลด้วยตัวเร่งปฏิกิริยาร่วมกับตัวดูดซับ (HYDROGEN RICH GAS PRODUCTION FROM PYROLYSIS-GASIFICATION OF BIOMASS WITH COMBINED CATALYST AND SORBENT) อ.ที่ปริกษาวิทยานิพนธ์หลัก: รศ. ดร. ประพันธ์ คุณลธาวา, 144 หน้า.

งานวิจัยนี้ศึกษาการผลิตแก๊สไฮโดรเจน ด้วยกระบวนการไพโรไลซิส-แกซิฟิเคชันด้วยไอน้ำของชีวมวล ร่วมกับตัวเร่งปฏิกิริยาและตัวดูดซับ ในเครื่องปฏิกรณ์แบบเบดนิ่ง 2 ชั้น ชีวมวลที่ใช้ในการศึกษาคือ ใบอ้อย ตัวเร่งปฏิกิริยาร่วมกับตัวดูดซับ ถูกเตรียมด้วยวิธีการฝังตัวด้วยสารละลายมากเกินพอ จากการศึกษาพบว่า ตัวเร่งปฏิกิริยานิกเกิลออกไซด์ (NiO)/แมกนีเซียมออกไซด์(MgO)/แคลเซียมออกไซด์(CaO) ที่มีปริมาณ NiO ร้อยละ 10 โดยมวล MgO ร้อยละ 5 โดยมวล และ CaO ร้อยละ 5 โดยมวล บนแกรมมา อะลูมินา (γ - Al_2O_3) มีประสิทธิภาพสูงสุดในเพิ่มการผลิตแก๊สไฮโดรเจนโดยใช้ตัวดูดซับ สำหรับกระบวนการไพโรไลซิสและแกซิฟิเคชันด้วยไอน้ำของชีวมวล และความเข้มข้นของแก๊สไฮโดรเจนสูงสุด และความเข้มข้นของแก๊สคาร์บอนไดออกไซด์ต่ำสุด ถูกพบเมื่อใช้ตัวเร่งปฏิกิริยาร่วมกับตัวดูดซับในลำดับ $Mg_5Ni_{10}Ca_5$ เพราะลำดับการฝังตัวเร่งปฏิกิริยาดังกล่าวมีปริมาณเฟส CaO สูงที่สุด ซึ่งเป็นเฟสที่สำคัญในการเพิ่มความสามารถการดูดซับของแก๊สคาร์บอนไดออกไซด์ได้ นอกจากนี้การศึกษาผลลัพธ์เชิงบวกของตัวดูดซับระหว่าง CaO และ MgO ที่ถูกเตรียมด้วยการผสมเชิงกายภาพ ทั้งแบบแห้ง และแบบเปียก พบว่าการเตรียมตัวดูดซับแบบเปียก ที่อัตราส่วนโดยโมลระหว่าง CaO และ MgO เท่ากับ 2:1 (WM2:1) ให้ปริมาณของแก๊สไฮโดรเจนสูงสุด เพราะเฟสแคลเซียมไฮดรอกไซด์ ($Ca(OH)_2$) ในการผสมเชิงกายภาพของตัวดูดซับแบบเปียก ทำให้ส่งเสริมประสิทธิภาพของการเพิ่มการผลิตแก๊สไฮโดรเจนโดยใช้ตัวดูดซับ และยังได้พบว่าอุณหภูมิการปล่อยสารระเหย และอุณหภูมิแกซิฟิเคชันที่ 600 องศาเซลเซียส เป็นอุณหภูมิที่ดีที่สุดที่จะช่วยส่งเสริมการผลิตไฮโดรเจนดังกล่าว ผลของปริมาณการฝังตัวของ NiO ลงบน WM2:1 ได้ถูกศึกษา พบว่าที่ปริมาณ NiO ร้อยละ 5 โดยมวล ($NiO_5/WM(2:1)$) เป็นปริมาณที่เหมาะสมที่สุดในการผลิตแก๊สไฮโดรเจน จากผลการศึกษาดังกล่าวสามารถนำไปประยุกต์ในการสังเคราะห์ตัวเร่งปฏิกิริยาร่วมกับตัวดูดซับ สำหรับการไพโรไลซิส-แกซิฟิเคชันของชีวมวลได้ในอนาคต

ภาควิชา เคมีเทคนิค

ลายมือชื่อนิสิต

สาขาวิชา เคมีเทคนิค

ลายมือชื่อ อ.ที่ปริกษาหลัก

ปีการศึกษา 2560

5772822423 : MAJOR CHEMICAL TECHNOLOGY

KEYWORDS: SORPTION-ENHANCED HYDROGEN PRODUCTION (SEHP); PYROLYSIS; STEAM-GASIFICATION; CATALYST AND SORBENT.

TEERAYUT BUNMA: HYDROGEN RICH GAS PRODUCTION FROM PYROLYSIS-GASIFICATION OF BIOMASS WITH COMBINED CATALYST AND SORBENT.
ADVISOR: ASSOC. PROF. PRAPAN KUCHONTHARA, Ph.D., 144 pp.

In this work, the hydrogen production during biomass steam pyrolysis-gasification with a combined catalysts and sorbent (catalyst/sorbents) was studied in a drop tube two-stages fixed bed reactor. The catalyst/sorbents were prepared by an excess-solution impregnation method. A nickel oxide (NiO)/magnesium oxide (MgO)/calcium oxide(CaO) catalyst/sorbents containing 10 wt. % NiO, 5 wt. % MgO and 5 wt. % CaO on gamma alumina (γ -Al₂O₃) showed the best activity in sorption enhanced hydrogen production (SEHP) for the pyrolysis-gasification of sugarcane leaves. Besides, the highest H₂ concentration and the lowest CO₂ concentration were attained using the Mg₅Ni₁₀Ca₅ catalyst/sorbents. Because Mg₅Ni₁₀Ca₅ catalyst/sorbents provided the dominant phases of CaO which can increase the CO₂ adsorption capacity to promote the H₂ production. Moreover, the synergistic effect between CaO and MgO sorbents which were prepared by dry- and wet-physical mixing with different molar ratios were investigated. The results indicated that the wet-mixed sorbent with the molar ratio between CaO and MgO of 2:1 (WM 2:1) afforded a higher H₂ yield because the Ca(OH)₂ phases in the wet-mixed sorbents induced high performance for SEHP. Furthermore, the devolatilization and gasification temperature of 600 °C gave the optimal condition for SEHP. The effect of NiO loading content on WM(2:1) was also examined for the H₂ production. The results showed that NiO 5 wt.% on WM (2:1) sorbents showed the optimal yield and concentration of H₂. The obtained results will be useful for the effective development of combined catalyst/sorbents for SEHP of biomass pyrolysis-gasification

Department: Chemical Technology Student's Signature

Field of Study: Chemical Technology Advisor's Signature

Academic Year: 2017

ACKNOWLEDGEMENTS

I would like to express my deepest gratitude my supervisors, Assoc. Prof. Prapan Kuchonthara, Ph.D who reviewed this dissertation during its preparation and offered many helpful suggestions, supervision and much encouragement throughout pass 4 years of my research

I would like to acknowledge Prof. Pattarapan Prasassarakich, Ph.D, Assoc. Prof. Prasert Reubroycharoen and Assoc. Prof. Napida Hinchiranan, Ph.D for their participation on the dissertation chairman and members of thesis committee, respectively.

I am grateful for the financial support from the ๑๐๐th Anniversary Chulalongkorn University Fund for Doctoral Scholarship, the ๙๐th Anniversary Chulalongkorn University Fund (Ratchadaphiseksomphot endowment Fund, GCUGR1125594015D), the Thailand Research Fund (IRG5780001), Chulalongkorn University and Faculty of Science of Chulalongkorn University.

Finally, I wish to acknowledge all of researcher in GLS Group for suggesting about my research work for my beloved family who always beside me throughout Ph.D period.

CONTENTS

	Page
THAI ABSTRACT	iv
ENGLISH ABSTRACT	v
ACKNOWLEDGEMENTS	vi
CONTENTS	vii
CHAPTER 1 INTRODUCTION	6
1.1 Motivation	6
1.2 Objectives	9
1.3 Scope of this work	9
CHAPTER 2 THEORY AND LITERATURE REVIEWS	11
2.1 Gasification process	11
2.2 Biomass Feedstock	12
2.2.1 General knowledge of biomass	12
2.2.2 Biomass situation in Thailand	17
2.2.2.1 Sugarcane	17
2.2.2.2 Rice	18
2.2.2.3 Oil palm	18
2.2.2.4 Other agricultural sources	18
2.3 Chemical Reactions	18
2.4 Heterogeneous Catalysis	23
2.5 Preparation of supported catalysts	25
2.5.1 Impregnation	26
2.5.1.1 Dry or incipient impregnation	26

	Page
2.5.1.2 Wet-diffusional impregnation.....	27
2.5.1.3 Mechanism of impregnation.....	27
2.5.1.4 Precursor distribution.....	28
2.5.2 Precipitation and Co-Precipitation.....	30
2.5.2.1 Mechanism of precipitation.....	30
2.5.2.2 Characteristic of sample from precipitation method.....	31
2.6 Review of catalytic for biomass gasification to enhanced H ₂ production.....	34
2.6.1 Catalysts for tar reduction	34
2.6.1.1 Commercial nickel catalyst as primary catalyst.....	34
2.6.1.2 Commercial nickel catalyst as secondary catalyst.....	37
2.6.2 Sorption enhanced H ₂ production (SEHP)	39
2.6.2.1 CaO based sorbents.....	40
2.6.2.2 MgO based sorbents	43
2.6.3 Combined catalyst and sorbent for H ₂ production.....	45
CHAPTER 3 EXPERIMENTAL APPARATUS AND ANALYTICAL METHOD.....	48
3.1 Materials.....	48
3.1.1 Feedstock and chemicals.....	48
3.1.2 Equipment.....	48
3.2 Experiment procedure	50
3.2.1 Biomass feedstock preparation.....	50
3.2.2 Catalyst and sorbent preparation.....	50
3.2.2.1 Physical mixing method	51
3.2.2.2 Excess solution impregnation method.....	52

	Page
3.2.3 Activity test for biomass pyrolysis - gasification	53
3.2.4 Activity test for pyrolysis of biomass	53
3.2.5 Regeneration process of catalyst/sorbents	54
3.3 Data analysis.....	54
3.4 Characterization Method	55
3.4.1 Proximate and CHN Analysis.....	55
3.4.2 Gas chromatography with thermal conductivity detector (GC-TCD).....	55
3.4.3 CO ₂ adsorption capacity.....	55
3.4.4 Gas chromatography with mass spectrometry (GC-MS).....	56
3.4.5 X-ray fluorescence (XRF).....	56
3.4.6 X-ray Powder Diffraction (XRD).....	56
3.4.7 Brunauer-Emmit-Teller (BET) analysis.....	56
3.4.8 Scanning electron microscopy with energy dispersive X-ray spectroscopy (SEM/EDX)	57
CHAPTER 4 NiMgCa/γ-Al ₂ O ₃ CATALYST/SORBENTS DURING THE PYROLYSIS-STEAM GASIFICATION OF SUGARCANE LEAVES.....	58
4.1 Chemical characteristics of sugarcane leaves.	58
4.2 Catalyst/sorbents characterization.	60
4.2.1 The element analysis of prepared catalysts/sorbent using XRF.....	60
4.2.2 The phases analysis of prepared catalysts/sorbent using XRD.....	61
4.3 Effects of metal loading content of metals on the H ₂ production from pyrolysis-gasification of sugarcane leaves.....	66
4.3.1 Effect of NiO loading content.....	66
4.3.2 Effect of CaO loading content.....	68

	Page
4.3.3 Effect of MgO loading content.....	72
4.4 The order of metal loading study on H ₂ production from pyrolysis-gasification of sugarcane leaves.....	75
4.4.1 Effect of metal loading sequence on H ₂ production with catalyst/sorbent addition at low gasification temperature (600°C).....	76
4.4.2 Effect of metal loading sequence on H ₂ production with catalyst/sorbent addition at low gasification temperature (800°C).....	80
4.5 The optimal condition of catalyst/sorbent on H ₂ production from pyrolysis-gasification of sugarcane leaves.....	85
4.5.1 Effect of the Mg ₅ Ni ₁₀ Ca ₅ catalyst/sorbent to biomass mass ratio.....	85
4.5.2 The regeneration of Mg ₅ Ni ₁₀ Ca ₅ catalyst/sorbent on H ₂ yield and gas concentration.....	86
4.6 Role of MgO and CaO study on γ -Al ₂ O ₃ with different gasification temperature on the H ₂ production from pyrolysis-gasification of sugarcane leaves.....	88
4.6.1 Effect of the gasification temperature on gas yield with MgO/ γ -Al ₂ O ₃	88
4.6.2 Effect of the gasification temperature on gas yield with CaO/ γ -Al ₂ O ₃	89
4.6.3 Effect of the gasification temperature on gas yield with CaO-MgO/ γ -Al ₂ O ₃	91
4.6.4 Regeneration process of CaO-MgO/ γ -Al ₂ O ₃ sorbent.....	92
CHAPTER 5 Ni/CaO-MgO CATALYTS/SORBENTS STUDY ON H ₂ PRODUCTION DURING THE PYROLYSIS-STEAM GASIFICATION OF SUGARCANE LEAVES.....	94
5.1 The preparation of supported CaO-MgO on H ₂ production.....	94
5.1.1 Effect of the CaO:MgO molar ratio on the gas yield and composition.	95

	Page
5.1.2 Effect of the sorbent preparation method on the gas yield and composition.....	99
5.2.3 Effect of the devolatilization temperature on the gas yield.	102
5.2 The Metal loading study with the prepared CaO-MgO on H ₂ production	109
5.2.1 Effect of NiO loading content of H ₂ production from pyrolysis-gasification of sugarcane leaves.	109
5.2.2 The regeneration process of NiO ₅ /WM(2:1) catalyst/sorbent	115
5.3 Comparison of Mg ₅ Ni ₁₀ Ca ₅ catalyst/sorbent and NiO ₅ /WM(2:1) on H ₂ production.....	116
CHAPTER 6 CONCLUSIONS AND RECOMMENDATIONS	118
6.1 Conclusions	118
6.2 Recommendations and future works.....	120
REFERENCES	123
REFERENCES	136
APPENDIX.....	137
APPENDIX A THE PHYSICAL PROPERTIES OF BIOMASS METHODS.....	138
A1 Moisture Content: ASTM D3173.....	138
A2 Volatile matter: ASTM D3175	139
A3 Ash content: ASTM D3174	140
A4 Fixed carbon content.....	141
APPENDIX B GAS YIELD AND COMPOSITION CALCULATION	142
VITA.....	144

LIST OF TABLES

TABLE	PAGE
Table 2.1 Types of lignocellulosic biomass and their chemical composition.....	15
Table 2.2 National production of sugarcane, paddy, and oil palm.....	17
Table 2.3 Distribution of precursor at different conditions of impregnation and drying.....	29
Table 2.4 Activity comparison of nickel catalysts used as primary catalyst in biomass gasification.....	36
Table 3.1 Condition of GC-TCD.....	55
Table 4.1 Proximate and elemental analysis of the sugarcane leaves.....	59
Table 4.2 Elemental analysis of prepared catalyst/sorbents using XRF with different loading contents.....	62
Table 4.3 CO ₂ sorption capacity of the fresh CaMgNi catalyst/sorbents.with different CaO loading content.....	71
Table 4.4 CO ₂ sorption capacity of the fresh catalyst/sorbents.....	78
Table 4.5 CO ₂ sorption capacity of the fresh catalyst/sorbents with the temperature of 800 °C.....	82
Table 4.6 Textural properties of the used catalyst/sorbents with different gasification temperature.....	84
Table 5.1 Corresponding name of prepared support.....	95
Table 5.2 CO ₂ adsorption capacity of the fresh mixed CaO/MgO sorbents.....	100
Table 5.3 Textural properties of the fresh (as-prepared) sorbents.....	102
Table 5.4 CO ₂ adsorption capacity with different NiO loading content at 600 °C.....	112
Table 5.5 Comparison of gas production from Mg ₅ Ni ₁₀ Ca ₅ catalyst/sorbent and NiO/CaO-MgO.....	117

LIST OF FIGURES

FIGURES	PAGE
Figure 2.1 Overall of gasification process with their products advantages.....	11
Figure 2.2 Gasification process with different gasifying and their products.....	12
Figure 2.3 The main components of lignocellulose.....	14
Figure 2.4 Main biomass conversion processes.....	16
Figure 2.5 Gasification step.....	19
Figure 2.6 The sequential reaction for biomass gasification.....	22
Figure 2.7 The example model of the heterogeneous catalysis.....	23
Figure 2.8 Reaction cycle and potential energy diagram for the catalytic oxidation of CO by O ₂	24
Figure 2.9 Schematic representation of basic processes involved during impregnation of precursors on porous support.....	28
Figure 2.10 Supersaturation dependence on concentration, T and pH.....	31
Figure 2.11 Properties of colloidal particles.....	32
Figure 2.12 Mechanism of CaO carbonation by CO ₂ in the presence of steam.....	41
Figure 3.1 Schematic representation of the experimental apparatus: (1) HPLC pump, (2) steam generator, (3) mass flow controller, (4) biomass feeder, (5) quartz wool, (6) catalyst bed, (7) tar trap, (8) gas bag and (9) gas tank.....	49
Figure 3.2 Concept of a two-stage fixed bed reactor.....	49
Figure 3.3 Photo of two-stage fixed bed reactor from laboratory.....	50
Figure 3.4 Dry-physical mixing method.....	51
Figure 3.5 Wet-physical mixing method.....	51
Figure 3.6 Excess solution impregnation method.....	52
Figure 4.1 The thermogravimetric analysis of sugarcane leaves.....	60

Figure 4.2 XRD pattern of fresh NiO/ γ -Al ₂ O ₃ catalysts with different NiO loading content	63
Figure 4.3 XRD pattern of fresh CaXMg5Ni10 catalyst/sorbents with different CaO (X = 0 – 15 wt.%) loading contents.....	65
Figure 4.4 XRD pattern of fresh Ca5MgXNi10 catalyst/sorbents with different MgO (X= 0 – 15 wt.%) loading contents	65
Figure 4.5 XRD pattern of fresh catalyst/sorbent with different order of metal loading.	66
Figure 4.6 Effect of NiO loading content (Ca0Mg0Ni0-15) on the (a) gas yield and (b) gas compositions from pyrolysis-gasification of sugarcane leaves.....	67
Figure 4.7 Effect of CaO loading content on the (a) gas yield and (b) gas composition from pyrolysis-gasification of sugarcane leaves.....	70
Figure 4.8 XRD pattern of used catalyst/sorbents with different CaO loading contents.....	71
Figure 4.9 Effect of MgO loading content on the (a) gas yield and (b) gas concentration from pyrolysis-gasification of sugarcane leaves.....	74
Figure 4.10 Effect of MgO loading content on the carbon deposition of used catalyst/sorbents. and tar conversion.....	75
Figure 4.11 Effect of the metal salt loading sequence on the subsequent gas distribution and H ₂ yield at the gasification temperature of 600 °C.....	76
Figure 4.12 Breakthrough curves of the different fresh catalyst/sorbents at a gasification reaction temperature of 600 °C.	78
Figure 4.13 XRD patterns of the used catalyst/sorbent (a) Ca5Mg5Ni10, (b) Ni10Mg5Ca5 (c) Mg5Ni10Ca5 at the gasification temperature of 600 °C.....	79
Figure 4.14 The schematic of the catalyst/sorbent mechanism for SEHP in pyrolysis-gasification of sugarcane leaves.	80

Figure 4.15 Effect of the gasification temperature on the gas yield with the Mg5Ni10Ca5 catalyst/sorbents.....	81
Figure 4.16 Effect of the metal salt loading sequence on the subsequent gas distribution and H ₂ yield at the gasification temperature of 800 °C.....	82
Figure 4.17 XRD patterns of the used catalyst/sorbent (a) Ca5Mg5Ni10, (b) Ni10Mg5Ca5 (c) Mg5Ni10Ca5 at the gasification temperature of 800 °C.....	85
Figure 4.18 Effect of the catalyst/sorbents: biomass mass ratio on the gas distribution and H ₂ yield at a low gasification temperature (600°C).....	87
Figure 4.19 The regeneration cycle of Mg5Ni10Ca5 catalyst/sorbents.....	87
Figure 4.20 SEM images of sorbent (a) 0 cycle, (b) 1 cycle, (c) 2 cycle.....	88
Figure 4.21 Effect of the gasification temperature on gas yield with 5 wt.% of MgO on γ -Al ₂ O ₃	89
Figure 4.22 Effect of the gasification temperature on gas yield with 5 wt.% of CaO on / γ -Al ₂ O ₃	90
Figure 4.23 Effect of the gasification temperature on gas yield with CaO-MgO/ γ -Al ₂ O ₃	92
Figure 4.24 XRD pattern of used sorbent (CaO-MgO/ γ -Al ₂ O ₃) for pyrolysis-gasification of sugarcane leaves.....	93
Figure 4.25 The regeneration cycle of CaO-MgO on / γ -Al ₂ O ₃ for biomass pyrolysis gasification on gas yield.....	93
Figure 5.1 Gas concentration from pyrolysis-gasification with the dry mixed CaO: MgO sorbents at different molar ratios.....	96
Figure 5.2 Gas yield obtained from pyrolysis-gasification (600 °C pyrolysis and gasification) of sugarcane leaves with the dry mixed CaO: MgO sorbents at different molar ratios.....	97

Figure 5.3 Breakthrough curves of the different fresh (unused) dry mixed CaO/MgO sorbents at different molar ratios (pyrolysis and gasification at 600 °C).	98
Figure 5.4 Gas yields obtained from the pyrolysis-gasification (600 °C pyrolysis and gasification) of sugarcane leaves with the dry and wet mixed CaO/MgO sorbents at different molar ratios.	99
Figure 5.5 Representative XRD pattern of the (a) fresh (before pyrolysis-gasification) wet and dry mixed CaO/MgO sorbents and (b) WM 2:1 before and after pyrolysis-gasification at different gasification temperatures.	101
Figure 5.6 Gas concentration and H ₂ yield obtained from the pyrolysis-gasification with WM 2:1 sorbent.	104
Figure 5.7 The product distribution obtained from the pyrolysis of sugarcane leaves without any sorbent at different devolatilization (pyrolysis) temperatures....	104
Figure 5.8 Effect of the devolatilization temperature on the GC-MS patterns of the volatiles obtained from the pyrolysis-gasification of sugarcane leaves at (a) 600 °C and (b) 800 °C without any sorbent.	106
Figure 5.9 The H ₂ yield and gas concentration obtained from the pyrolysis-gasification of sugarcane leaves at different gasification temperatures (pyrolysis at 600 °C) in the presence of (a) WM 2:1 or (b) no sorbent.	108
Figure 5.10 Effect of NiO ₅ /WM (2:1) loading content on (a) gas yield and (b) gas concentration from pyrolysis-gasification of sugarcane leaves.	110
Figure 5.11 Breakthrough curves of the different NiO loading content of fresh catalyst/sorbents at a gasification reaction temperature of 600 °C.	112
Figure 5.12 XRD pattern of (a) fresh and (b) used catalyst/sorbent with different NiO loading content on WM (2:1).	114
Figure 5.13 The regeneration cycle of NiO ₅ /CaO-MgO catalyst/sorbent.	115

CHAPTER 1

INTRODUCTION

1.1 Motivation

The world's energy consumption is annually increasing due to the increase in the global population, economics and level of technologies. This induces high depletion rate of the non-renewable fossil fuels. Moreover, the use of such levels of fossil fuels leads to the release of carbon dioxide (CO₂), one of greenhouse gases, at higher volumes than that can be autographically fixed [1]. However, concerns in relation to environment issue, make it necessary to consider the development of renewable energy instead of fossil fuels.

The renewable energy is collected from renewable resources which are naturally replenished on a human timescale such as sunlight, wind, geothermal, solar and water. Nevertheless, Thailand is an agricultural based country with a vast supply of biomass resources. Therefore, several types of biomass including rice straw, sugarcane, bagasse, palm oil waste and wood chips are known as one of the promising sources due to their relatively low cost and high production rate. Moreover, the biomass is carbon neutral and can be efficiently converted into several kinds of energy forms.

Meanwhile, hydrogen (H₂) is one of the key clean energy carriers, which can be used for hydrogen engines and hydrogen-fuel cells, since it only generates water from combustion. In addition, hydrogen is necessary for the petroleum industry as petrochemical feedstock and for steel plants as a reduction agent. Currently, hydrogen production from renewable resources such as biomass is an attractive potential technology option [2].

The technologies available for conversion of biomass into H₂ rich gas can be classified into biological and thermochemical processes [3]. However, the biological process has low productivity, long fermentation time and high operating cost. Therefore, the thermochemical process would be a suitable way to convert the biomass into the H₂ rich gas. Combustion, gasification and pyrolysis can be used for power generation and biofuel production. Among these processes, biomass pyrolysis-gasification has been perceived as an attractive process for producing syngas rich in H₂ [4, 5].

The pyrolysis-gasification process is the process to convert organic components in biomass into combustible gases in the presence of gasifying agent including steam, CO₂ and H₂. The principle mechanisms of gasification process are composed of drying, pyrolysis, oxidation and reduction. In the pyrolysis zone, the dried biomass descending from drying zone is pyrolyzed using energy from the partial combustion of pyrolysis products in the oxidation zone, with generation of pyrolysis gaseous products (such as tar, H₂, H₂O, CO₂, carbon monoxide (CO)) and char. In the reduction zone (gasification zone), the char is converted into gas by the reaction with the hot gases from the pyrolysis zone.

The main problem from biomass gasification is the tar formation. Tar, which is produced in a series of complex thermochemical reactions, decrease the gas yield in gasification product and provides higher corrosion of equipment. The yield of hydrogen from biomass gasification is also low. Hence, catalysts are interesting to reduce the tar formation and also on hydrogen production [6].

Many types of catalysts have been investigated biomass gasification including nickel (Ni), iron (Fe) [7], rhodium (Rh) [8], ruthenium (Ru) [9], platinum (Pt), and palladium (Pd). Generally, Ni-based catalysts have been widely used with steam as for tar reduction and H₂ production because of its high activity, stability and relatively cheap price [10]. However, H₂ concentration in the syngas from conventional biomass

with steam is limited by the thermodynamic equilibrium. In order to enhance H₂ production, utilization of sorbent has been proposed [11].

Sorption-enhanced hydrogen production (SEHP) has been intensively investigated in the last two decades [12]. Nowadays, the researches on SEHP have been widely involved in the fields of methane (CH₄), coal, heavy oil, and biomass gasification to produce H₂ [13, 14]. SEHP can shift the thermodynamic equilibrium of the water-gas shift reaction by adsorption of CO₂ as shown in reaction (1.1), resulting in higher hydrogen yield and hydrogen concentration in produced gas. Theoretically, almost pure hydrogen can be generated as shown in reaction (1.2).

Carbonation reaction (CO₂ adsorption)



Sorption-enhanced hydrogen production (SEHP)



Currently, the sorbents are usually used in SEHP including calcium-based oxides (CaO), magnesium oxides (MgO), hydrotalcite, and mixed metal oxides of lithium (Li) and sodium (Na). Among these sorbents, CaO and MgO have the greatest potential based on availability and cost [15].

Herein, a combined catalyst and sorbent for biomass gasification process is considered to play roles as both the reforming catalyst and the CO₂ sorbent. The mechanism the gasification by using combined catalyst and sorbent (Ni-Al-Ca) can be explained as follow [16].

Firstly, pyrolysis product of feedstock (wood sawdust and propylene) was introduced to the gasification zone, where the reaction with oxidizing agent (steam) in the presence of Ni-Al-Ca catalyst occurs. The nickel oxide (NiO) plays a role as a catalyst in the gasification of pyrolysis product consuming water and producing H₂, CO, CO₂ and another hydrocarbon. Then, the produced CO and H₂O derived from steam can be

converted into H_2 and CO_2 by the water-gas shift reaction, which was enhanced H_2 production by CaO through CO_2 adsorption.

However, few of attention have been focused on direct gasification of biomass with catalyst and sorbent bed to produce high purity of H_2 gas. Therefore, this research aimed to investigate effects of operating parameters of each stage (pyrolysis and gasification stage) on product yield and selectivity in pyrolysis-gasification of biomass.

1.2 Objectives

1. To investigate effects of reaction parameters on biomass gasification using combined catalyst and sorbent
2. To study the role of CO_2 sorbent and metal oxide on biomass gasification

1.3 Scope of this work

This work is divided into two parts. The first part, three metal loading including nickel oxide (NiO), magnesium oxide (MgO) and calcium oxide (CaO) on gamma alumina ($\gamma-Al_2O_3$) which were prepared by the excess solution impregnation method. The experiments were carried out in two stage fixed bed reactor. The effect of metal loading content including NiO, CaO and MgO (3-15 wt.% on $\gamma-Al_2O_3$), the order of metal loading (NiMgCa/ $\gamma-Al_2O_3$, MgNiCa/ $\gamma-Al_2O_3$ and CaMgNi/ $\gamma-Al_2O_3$ catalyst/sorbents) and the gasification temperature (300 – 800 °C) on the hydrogen production from the pyrolysis-gasification of biomass were investigated. In addition, the characterization of the sample such as fresh-used catalyst/sorbent were analyzed by breakthrough test, BET, XRF and XRD methods.

In the second part, synthetic CaO-based adsorbents with the addition of MgO on the H_2 production from the pyrolysis-gasification of biomass were studied. The CaO/MgO sorbents were prepared by physical mixing. They were characterized by

means of Brunauer-Emmitt-Teller (BET), X-ray diffractometry (XRD) and their CO₂ adsorption capacity. Their influence in the steam pyrolysis-gasification of biomass was evaluated using a two-stage fixed bed reactor. However, the volatile components, which are released from different pyrolysis (devolatilization) temperatures, have a greater effect on the SEHP system. The effect of the CaO to MgO molar ratios (0:1, 1:2, 1:1, 2:1, 1:0), the preparation method (dry- and wet- physical mixing), the NiO loading content (3 – 15 wt.% on prepared support), devolatilization temperatures (400 – 800°C) and gasification temperatures (600 – 800 °C) were examined.



CHAPTER 2

THEORY AND LITERATURE REVIEWS

2.1 Gasification process

Gasification involves turning organic fuels (such as biomass resources) into gaseous compounds by supplying less oxygen than that is needed for complete combustion of the fuel. Gasification occurs at temperatures between 600 °C and 1500 °C and produces a low-to medium-energy gas depending upon the process type and operating conditions. The gasification of biomass has been already used to produce bioenergy and bioproducts for dual-mode engines to produce heat, steam and electricity. Studies are underway to develop biomass gasification technologies to economically produce hydrogen, organic chemicals and ethanol for use as transportation fuel in cars and trucks and to extend its use as a source of electricity [17]. Figure 2.1 shows the overall of gasification process with their products advantages [18].

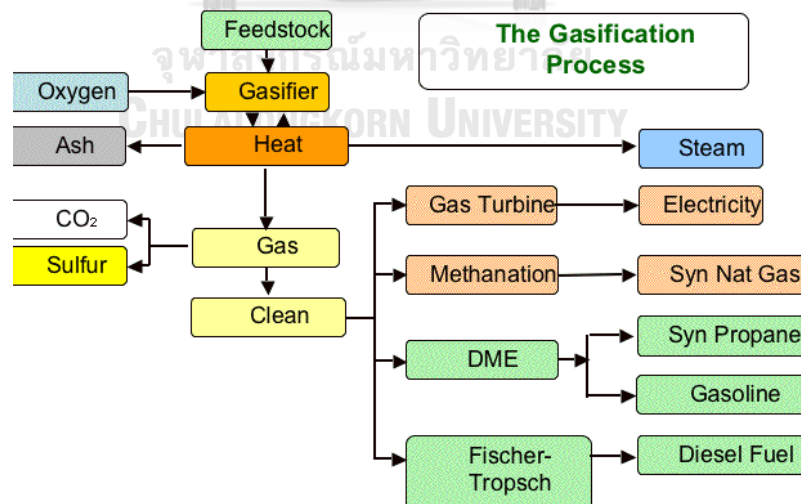


Figure 2.1 Overall of gasification process with their products advantages.

The gasification process has to use a gasifying agent such as air, oxygen, hydrogen or steam to convert carbonaceous materials into gaseous products. Figure 2.2 shows the gasification process with different gasifying and their products [19].

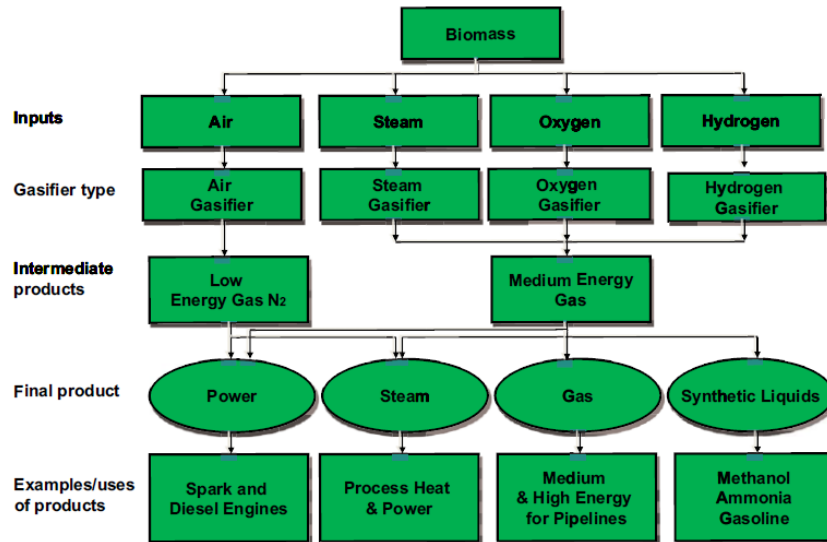


Figure 2.2 Gasification process with different gasifying and their products.

2.2 Biomass Feedstock

2.2.1 General knowledge of biomass

Biomass is an organic material that has stored sunlight in the form of chemical energy. It is commonly recognized as an important renewable energy, which can refer to non-fossilized and biodegradable organic material originating from plants, animals, and microorganisms derived from biological sources. It includes products, byproducts, residues and waste from agriculture, forestry and related industries, as well as the non-fossilized and biodegradable organic fractions of industrial and municipal solid wastes. The biomass also includes gases and liquids recovered from the decomposition of non-fossilized and biodegradable organic material. Biomass residues mean biomass byproducts, residues and waste streams from agriculture, forestry, and related industries [20].

The lignocellulosic biomass is one of the promising biomasses for the production of renewable energy [21]. It is mainly composed of three polymers; cellulose, hemicellulose and lignin together with small amounts of other components, like acetyl groups, minerals and phenolic substituents (Figure 2.3).

Depending on the type of lignocellulosic biomass, these polymers are organized in complex non-uniform three-dimensional structures to different degrees and varying relative composition. Lignocellulose has evolved to resist degradation and this robustness or recalcitrance of lignocellulose stems from the crystallinity of cellulose, hydrophobicity of lignin, and encapsulation of cellulose by the lignin-hemicellulose matrix [22].

The major component of lignocellulosic biomass is cellulose. Unlike to glucose in other glucan polymers, the repeating unit of the cellulose chain is the disaccharide cellobiose. Its structure consists of extensive intramolecular and intermolecular hydrogen bonding networks, which tightly binds the glucose units (Figure 2.3) [23]. Since about half of the organic carbon in the biosphere is present in the form of cellulose, the conversion of cellulose into fuels and valuable chemicals has a paramount importance [24, 25].

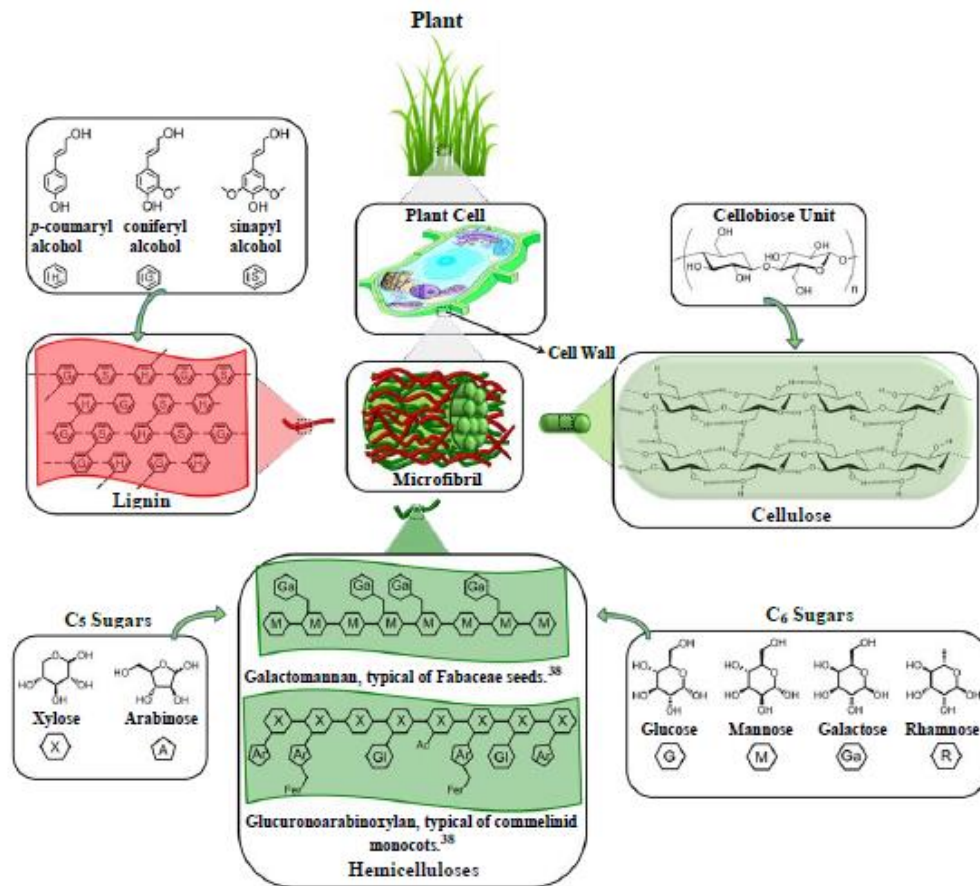


Figure 2.3 The main components of lignocellulose.

Hemicellulose is the second most abundant polymer. Unlike cellulose, hemicellulose has a random and amorphous structure, which is composed of several heteropolymers including xylan, galactomannan, glucuronoxylan, arabinoxylan, glucomannan and xyloglucan (Figure 2.3). Hemicelluloses differ in composition too; hardwood hemicelluloses contain mostly xylans, whereas softwood hemicelluloses contain mostly glucomannans. The heteropolymers of hemicellulose are composed of different 5- and 6-carbon monosaccharide units; pentoses (xylose, arabinose), hexoses (mannose, glucose, galactose) and acetylated sugars. Hemicelluloses are imbedded in the plant cell walls to form a complex network of bonds that provide structural strength by linking cellulose fibers into microfibrils and cross-linking with lignin (Figure 2.3).

Finally, lignin is a three-dimensional polymer of phenylpropanoid units. It functions as the cellular glue which provides compressive strength to the plant tissue and the individual fibres, stiffness to the cell wall and resistance against insects and pathogens [26]. The oxidative coupling of three different phenylpropane building blocks; monolignols: p-coumaryl alcohol, coniferyl alcohol, and sinapyl alcohol, forms the structure of lignin. The corresponding phenylpropanoid monomeric units in the lignin polymer are identified as p-hydroxyphenyl (H), guaiacyl (G), and syringyl (S) units, respectively [27]. Table 2.1 shows the chemical composition of various types of lignocellulosic biomass [28].

Table 2.1 Types of lignocellulosic biomass and their chemical composition.

Lignocellulosic Biomass		Cellulose (%)	Hemicellulose (%)	Lignin (%)
Hardwood	Poplar	50.8-53.3	26.2-28.7	15.5-16.3
	Oak	40.4	35.9	24.1
	Eucalyptus	54.1	18.4	21.5
Softwood	Pine	42.0-50.0	24.0-27.0	20.0
	Douglas fir	44.0	11.0	27.0
	Spruce	45.5	22.9	27.9
Agricultural Waste	Wheat Straw	35.0-39.0	23.0-30.0	12.0-16.0
	Barley Hull	34.0	36.0	13.8-19.0
	Barley Straw	36.0-43.0	24.0-33.0	6.3-9.8
	Rice Straw	29.2-34.7	23.0-25.9	17.0-19.0
	Rice Husks	28.7-35.6	12.0-29.3	15.4-20.0
	Oat Straw	31.0-35.0	20.0-26.0	10.0-15.0
	Ray Straw	36.2-47.0	19.0-24.5	9.9-24.0
	Corn Cobs	33.7-41.2	31.9-36.0	6.1-15.9
	Corn Stalks	35.0-39.6	16.8-35.0	7.0-18.4
	Sugarcane Bagasse	25.0-45.0	28.0-32.0	15.0-25.0
Sorghum Straw	32.0-35.0	24.0-27.0	15.0-21.0	
Grasses	Grasses	25.0-40.0	25.0-50.0	10.0-30.0
	Switchgrass	35.0-40.0	25.0-30.0	15.0-20.0

When biomass is used directly in an energy application without chemical processing then it is combusted. Conversion may be affected by thermochemical, biological, or chemical processes. These may be categorized as follows: direct combustion, pyrolysis, gasification, liquefaction, supercritical fluid extraction, anaerobic digestion, fermentation, acid hydrolysis, enzyme hydrolysis, and esterification. Figure 2.4 shows main biomass conversion processes. Biomass can be converted to biofuels such as bioethanol and biodiesel, and thermochemical conversion products such as syn-oil, syngas and biochemical [29].

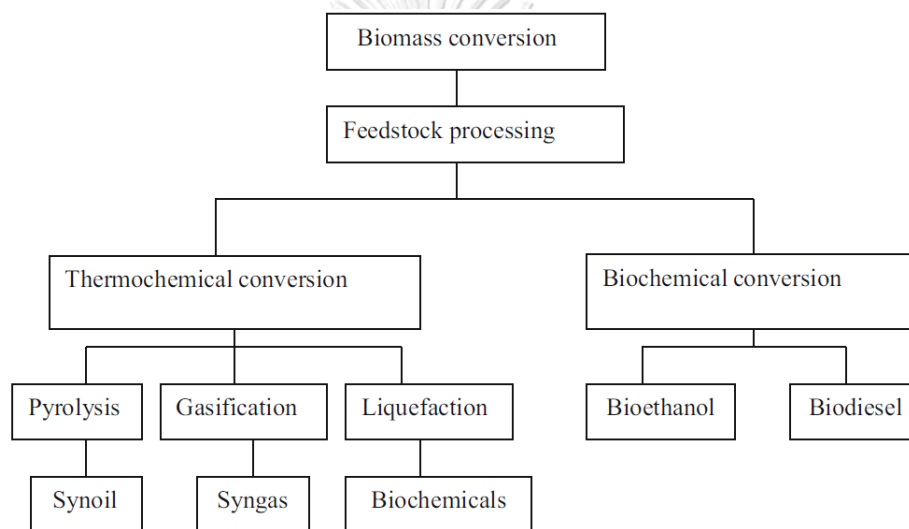


Figure 2.4 Main biomass conversion processes.

Thermochemical process is the suitable way to use dry feedstock. Pyrolysis involves heating biomass in the absence of oxygen at temperature up to 500 °C and produces an energy-dense bio-oil along with some gaseous and char products. Gasification involves the partial oxidation of biomass at high temperature (>500 °C) and yield mixture of CO and H₂ along with some CH₄, CO₂, water and small of carrier gas and heavy hydrocarbon. Liquefaction involves the attraction of solvent at high temperature and pressure and produces.

2.2.2 Biomass situation in Thailand

Biomass is the most important renewable energy source for areas in Thailand. Nowadays, in Thailand, biomass materials can be used to generate electricity, heat, or liquid fuel such as ethanol for motor vehicles that have substantially lower environmental impacts than traditional fossil fuels.

Three major potential sources of the biomass from agriculture-based industries in Thailand are sugarcane, rice, and oil palm sectors. Sugarcane and rice are mostly concentrated in northern and northeastern regions of the country, while the oil palm is found in the southern region [30, 31] Table 2.2 shows the national production trends in tons of sugarcane, paddy, and oil palm from 2010 – 2015 [32].

Table 2.2 National production of sugarcane, paddy, and oil palm.

(Unit: 1,000 Tons)

Crop year	Sugarcane	Paddy	Oil Palm (Fresh Fruit Bunches)
2010/11	45,873	22,580	2,781
2011/12	51,442	23,999	2,356
2012/13	53,912	25,182	3,621
2013/14	50,563	26,552	3,241
2014/15	60,114	26,861	4,002
2015/16	74,266	25,145	4,910
Average	56,028	25,053	3,485

2.2.2.1 Sugarcane

Sugarcane is grown mostly in the central region of the country, and some productions are found in the northern and northeastern region. Sugarcane production over period from 2010/11 to 2015/16 has average value of about 56 million tons per

year. Most of residues from sugarcane processing can be found at the mills except the sugarcane tops (Stumps and leaves, etc.) that are usually persist in field by farmers.

2.2.2.2 Rice

Rice is grown in every region of Thailand. Paddy production over period from 2010/11 to 2015/16 has average value of about 25 million tons per year. The cropping pattern for paddy consists of the major rice growing during the rainy months of May to September, and the second rice cultivating during the dry months of November to February. Most of the paddy fields in Thailand are in small size. However, there are 215 mills that have capacities ranging from 100 to 2000 tons of paddies per day.

2.2.2.3 Oil palm

The southern region of the country is the major area of the oil palm planting, while the eastern region has only small area for the oil palm planting and palm oil production. Oil palm production over period from 2010/11 to 2015/16 has average value of about 3.4 million tons per year. The raw material for the palm oil industry is fresh fruit bunches (FFB), which is harvested from oil palm trees [33].

2.2.2.4 Other agricultural sources

Two other biomass sources in the country that should be mentioned are coconut and tapioca. The coconut is a traditional crop in Thailand, which is grown for the domestic market. The coconut residues e.g. husk and shells have been used for the production of higher value-added products in the local and export markets since 1998. For tapioca, it is grown almost in all areas in the northeastern Thailand. In tapioca fields, there are a lot of residues which are not utilized. However, these residues are difficult to collect because they usually scattered all over the field.

2.3 Chemical Reactions

It is conceivable that the gasification consists of two steps; pyrolysis followed by gasification (Figure 2.5). Pyrolysis, which is called devolatilization, is decomposition

by the thermal. There is endothermic reaction. The main compound from the pyrolysis of biomass is the volatile component (more than 80-95 wt.%), including non-condensable gases and condensable liquid. The remaining solid, which is called char has mainly the carbon content [34].

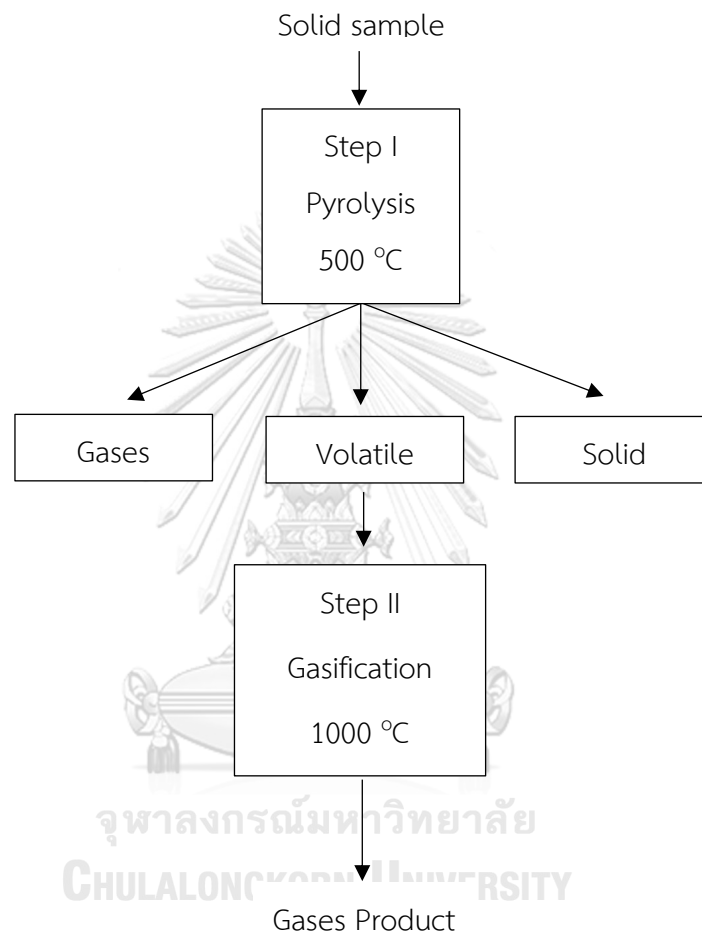
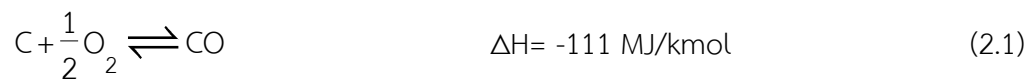


Figure 2.5 Gasification step.

The volatile component and char which are consisted of the hydrocarbon are converted into the gases product. In the gasification process, the fundamental chemical reaction reactions are those involving carbon (C), carbon monoxide (CO), carbon dioxide (CO₂), hydrogen (H₂), and methane (CH₄) [35].

Combustion reactions



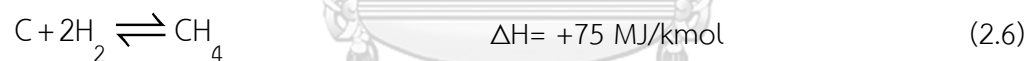
Boudouard reaction



Water gas reaction



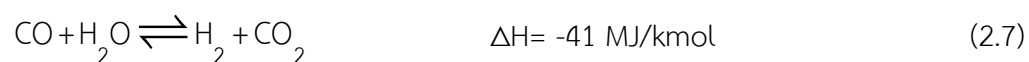
Methanation reaction



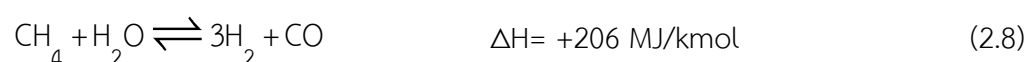
There are related to determination of the composition of syngas at equilibrium. Three heterogeneous (i.e gas and solid phases) reactions (2.4) to (2.6) are the most important for syngas production.

In general, we are concerned with situations where the carbon conversion is also completed. Under this situation, the equation from (2.4) to (2.6) can be reduced into the two following homogeneous gas reactions:

Water-gas shift reaction



Steam reforming of methane



The above reactions consist of (2.4), (2.5), (2.7) and (2.8) can explain four pathway which the carbon source sample are can be gasified.

Pathway 1: Reaction (2.4) is necessary for pure CO production when gasifying carbon source with mixing O₂ and CO.

Pathway 2: Reaction (2.5) plays an important role for the yield of syngas production.

Pathway 3: Reaction (2.7) is the most important for controlling the ratio between CO and H₂ which are produced from the gasification process

Pathway 4: The CH₄ which is produced from (2.6) can be reformed by the steam to produce syngas

However, most gasification process rely on a balance between partial oxidation (2.1) and water gas reaction (2.5).

For real fuels, including biomass which also contains carbon, the overall reaction can be written as:



Where,

- For gas, as pure CH₄, m = 4 and n=1, hence $\frac{m}{n} = 4$
- For oil, m = 2 and n = 1, hence $\frac{m}{n} = 2$
- For biomass, m = 1 and n = 1

A simplified reaction sequence for biomass gasification can be also explained a Figure 2.6 [36].

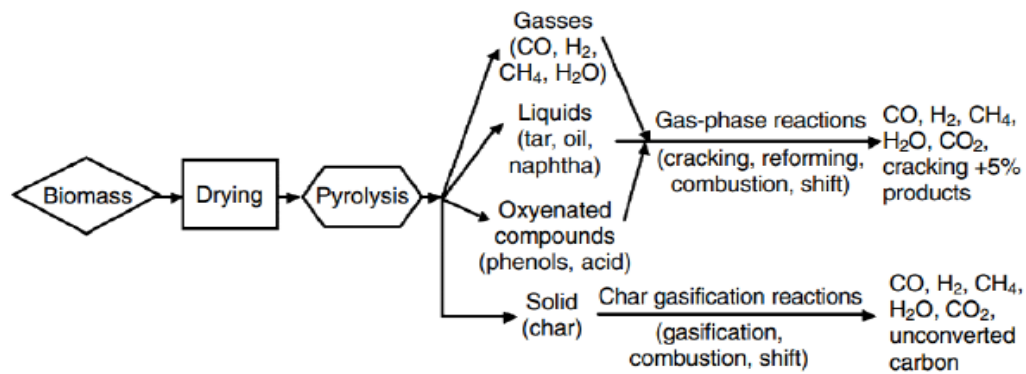


Figure 2.6 The sequential reaction for biomass gasification.

Gasification occurs in a set of four steps: drying, pyrolysis, oxidation and reduction. Firstly, drying process removes water in the biomass and converts it into steam. The steam produced by drying process can lead the thermal decomposition of biomass into bio-syngas. Pyrolysis is the chemical decomposition through the application of heat in the absence of oxygen. It can convert biomass to liquid product (also known as bio-oil or tar), a solid residue (also known as char) and several light gaseous compounds (e.g. H₂, CO, CO₂ and light hydrocarbon). Oxidation process takes place between oxygen in the air and biomass, producing carbon dioxide and water. Reduction process is a high temperature chemical reaction, occurring in the absence of oxygen. The main reactions in the reduction process are boudouard reaction (2.4), steam reaction (2.5), water-shift reaction (2.7) and methanation (2.6). These reactions are endothermic reaction which needs the energy to be occurred, except methanation (2.6). Gasification of biomass needs gasifying agent. Gasifying agent reacts with solid carbon and heavier hydrocarbons to convert them into low-molecular- weight gases like CO and H₂, as primary product of bio-syngas. The main gasifying agent used for gasification are oxygen, steam and air. Air has been widely used as the oxygen source for gasification because steam requires additional energy cost for increasing temperature and oxygen requires oxygen production equipment which increases the cost of gasification process [37].

2.4 Heterogeneous Catalysis

In heterogeneous catalysis, solids catalyze reactions of molecules in gas or solution. As solids – unless they are porous – are commonly impenetrable, catalytic reactions occur at the surface. To use the often-expensive materials (e.g. platinum) in an economical way, catalysts are usually nanometer-sized particles, supported on an inert, porous structure (Figure. 2.7). Heterogeneous catalysts are the workhorses of the chemical and petrochemical industry [38].

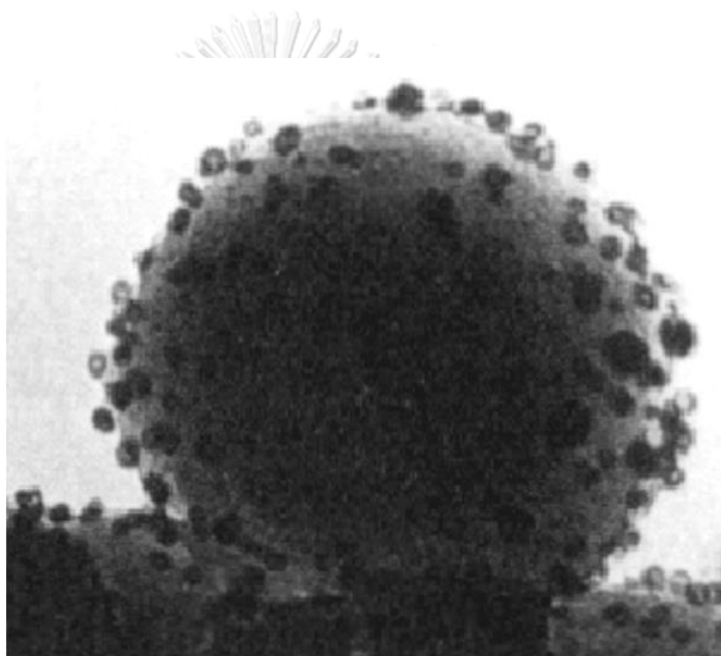
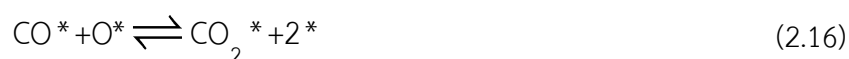


Figure 2.7 The example model of the heterogeneous catalysis.

As an introductory example we take one of the key reactions in cleaning automotive exhaust, the catalytic oxidation of CO on the surface of noble metals such as platinum, palladium and rhodium. To describe the process, we will assume that the metal surface consists of active sites, denoted as “*” We define them properly later on. The catalytic reaction cycle begins with the adsorption of CO and O₂ on the surface of platinum, whereby the O₂ molecule dissociates into two O atoms. (X* indicates that the atom or molecule is adsorbed on the surface, i.e. bound to the site *)



The adsorbed O atom and the adsorbed CO molecule then react on the surface to form CO₂, which, being very stable and relatively unreactive, interacts only weakly with the platinum surface and desorbs almost instantaneously:



Note that in the latter step the adsorption sites on the catalyst are liberated, so that these become available for further reaction cycles. Figure 2.8 shows the reaction cycle along with a potential energy diagram [39].

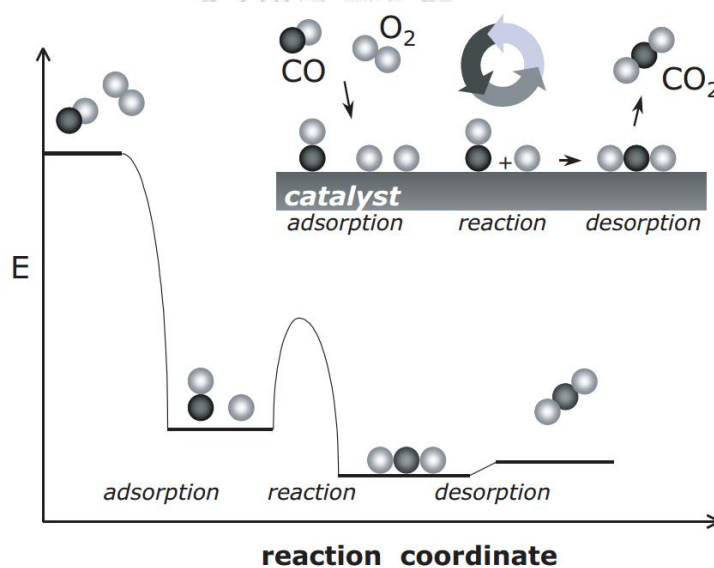


Figure 2.8 Reaction cycle and potential energy diagram for the catalytic oxidation of CO by O₂.

Suppose we carry out the reaction in the gas phase without a catalyst. The reaction will proceed if we raise the temperature sufficiently for the O₂ molecule to dissociate into two O atoms (radicals). Once these radicals are available, the reaction with CO to CO₂ follows instantaneously. The activation energy of the gas phase reaction will be roughly equal to the energy required to split the strong O–O bond in O₂, i.e.

about 500 kJ mol^{-1} . In the catalytic reaction, however, the O_2 molecule dissociates easily in fact without an activation energy on the surface of the catalyst. The activation energy is associated with the reaction between adsorbed CO and O atoms, which is of the order of $50\text{--}100 \text{ kJ mol}^{-1}$. Desorption of the product molecule CO_2 costs only about $15\text{--}30 \text{ kJ mol}^{-1}$ (depending on the metal and its surface structure). Hence if we compare the catalytic and the uncatalyzed reaction, we see that the most difficult step of the homogeneous gas phase reaction, namely the breaking of the O–O bond is easily performed by the catalyst. Consequently, the ease with which the CO_2 molecule forms determines the rate at which the overall reaction from CO and O_2 to CO_2 proceeds. This is a very general situation for catalyzed reactions, hence the expression: A catalyst breaks bonds, and lets another bonds form. The beneficial action of the catalyst is in the dissociation of a strong bond, the subsequent steps might actually proceed faster without the catalyst (which is a hypothetical situation of course).

2.5 Preparation of supported catalysts

Supported catalysts are prepared by deposition of the active metal on the support materials. The main purpose of using a support is to achieve an optimal dispersion of the catalytically active component and to stabilize it against sintering. But in many reactions the support is not inert and the overall process consists of two catalytic functions both for active components and support [40].

Supported catalysts are prepared in two main steps:

1. Deposition of the precursor of the active component on the support.
2. Transformation of this deposited precursor to catalytically active site.

The final active component can be in metallic state, oxide form or reduced from depending on the requirements.

There are various deposition methods. Most of these involve aqueous solutions and liquid solid interface. In some cases, deposition is also done from the gas phase and involves gas- solid interface. The methods most frequently used are impregnation, precipitation and co-precipitation

2.5.1 Impregnation

Impregnation can be classified in two categories according to the volume of solution used as following:

2.5.1.1 Dry or incipient impregnation

In this method, a previously dried support is contacted with volume of solution equal to its pore volume. The solution contains the required amount of the precursors of the active phase. As soon as the support is placed in contact with the solution, the solution is drawn into the pores by capillary suction. In case of proper wetting, no excess solution remains outside the pore space. Part of the air present in the pores is imprisoned and compressed under the effect of capillary forces. The pressure developed inside the imprisoned gas bubbles depends on the radius, r , of the curve of the liquid -gas meniscus and may reach several MPa when $r < 100$ nm as a result of Young - Laplace law as follow

$$\Delta P = P - P' = \frac{2\gamma}{r},$$

where, γ is the liquid- gas interfacial tension. Considerable forces will thus be exerted on the portions of the pore walls in contact with these bubbles. The walls that are not strong enough may break down causing a degradation of the mechanical properties.

Occasionally, even bursting of the catalyst grains occurs. However, the development of the high pressure is a transitory phenomenon. Under highly compressed conditions, air dissolves and progressively escapes from the solid.

2.5.1.2 Wet-diffusional impregnation

In this method, the pore space of the support is first filled with the same solvent as used in the impregnating precursor solution. The wetted support is then treated with the impregnating precursor solution. Here the actual impregnation takes place in diffusional condition when solvent filled support is dipped in the precursor solution.

The first phase of saturation of the support by solvent involves the characteristics of dry impregnation. But in the second phase, when solvent saturated support is added to the impregnating solution, high pressure is not developed within the pores. The precursor salt migrates progressively from the solution into the pores of the support. The driving force at all times is the concentration gradient between the bulk solution and the solution within the pores. The impregnation time is much longer than for dry impregnation.

Wet impregnation should be avoided when the interaction between the precursors and the support is too weak to guarantee the deposition of the former.

2.5.1.3 Mechanism of impregnation

The mechanism of wet impregnation is simpler compared to dry impregnation. In wet impregnation, the distribution of the solute inside the pores is assumed to be governed by two phenomena (Figure 2.9)

- Diffusion of the solutes within the pores. It is described by Fick's law
- Adsorption of the solute onto the support. This depends on the adsorption capacity of the surface and on the adsorption equilibrium constant.

The distribution of the precursors within the pellets depends on the balance between these diffusion and adsorption phenomena.

In case of dry impregnation, in addition to diffusion and adsorption processes, another phenomenon occurs, which is the pressure driven capillary flow of the solution inside the empty pores. This can be represented by Darcy's law. An important parameter from introduction of Darcy law is the solution viscosity ' μ '. In case of aqueous solution and in the common range of concentration used for impregnation, viscosity increases almost proportionally with concentration. It also increases with the presence of organic ligands attached to the metal ions. Viscosity and concentration have opposite effects on precursor diffusion; a high concentration tends to favor the diffusion of the solute towards the center of the pellet, while a high viscosity tends to hinder the diffusion [41].

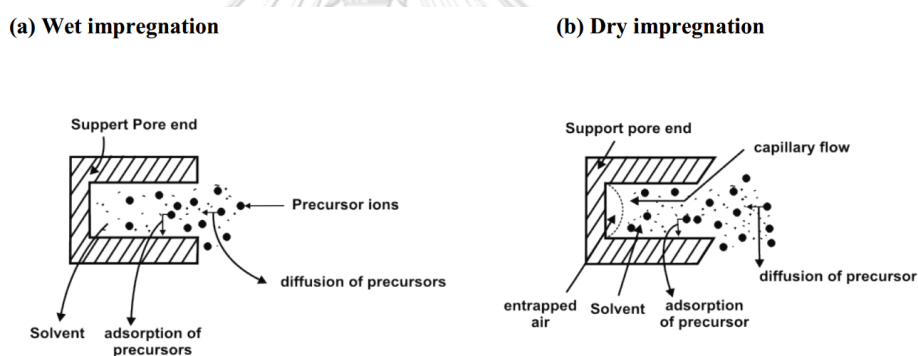



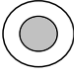
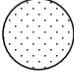
Figure 2.9 Schematic representation of basic processes involved during impregnation of precursors on porous support.

2.5.1.4 Precursor distribution

The distribution of precursors within the pores of support depends on various factors. The different conditions of impregnation and drying can result in broadly three types of precursor distribution as described in Table 2.3. In Egg shell type distribution, the precursors are preferentially accumulated near the pore wall. This type of distribution is obtained if during impregnation precursors are strongly adsorbed on the pore wall. High viscosity of the solution also tends

to result in egg shell distribution. For slow drying, egg shell distribution can result even in low viscosity and weak adsorption conditions. In egg yolk type distribution, the precursors are accumulated in the interior core of the pores. Egg yolk distribution is obtained if during impregnation, the competing ions are present that have stronger interaction with the pore wall of supports. Fast drying regime with predominant back diffusion also results in egg yolk distribution. In uniform precursor distribution, precursors are uniformly distributed across the pores. If the adsorption of the solutes is weak and the time is long enough, distribution tends to be uniform. Uniform distribution also results when precursors and competitors interact equally with the surface or the impregnating solution is concentrated and viscous. Room temperature drying with weakly adsorbing precursors also tends to give uniform precursor distribution. For powders, the equilibrium is reached within few minutes. However, in case of pellets it may take up to several hours to reach a uniform distribution of the precursors [42, 43].

Table 2.3 Distribution of precursor at different conditions of impregnation and drying.

Precursor distribution	Conditions of Impregnation and drying
Egg shell distribution 	<ol style="list-style-type: none"> 1. Strong adsorption of precursors during impregnation 2. High viscosity of impregnating solution 3. Slow drying regime for low concentration, low viscosity and weak adsorption conditions
Egg yolk distribution 	<ol style="list-style-type: none"> 1. In presence of competitor ions that have stronger interaction with the supports 2. Fast drying regime with predominant back diffusion
Uniform distribution 	<ol style="list-style-type: none"> 1. Precursors and competitors interact equally with the surface. 2. Impregnating solution is concentrated and viscous 3. Room temperature drying with weakly adsorbing precursors

2.5.2 Precipitation and Co-Precipitation

Precipitation is the creation of a solid from a solution. When the reaction occurs in a liquid solution, the solid formed is called the 'precipitate'. The chemical that causes the solid to form is called the 'precipitant'.

2.5.2.1 Mechanism of precipitation

Precipitation occurs in three steps: supersaturation, nucleation and growth. Pertinent parameters producing supersaturation are shown in Figure. 2.10 Solubility curves are functions of temperatures and pH. In the supersaturation region the system is unstable and precipitation occurs with any small perturbation. The supersaturation region can be approached either by increasing the concentration through solvent evaporation (A to C), lowering the temperature (A to B) or increasing the pH (which moves the solubility curve to D and A into the supersaturation region). This last approach is quite usual in the preparation of hydroxides and sulfides. Particles within the supersaturation region develop in a two-stage process: nucleation and growth. Nucleation may proceed spontaneously (homogeneous nucleation) or be initiated with seed materials (heterogeneous nucleation). These are solid impurities such as the dust or the rough edges of the vessel surface. The rate of nucleation can be accelerated by deliberate addition of seed nuclei. The growth process depends on concentration, temperature, pH and ripening [44].

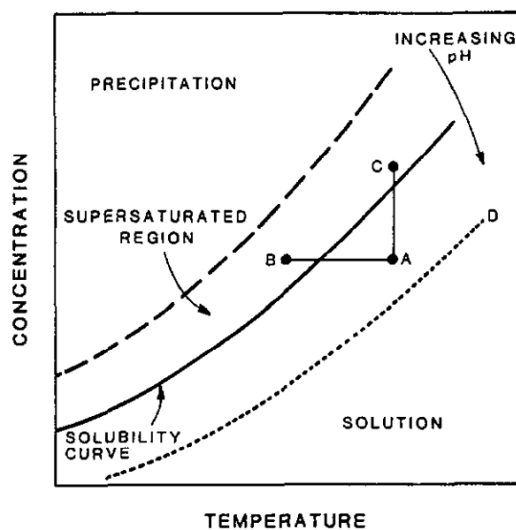


Figure 2.10 Supersaturation dependence on concentration, T and pH.

The size of the precipitated crystal diminishes as their equilibrium solubility diminishes (i.e. as supersaturation increases), as Ostwald ripening is slowed down by the reduced transfer rate between the suspended particles [45].

2.5.2.2 Characteristic of sample from precipitation method

Most precipitates are crystalline precipitates. Depending on the precipitation conditions it is possible to obtain amorphous solids. If the supersaturation is very high, the aggregation rate can exceed the orientation rate and the solid obtained is amorphous. However, by ripening in the presence of the mother liquor, the amorphous solid can become crystalline. Precipitation can be performed starting from either 'true' solutions or colloidal solutions (sols). Figure 2.11 shows the characteristics of such solutions. Particles which show little or no attraction for water form hydrophobic colloids. These are easily flocculated and the resulting colloidal precipitates are easily filtered (e.g. arsenic trisulfide, silver chloride). Particles which show a strong

affinity to water form hydrophilic colloids. These are very difficult to flocculate and the resulting jellylike mass is difficult to filter. Hydrophilic colloidal solutions can be prepared from many inorganic compounds, such as silicic acid and the hydrous oxides of aluminum and tin [46].

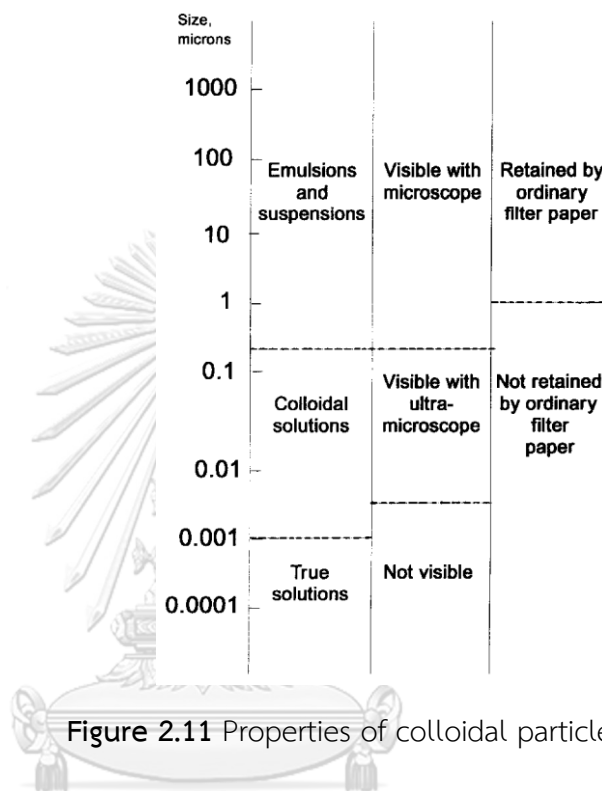


Figure 2.11 Properties of colloidal particles.

Precipitation procedures can be used to prepare either single component catalysts and supports or mixed catalysts. The main purpose in the latter case is the intimate mixing of the catalyst components that can be achieved either by the formation of very small crystallites or by the formation of mixed crystallites containing the catalyst constituents. Hydroxides and carbonates are the preferred precipitated intermediates for the following reasons [47]:

(1) The solubility of these salts of transition metals are very low. Consequently, very high supersaturations can be reached, leading to very small precipitate particle sizes.

(2) Hydroxides and carbonates are easily decomposed by heat to oxides of high area without leaving potential catalyst poisons (as, for example, the sulfur left by sulfates calcination).

(3) Safety and environmental problems arising from the calcination of hydroxide and carbonates are minimal.

During coprecipitation care must be taken in order to avoid independent or consecutive precipitations. Besides, the pH should be adjusted and kept constant during the operation: this can be done by mixing the starting solution continuously, instead of adding one solution to the other [48].



2.6 Review of catalytic for biomass gasification to enhanced H₂ production

Catalysts for use in biomass conversion may be divided into two distinct groups which depend on the objective for the development of biomass gasification [49].

The first group of catalysts is added to the biomass prior to gasification, which catalyze the reactions which is already explained in section 2.3. The addition is either by wet impregnation of the biomass material or by dry mixing of the catalyst with it. These catalysts have the purpose of reducing the tar content and have little effect on the conversion of methane and C₂₋₃ hydrocarbons in the product gas.

The second group is called sorbent catalysts. It is the novel systems for hydrogen production have been carried out as sorption enhanced hydrogen production (SEHP) with in-situ CO₂ removal, which has been considered to change the normal equilibrium limits of shift reactions for producing high-purity hydrogen.

2.6.1 Catalysts for tar reduction

The most significant of literature published on the area of hot gas cleaning for biomass gasification concerns nickel catalysts. The several researches have investigated a system of raw gas cleaning that involves a dolomite or alkali catalyst for the removal of tar up to 95% followed by the adjustment of the gas composition (reforming of the methane and the remaining tar) using a nickel steam reforming catalyst [50-52]. The literatures can be divided into two groups. The first group focuses on using nickel catalyst as the primary catalyst in the gasifiers and the second group concentrates on using it as the secondary catalyst in post gasification or post pyrolysis reactor.

2.6.1.1 Commercial nickel catalyst as primary catalyst

There are several benefits of using nickel catalyst as the primary catalyst. First, nickel is one of the most effective transition metals for tar cracking and reforming. In addition to reducing the tar content, nickel catalyst improves the quality of the gaseous product in biomass

gasification. Second, it is economically attractive. Because both gasification and gas clean-up processes occur in-situ, no downstream reactor or extra heating is required, which results in lower plant capital and operating cost [53].

Baker *et al.* [54] examined the performance of G-90C catalyst used as primary and secondary catalysts in biomass steam gasification (Table 2.2) In a fluidized bed experiment with G-90C as primary catalyst, synthesis gas yield of 1.8 m³/kg was obtained in the first 5 h of run. However, gas yield started to decline after 5 h and the catalyst was completely deactivated after 7 h. For comparison, the maximum theoretical gas yield with a H₂/CO ratio of 2.0 is 2.4 m³/kg. Similar behavior was observed in the experiments with G-90C used as a secondary catalyst. The initial activity was high but gradually reduced thereafter. After 16 h of on stream testing, synthesis gas yields of the secondary fixed bed reactor and the secondary fluidized bed reactor stabilized at 1.25 – 1.30 m³/kg and 1.50 m³/kg respectively. The G-90C catalyst performed better as secondary catalyst over longer time period because of lower carbon fouling (1/3rd) compared to the primary catalyst.

Li *et al.* [55] also conducted a study using commercial nickel catalyst as primary catalyst in biomass gasification (Table 2.4). The main focus of their studies was to investigate the impact of operating parameters on the final gaseous product composition in a circulating fluidized bed gasifier and to develop a model for the air-blown circulating fluidized bed biomass gasification. They reported that tar yields in two of the runs with Sud-Chemie catalyst C11-9 LDP were substantially lower when compared with the runs with no catalyst

added under the same operating temperature. The tar yield reduced from 10.26 g/N m³ to 2.35 g/N m³ and 0.04 g/N m³ respectively. However, no further investigation and characterization was conducted on the spent catalyst and deactivation of the catalyst was not reported.

Table 2.4 Activity comparison of nickel catalysts used as primary catalyst in biomass gasification.

Catalyst	NiO (wt%)	Support	Reactor condition		Carbon conversion		
			Temp (°C)	Pressure (kPa)	Gas (%)	Solid (%)	Liquid (%)
Blank	-	-	750	101	80.0	13.0	7.0
G-90C	15	Al-CaO	750	101	90.0	10.0	0.0
Blank	-	-	728	119	89.8	6.9	3.3
C11-9P	N/A	Al	739	119	95.0	4.2	0.8

Both Baker and Li studies demonstrated the advantages and limitations of commercial nickel catalyst used as primary catalyst in biomass gasification. The catalysts were effective in increasing the gaseous product yield and reducing tar yield. However, the catalysts suffered from rapid deactivation. The deactivation of nickel catalyst in in-situ gasification is commonly caused by carbon formation on the catalyst surface and nickel sintering [56]. The deactivation of catalysts in gasification may be minimized through the use of additives and promoters.

2.6.1.2 Commercial nickel catalyst as secondary catalyst

Secondary catalysts are used in post gasification or post pyrolysis reactor to improve the quality of the product gas or to reform the bio-oil produced in the primary reactor. Secondary catalysts are active for longer duration because coke formation on the catalyst surface is minimized in a downstream reactor.

Caballero *et al.* [57] and Aznar *et al.* [58] studied the feasibility of using commercial nickel catalyst as secondary catalyst in biomass gasification. Four out of eight catalysts used in their studies were made for heavy hydrocarbons steam reforming, while the remaining were made for light hydrocarbons steam reforming. Catalysts were tested in pine wood chips gasification process. It was found that catalysts made for heavy hydrocarbons steam reforming were more effective in eliminating tar, promoting hydrogen and carbon monoxide productions and suppressing the formations of the undesired methane and carbon dioxide. No catalyst deactivation was reported after 45 h of on-stream testing in a temperature range of 780–830 °C.

Pfeifer *et al.* [59] tested six commercial nickel catalysts, also made for heavy and light hydrocarbons reforming, in toluene steam reforming reaction with a fixed bed quartz reactor. They found that heavy hydrocarbons steam reforming catalysts were more effective in converting tars and ammonia into gaseous product than light hydrocarbons reforming catalysts. High conversion of tar (98%) and ammonia (40%) was achieved at a space velocity of 1200 h⁻¹ and operating temperature of 850–900 °C. Selectivity toward CO formation was higher with heavy hydrocarbons reforming catalysts. No

deactivation of catalyst was reported from the 12-hr. test which implies that these catalysts were able to suppress coke deposition.

One of the catalysts, G-90B, studied by Pfeifer was also used by Kinoshita *et al.* [60] in sawdust gasification investigation. Using in an indirectly heated fluidized bed catalytic reformer, they noticed that carbon conversion, tar conversion and gas yield, particularly carbon monoxide and hydrogen yield, increased as the temperature and space time increased. Complete conversion of tar was achieved at 700–800 °C at space velocity 41.2 s. Hydrogen to carbon monoxide ratio also improved by increasing steam to biomass ratio. However, increasing the steam to biomass ratio lowers the heating value of the product gas due to high vapor content in the product gas.

In summary, commercial catalysts used in heavy hydrocarbons reforming performed better in converting tar and suppressing coke formation. The nickel loading of the heavy hydrocarbons reforming catalysts is typically 5 – 10 wt% higher than light hydrocarbons reforming catalysts. The catalyst BET surface area of the heavy hydrocarbons reforming catalyst was on average 3 times the surface area of the light hydrocarbons reforming catalysts. High BET surface area along with higher metal loading would provide large metal surface area which is one of the reasons for better activity of heavy hydrocarbon catalysts. Another reason is the presence of magnesium compounds in the heavy hydrocarbons reforming catalysts. Oxides of magnesium play a key role in suppressing coke formation in gasification [61, 62].

2.6.2 Sorption enhanced H₂ production (SEHP)

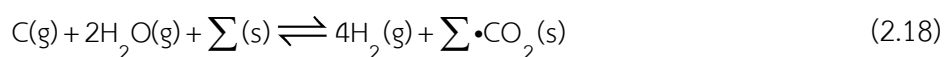
In the past few decades, the studies on a new technology for hydrogen rich gas production have been carried out as SEHP with in-situ CO₂ removal, which has been considered to change the normal equilibrium limits of shift reactions for producing high-purity hydrogen and increasing hydrocarbons conversion [63-65]. In addition, it is a low-cost hydrogen production due to reducing the number of processing steps required for subsequently separating CO₂ and decreasing the reaction temperatures for energy usage [66-68].

The primary reactions involved in H₂ production from natural gas are water gas reaction (2.5) methane steam reforming (2.8) and water gas shift (2.7)

Water gas reaction and methane steam reforming are highly endothermic while the water gas shift reaction is moderately exothermic. All reactions are equilibrium limited, and it is impossible to achieve complete conversion of carbon source (C) in biomass and CO in a single reactor under normal reaction conditions. However, if the CO₂ can be removed from the gas phase as it is formed, the normal equilibrium limits are displaced and complete conversion can be closely approached. In sorption enhanced H₂ production, the CO₂ is removed using an appropriate solid sorbent that for the time being we represent by the symbol Σ . The CO₂ capture reaction may be written as



The overall reaction thus becomes



As will be seen, the sorbent may truly react with CO₂ to form a solid carbonate or may be physically or chemically adsorbed on the surface of the sorbent. Because the sorbent is effectively consumed in reaction 2.17, sorption-enhanced processes are inherently dynamic in operation. A sorbent

regeneration step is necessary, and the sorbent must maintain activity through many cycles for the process to be economically viable.

The several research works studied the H₂ rich gas production in steam reforming process with different sorbent material. However, calcium oxide (CaO) and magnesium oxide (MgO) known as a tar reforming agent are also an effective and commonly used solid sorbent due to its low cost and abundance. This literature review is divided into CaO and MgO sorbent for SEHP.

2.6.2.1 CaO based sorbents

The advantages of low-cost sorbents for hydrogen production are very apparent. To date, CaO-based sorbents have been one of the most promising candidates for their CO₂ sorption capacities under the conditions for steam reforming, and it is believed to be thermodynamically the best candidate among metal oxides for CO₂ capture in zero emission power generation systems. CaO is capable of scavenging CO₂ to very low concentrations at moderate temperatures (450–750 °C) and at atmospheric pressure.

For the carbonation process of CaO, the initial stage is fast and controlled by chemical kinetics, and the next stage is slow and controlled by the diffusion in the solid product (CaCO₃) layer. The formation of a critical size of CaCO₃ “product islands” on the reacting CaO particles surface can lead to reduction of the conversion rate which is strongly affected by temperature [69, 70]. Figure 2.23 illustrates the CaCO₃ product formation during the carbonation reaction of CaO involved with steam. During the initial stage, certain amount of CaCO₃ is produced and grows as the morphology of the island, meaning a part of CaO particle surface is covered by these CaCO₃ islands, whereas the

other part of CaO surface remains in contact with CO_2 [71]. In the product layer diffusion-controlled stage, the produced CaCO_3 (higher molar volume of $36.9 \text{ cm}^3/\text{g}$) covers almost all the CaO ($16.7 \text{ cm}^3/\text{g}$) particle surface so as to hinder the direct contact of CaO with CO_2 . In this case, the carbonation process is controlled by ion diffusion through the CaCO_3 product layer. As it is proposed [72], the counter-current and co-current diffusion process occurs on the surface of the particle. CO_3^{2-} diffuses inward from the CaCO_3 -CaO gas interface to the CaCO_3 -CaO interface, whereas O^{2-} diffuses in the opposite directions. The involved H_2O molecule dissociates to H^+ and OH^- . With a very small radius, H^+ easily diffuses through the CaCO_3 product layer to the CaCO_3 -CaO interface and interacts with O^{2-} to form OH^- . Then, OH^- diffuses outwardly to the CaCO_3 -CaO gas interface to react with CO_2 , as shown in Figure 2.12.

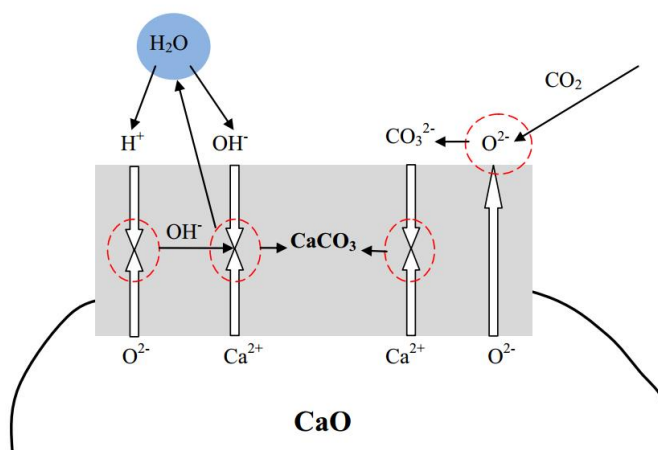


Figure 2.12 Mechanism of CaO carbonation by CO_2 in the presence of steam.

On the other hand, dry gas–solid carbonation of CaO can be reactivated at relatively high temperature. At high temperature atomic excitation allows the local migration of oxygen atoms from CaO toward the adsorbed CO_2 leading to its mineralization into carbonate around

CaO particles; chemically the mineralization of CO₂ also implies the breaking of one covalent bond in the CO₂ molecule [73].

Qin *et al.* [74] studied three types of fabricated sorbent using various calcium and support precursors via a simple mixing method, in order to develop highly effective, durable, and cheap CaO-based sorbents suitable for CO₂ capture. The sorption performance and morphology of the sorbents were measured in a thermogravimetric analyzer and a scanning electron microscopy, respectively. The experimental results indicate that cement is a promising low-cost support precursor for contributing to the enhancement of cyclic CO₂ sorption capacity, especially when organometallic calcium precursors were used. A sorbent (with 75% CaO content) made from calcium L-lactate hydrate and cement showed the highest CO₂ sorption capacity of 0.36 g of CO₂/g of sorbent and its capacity decreased only slightly after 70 cycles of carbonation and calcination.

Wu *et al.* [75] studied the properties of nano CaO/Al₂O₃ as a high-temperature CO₂ sorbent for its use in an adsorption enhanced reforming reaction. The sorbent containing nano CaCO₃ precursors and aluminum oxide was prepared, and evaluation of the CO₂ adsorption properties by a thermogravimetric analyzer, the results show that nano CaO/Al₂O₃ has a faster decomposition rate and has a higher CO₂ adsorption ratio than micro CaO/Al₂O₃. The maximum adsorption ratio occurs at temperatures of 650 °C under a CO₂ partial pressure of 0.33 atm. Durability studies show that the CO₂ adsorption ratio remains at 68.3% after 50 cyclic runs under a carbonation temperature of 650 °C and calcination temperature of 800 °C, respectively. XRD, SEM, and BET were used for studying the change of micro characteristics of the CO₂

sorbents before and after multiple carbonation-calcination runs. The results showed that the pore size of CaO/Al₂O₃ sorbents was enlarged and that a new substance (Ca₁₂Al₁₄O₃₃) was formed even under a temperature of 800 °C for the function of keeping the compound stable and durable.

2.6.2.2 MgO based sorbents

As reported, magnesium oxides are plausible CO₂ sorbent candidate for their moderate CO₂ sorption capacity. They perform well under wide operating temperatures from room temperature to around 500 °C and also under water vapor concentration of 8 – 17 vol% [76]. Also, their advantages are wide availability in natural minerals and low cost. Based on MgO–CO₂ carbonation/decomposition equilibrium diagram, it is theoretically possible to carry out a regenerative MgO-based process for CO₂ sorption. In order to make this process economically viable, highly durable, reactive, and mechanically strong, those MgO-sorbent candidates are required to minimize attrition losses and the fresh sorbent make up rate. Modified MgO-based sorbents are usually promoted with elements of K, Na, Al, Ti etc. by co-precipitation or impregnation methods. Mesoporous magnesia synthesized with mesoporous silica SBA-15 (treated with sucrose and sulfuric acid to obtain mesoporous carbon, CMK-3) through the nano-casting process exhibit superior CO₂ adsorption capacity [77]. The CO₂ sorption capacities over MgO-based sorbents were studied at temperatures lower than Ca-based sorbents (both carbonation and regeneration temperatures).

Li *et al.* [78] studied the MgO/Al₂O₃ sorbent for CO₂ capture under low temperatures via fixed bed reactor. It was found that, with MgO loading of 10 wt %, MgO/Al₂O₃ sorbent showed a maximum CO₂ capture capacity, which originated from the balance of physical adsorption and chemical absorption of the sorbent. The CO₂ capture capacity increased with the water vapor at first and then decreased. Typically, the total CO₂ capture capacities were as high as 0.97 and 1.36 mmol/g, with water vapor concentration of 0 and 13 vol %, respectively, at 60 °C with 13 vol % CO₂. The high CO₂ concentration could be approached by the multistage absorption/desorption cycles, during which the sorbent could be regenerated at 350 °C and maintained stable even after 5 cycles. In addition, a deactivation model was proposed that gave good predictions of the CO₂ breakthrough curves. Results showed that sorption rate parameters obtained in the presence of water vapor were found to be larger than the corresponding values in the absence of water vapor. It was possibly caused by increasing the reactivity of the sorbent prior to the sorption of CO₂ in the presence of water vapor.

Han *et al.* [79] examined nano-structured MgO–Al₂O₃ aerogel adsorbents (denoted as MgAl-AE-X) with different Mg/Al molar ratio (X) using a single-step epoxide-driven sol–gel method and a subsequent CO₂ supercritical drying method. The effect of Mg/Al molar ratio of nano-structured MgO–Al₂O₃ aerogel adsorbents on their physicochemical properties and CO₂ adsorptive performance at elevated temperature (200 °C) was investigated. Successful formation of flower-like nano-structured MgAl-AE-X adsorbents was confirmed by N₂ adsorption–desorption isotherms and SEM analyses. The crystalline

structure of MgAl-AE-X adsorbents was transformed in the sequence of $\text{Al}_2\text{O}_3 \rightarrow \text{MgAl}_2\text{O}_4 \rightarrow \text{MgO-MgAl}_2\text{O}_4$ with increasing Mg/Al molar ratio from 0 to 3. All the MgAl-AE-X adsorbents were found to possess weak base site and medium base site except for strong base site. In the dynamic CO_2 adsorption, both the total CO_2 capacity and the 90% breakthrough CO_2 capacity showed volcano-shaped curves with respect to Mg/Al molar ratio, and they were decreased in the order of MgAl-AE-0.5 > MgAl-AE-1.0 > MgAl-AE-2.0 > MgAl-AE-3.0 > MgAlAE-0. It was found that the 90% breakthrough CO_2 capacity increased with increasing medium basicity of the adsorbents. Among the adsorbents tested, MgAl-AE-0.5 (Mg/Al = 0.5) adsorbent with the highest medium basicity showed the best CO_2 adsorptive performance. Thus, medium basicity of nano-structured MgO- Al_2O_3 aerogel adsorbents served as a crucial factor in determining CO_2 adsorptive performance at elevated flue gas temperature (200 °C).

2.6.3 Combined catalyst and sorbent for H_2 production.

A few attentions studied about the combined catalyst and sorbent for H_2 production in biomass gasification process as followed

Mostafavi *et al.* [80] studied novel development of mixed catalyst-sorbent pellets for steam gasification of coal chars with in situ CO_2 capture. Novel mixed catalyst-sorbent pellets were prepared with different contents of potassium carbonate and calcium oxide as the catalyst and sorbent, respectively. The pellets were used in steam gasification experiments of two different types of coal. The results showed that the maximum hydrogen molar percentage of 80% was obtained from the steam gasification of coal at 700 °C. Small amounts of CO_2 and CO were detected. The pellets with a catalyst

content of 50% demonstrated the best performance, in terms of maximum achievable hydrogen yield. Lignite Boundary Dam coal showed a higher reactivity than the Genesee sub-bituminous samples. The residual results from the ultimate analyses and burn-off tests also confirmed the same trend at a catalyst content of 50% and revealed that carbon conversion and hydrogen production increased with increasing catalyst content in the pellets up to 50%, after which the opposite trend was observed. This trend with a maximum value may be a result of the solid-state reaction between the sorbent and the catalyst. The dispersion of catalyst particles on CaO and binder and the concentration of active catalyst sites on the pellets are other positive benefits in the enhancement of gasification.

Kumagai *et al.* [81] studied hydrogen production for the pyrolysis-gasification of a biomass/plastic mixture by using Ni-Mg-Al-Ca co-precipitation catalyst. The Ca content catalyst and catalyst calcination temperature were investigated. The results indicated that increasing the Ca content in the catalyst, hydrogen yield was improved to 33.2 mole H₂ g⁻¹ Ni since the water-gas shift reaction was enhanced by in situ CO₂ sorption. In addition, lower calcination temperature was preferred for hydrogen production due to the presence of reactivity CaO in the catalyst, resulting in the highest hydrogen yield of 39.6 mole H₂ g⁻¹ Ni using the catalyst produced at a lower calcination temperature.

Zamboni *et al.* [82] studied synthesis of Fe/CaO active sorbent for CO₂ absorption and tars removal in biomass gasification. In this work different Fe/CaO sorbent were prepared using three CaO precursors including CaO, CaCO₃, and Ca(CH₃COO)₂·H₂O and two iron salts, Fe(CH₃COO)₂ and Fe(NO₃)₃·9H₂O. The results showed that the sorbent prepared from Ca(CH₃COO)₂·H₂O have a higher BET surface area and CO₂ sorption capacity than the sorbent prepared from CaO and CaCO₃. In addition, Fe(CH₃COO)₂ is the

adequate salt to lead to the formation of Fe_2O_3 phase in Fe/CaO sorbent, thus iron can be more available for tar steam reforming. Moreover, mechanical mixture was identified as the best method to prepare Fe/CaO sorbents because it avoids the formation of $\text{Ca}_2\text{Fe}_2\text{O}_5$ phase.



CHAPTER 3

EXPERIMENTAL APPARATUS AND ANALYTICAL METHOD

3.1 Materials

3.1.1 Feedstock and chemicals

- Sugarcane leaves with particle sizes 250 – 300 μm
- Nickel nitrate hexahydrate ($\text{Ni}(\text{NO}_3)_2 \cdot 6\text{H}_2\text{O}$) from Fluka
- Calcium nitrate tetrahydrate ($\text{Ca}(\text{NO}_3)_2 \cdot 4\text{H}_2\text{O}$) from Sigma Aldrich
- Magnesium nitrate hexahydrate ($\text{Mg}(\text{NO}_3)_2 \cdot 6\text{H}_2\text{O}$) from UNILAB
- Ammonia solution (NH_3) from Sigma Aldrich
- Commercial calcium oxide (CaO) 500 μm from Sigma Aldrich
- Commercial magnesium oxide (MgO) 500 μm from Sigma Aldrich
- Gamma alumina ($\gamma\text{-Al}_2\text{O}_3$) with diameter of 150 μm from Sumitomo
- Alumina ball (inert- Al_2O_3) with diameter of 150 μm from Sumitomo
- Argon gas 99.99% from Praxair (Thailand)

3.1.2 Equipment

In this study, the two-stage fixed bed reactor (TFBR) was used for steam gasification of sugarcane leaves. A schematic diagram of TFBR is shown in Figure 3.1 and 3.2. The TFBR consists of two quartz reactors (inner tube with 9 mm-ID and 60 cm and outer tube with 19 mm-ID and 89 cm-length), two external electric furnaces (Carbolite model MTP 12) with temperature controller, Ar cylinder with mass flow controller, liced-tar trap, moisture trap, steam temperature controller, distilled water bath, HPLC pump and sample feeder. The heating zone was located in the middle of the outer tube with the length of 67 cm. The reactor is divided into two zones; The first zone (Upper) called

“Pyrolysis”, and the second zone (Lower) called “Gasification” the conceptual diagram of this reactor is shown in Figure 3.2 and the image of laboratory instrument is shown in Figure 3.3.

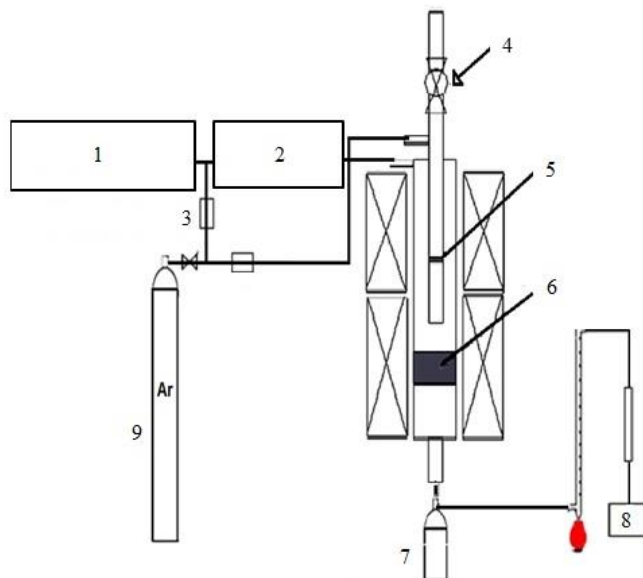


Figure 3.1 Schematic representation of the experimental apparatus: (1) HPLC pump, (2) steam generator, (3) mass flow controller, (4) biomass feeder, (5) quartz wool, (6) catalyst bed, (7) tar trap, (8) gas bag and (9) gas tank.

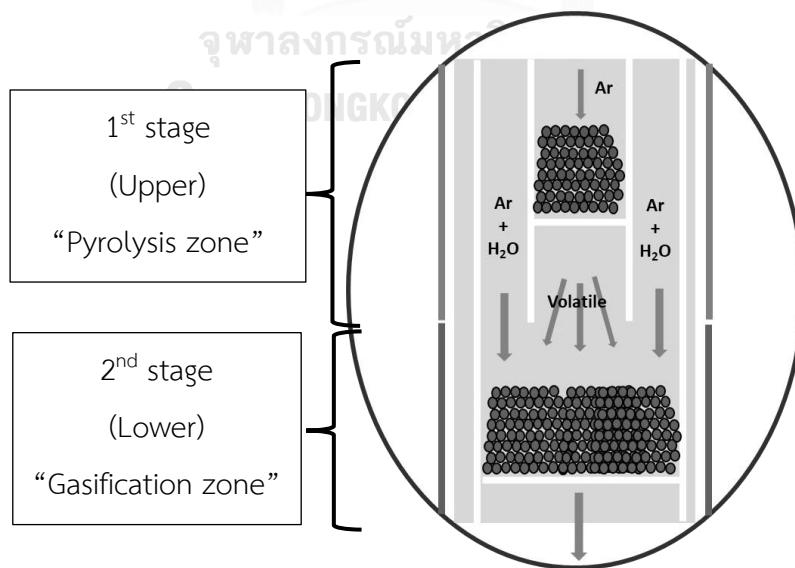


Figure 3.2 Concept of a two-stage fixed bed reactor.

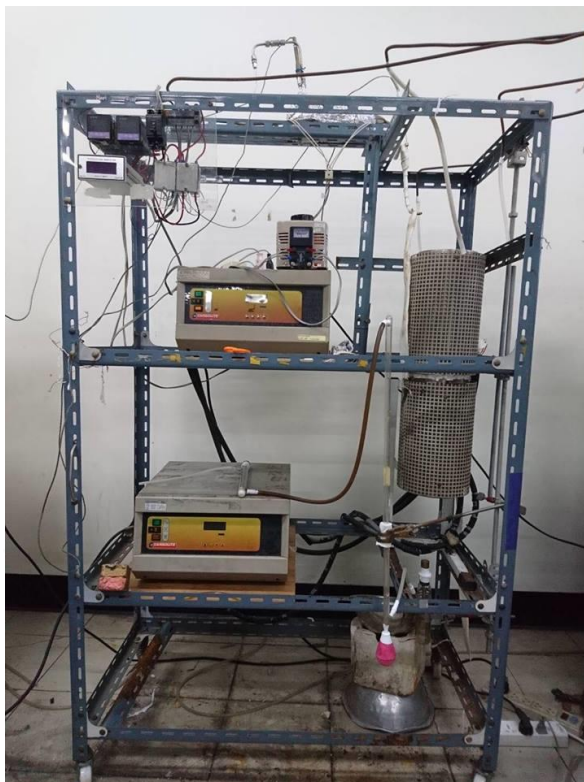


Figure 3.3 Photo of two-stage fixed bed reactor from laboratory

3.2 Experiment procedure

3.2.1 Biomass feedstock preparation

Sugarcane leaves, which are a widespread agricultural waste in Thailand, with particle sizes ranging from 250–300 μm were employed as the biomass feedstock in this study. The biomass feedstock was oven-dried at 110 °C for 24 h. to remove the effect of moisture content, and then stored in a desiccator before using in experimental section.

3.2.2 Catalyst and sorbent preparation

Three catalyst and sorbent preparations were used in this study. The prepared catalyst and sorbent were synthesized by using the dry/wet physical mixing and co-precipitation and the excess solution (wet) impregnation method. The detail of each method was explained as follow.

3.2.2.1 Physical mixing method

Commercial CaO and MgO with particle sizes 500 μm were calcined at 850 $^{\circ}\text{C}$ for 3 h. The CaO/MgO mixed sorbents were physically mixed by either dry or wet mixing.

For the dry mixing, CaO and MgO were mixed together at the desired molar ratio. The mixed sorbent was blended using the shaker for 3 hrs and calcined at 850 $^{\circ}\text{C}$ before Prepared catalyst and sorbent designated as “DM X:Y”, where X and Y are the molar ratios of CaO and MgO, respectively. The process flow of dry physical mixing is shown in Figure 3.4.

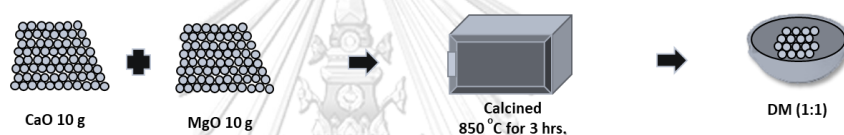


Figure 3.4 Dry-physical mixing method

For the wet mixed sorbents, the desired molar ratios of CaO and MgO were mixed in deionized water and stirred well using a magnetic bar. The mixed solution was dried at 105 $^{\circ}\text{C}$ for 24 h, and then calcined at 850 $^{\circ}\text{C}$ for 3 h and designated as “WM X:Y”, with the same designations for X and Y as above. For instance, WM 1:1 stands for the CaO/MgO sorbent prepared by wet mixing at a CaO: MgO molar ratio of 1:1. The process flow of dry physical mixing is shown in Figure 3.5.

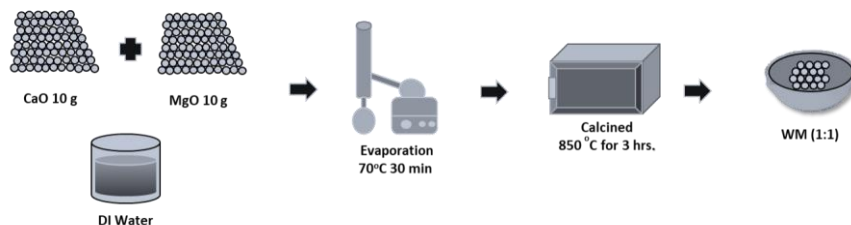


Figure 3.5 Wet-physical mixing method

3.2.2.2 Excess solution impregnation method.

The excess-solution impregnation method was used for doping the metal on the support. The example catalyst preparation is shown in Figure 3.6. First, the support (γ - Al_2O_3 and CaO/MgO) were calcined at desired calcination temperature for 3 h. Then the support was mixed with the solution of the first metal nitrate and evaporated at 70 °C before being calcined for 3 h. The procedure was then repeated sequentially for the second and third metal nitrates, respectively, using calcination temperatures of 650, 500 and 850 °C for the magnesium nitrate ($\text{Mg}(\text{NO}_3)_2 \cdot 6\text{H}_2\text{O}$), nickel nitrate ($\text{Ni}(\text{NO}_3)_2 \cdot 6\text{H}_2\text{O}$) and calcium nitrate ($\text{Ca}(\text{NO}_3)_2 \cdot 6\text{H}_2\text{O}$), respectively. The concentration of each metal nitrate solution was selected so as to 2 mol/L. The amount of each solution was calculated to provide the desired metal loading on the alumina support.

Each prepared catalyst/sorbent is hereafter named XYZ, where X was the first metal nitrate loaded, followed by Y and Z, respectively, omitting the Al_2O_3 support for brevity. The order of metal loading can be changed for studying the metal order to enhanced H_2 rich gas production in this study.

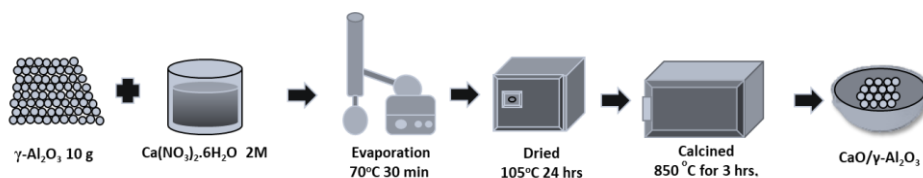


Figure 3.6 Excess solution impregnation method.

3.2.3 Activity test for biomass pyrolysis - gasification

The schematic diagram of the experimental apparatus is shown in Figure 3.1. Before the reactor was heated up, 8 g of mixed catalyst and inert material (inactive alumina) to maintain the bed height of 2 cm was added into the gasification zone. The reactor was purged with argon (Ar) gas at a total flow rate of 100 ml/min for 30 min. Then, both electric furnaces were heated up to the desired temperature pyrolysis and gasification zone. Meanwhile, the water was fed into the gasification zone with a HPLC pump at a volumetric flow rate of 0.14 ml/min so as to maintain the steam concentration at 60% (v/v). When the temperature reached the set point, 0.12 g of sugarcane leaves was dropped into the pyrolysis zone, whereupon the pyrolysis took place immediately. The released volatiles from the pyrolysis were transported by the Ar flow into the gasification zone, where the catalytic reaction with steam occurred. The tar and unreacted water were trapped in a cooler bottle containing isopropanol, while the gas products were collected using a gas bag. The amount of char and tar were defined as the solid residue in the reactor and the remaining tar in the trapped solution after evaporation.

3.2.4 Activity test for pyrolysis of biomass

The experimental setup is similar to the pyrolysis-gasification system. Only alumina ball (inactive alumina) was placed to maintain the bed height of 2 cm in the gasification zone. The Ar gas was purged into the reactor with the flow rate of 100 ml/min for 30 min. Then, both electric furnaces were heated up to the same temperature which was called the pyrolysis temperature. However, the pyrolysis study was not fed into the reactor. When the temperature reached the set point, the sugarcane leaves was dropped into the pyrolysis zone. The output materials were collected with the same process in the section 3.2.3.

3.2.5 Regeneration process of catalyst/sorbents

The used catalyst/sorbent were regenerated by using the calcination method. It was calcined with the calcination temperature of 850 °C for 3 h to confirm that all CaCO₃ phase was converted into the CaO phase by reverse carbonation reaction.

3.3 Data analysis

For the tar reduction study, the tar reduction is calculated by using the following equations to find the percentage of the tar reduction.

$$\% \text{Tar_reduction} = \left(\frac{X_{\text{catalyst}} - X_{\text{blank}}}{X_{\text{blank}}} \right) \times 100 \quad (3.1)$$

Where, X_{blank} = mass of tar without catalyst/sorbents

X_{catalyst} = mass of tar without catalyst/sorbents

For the carbon deposition which represents the coke formation on the catalyst/sorbents are given as

$$C_{\text{dep}} \text{ (wt.\%)} = \frac{m_c}{m_s} \times 100 \quad (3.2)$$

Where, m_c = mass of carbon deposition which is provided by using TGA result (The method was explained in section 4.3.3)

m_s = mass of used catalyst/sorbents

For the synergistic study, the experimental yields have to compare with the theoretical yield. The predicted yield ($Y_{\text{predicted}}$) was obtained by following equation to compare with the experimentally derived value.

$$Y_{\text{predicted}} = X_{\text{CaO}} \times Y_{\text{CaO}} + (1 - X_{\text{CaO}}) \times Y_{\text{MgO}} \quad (3.3)$$

where, X_{CaO} is the mass fraction of CaO in the mixing sorbent, and Y_{CaO} and

Y_{MgO} stand for the individual yield of pure CaO and MgO, respectively.

3.4 Characterization Method

3.4.1 Proximate and CHN Analysis

The proximate and ultimate analyses, in terms of the C, H and nitrogen (N) elemental compositions, of the biomass were performed following standard D3172-3175 using a CHN 2000 elemental analyzer (Figure 3.7). The oxygen (O) element was computed by the mass difference. The low heating value was analyzed using a bomb calorimeter.

3.4.2 Gas chromatography with thermal conductivity detector (GC-TCD).

The gas product (mainly H_2 , CO , CH_4 and CO_2) from the TFBR was analyzed by gas chromatography (Shimadzu GC-2014) with a thermal conductivity detector (TCD) using Unibeads C column (3.00 mm ID \times 2000 mm length). The conditions were used for gas analysis as shown in Table 3.1.

Table 3.1 Condition of GC-TCD

	Conditions
Carrier gas	Ar
Column type	Unibeads C column
Injector temperature ($^{\circ}C$)	120
Column temperature ($^{\circ}C$)	60 for 2 min and 120 for 9 min
Detector type	TCD
Detector temperature ($^{\circ}C$)	180

3.4.3 CO_2 adsorption capacity

The CO_2 capture (adsorption) capacity was examined in a fixed bed reactor (Figure 3.1). For this, 1 g of catalyst and sorbent were placed inside the reactor. Argon (Ar) and CO_2 were fed through it at a flow rate of 100 mL/min

and 0.05 mL/min, respectively. The furnace was heated up to a desired temperature (similar to in the gasification zone). The outlet gas was collected periodically by a gas bag and analyzed by GC-TCD. The breakthrough curve was obtained from the CO₂ outlet concentration and the amount of CO₂ capture capacity was determined by integrating the area under the curve.

3.4.4 Gas chromatography with mass spectrometry (GC-MS)

The chemical composition of condensed volatile in the tar trap was analyzed by using a GC-MS (a Varian Model Saturn 2200 equipped with a capillary column, 0.25 mm-OD × 0.25 mm-film thickness × 30 m-length, DB-5ms, J&W Scientific) with helium (He) as the carrier gas. The molecular weight scan range was 50-650 m/z with a 5 min of solvent cut time. The column was held at 50 °C for 3 min, and then the temperature was increased to 220 °C at heating rate of 20 °C/min and held for 40 min.

3.4.5 X-ray fluorescence (XRF)

The catalyst and sorbent were characterized the amount of chemical composition using XRF technique (Philips model PW2400). The elements are consisting of Ni, Mg, Ca, and Al₂O₃ was calculated by the theoretical formulas “fundamental parameter calculations” method.

3.4.6 X-ray Powder Diffraction (XRD)

The fresh and used catalysts and sorbents were analyzed by XRD using a Philips X'pert diffraction-meter with Cu K α (λ = 0.154 nm) generated at 40 kV and 20 mA.

3.4.7 Brunauer-Emmit-Teller (BET) analysis.

The specific surface area, pore volume and pore size of the prepared catalyst and sorbent were measured by N₂ adsorption at -196 °C using Brunauer-Emmit-Teller, BET method (model Quantachrome, Autosorb-1 MP) by degassing of sample before adsorption at 300 °C for 6 h.

3.4.8 Scanning electron microscopy with energy dispersive X-ray spectroscopy (SEM/EDX)

The morphology of produced chars was also characterized by Scanning electron microscopy with energy dispersive X-ray spectroscopy (SEM, model JEOL, JSM-5410V) method.



CHAPTER 4

NiMgCa/ γ -Al₂O₃ CATALYST/SORBENTS DURING THE PYROLYSIS-STEAM GASIFICATION OF SUGARCANE LEAVES

In this chapter, the pyrolysis-steam gasification of sugarcane leaves was investigated with the NiMgCa/ γ -Al₂O₃ which was prepared using the excess solution impregnation method. The experimental was carried out in a drop-tube two-stage fixed bed reactor (TFBR) as described in Chapter 3. The results are divided into six aspects; (I) the characteristics of sugarcane leaves, (II) catalyst characterization, (III) the metal loading content (IV) the order of metal loading, (V) the optimal condition of catalyst/sorbents and (VI) role of CaO and MgO. In section 4.1, the proximate analysis, ultimate analysis and the gross heating value (GHV) were reported. In the section 4.2, the fresh catalyst/sorbents characterization was performed using XRF, XRD, and BET. In the section 4.3 to 4.6, the effects of metal loading content, the order of metal loading content, the catalyst/sorbents to biomass mass ratio and the regeneration of catalyst/sorbents and the role of MgO content on H₂ production were examined at different gasification temperatures.

4.1 Chemical characteristics of sugarcane leaves.

Proximate, ultimate analysis and gross heating value of sugarcane leaves of sugarcane leaves are summarized in Table 4.1. The sugarcane leaves have high value of the volatile component and oxygen element. It can be explained by the molecular structure and thermal behavior of sugarcane leaves. The sugarcane leaves are the representative of lignocellulosic material which contains cellulose, hemicellulose and lignin. Cellulose and hemicellulose are mainly decomposed to the volatiles, including

condensable and non-condensable volatile, over the range of temperature between 200 to 500 °C [83].

Table 4.1 Proximate and elemental analysis of the sugarcane leaves.

Proximate analysis (wt.%, as received)			
Moisture	Volatile	Fixed carbon	Ash
10.0±0.7	69.5±0.9	12.9±0.4	7.6±0.5
Elemental analysis (wt.%, daf ¹)			
Carbon	Hydrogen	Nitrogen	Oxygen ²
51.8±0.5	9.3±0.6	0.9±0.1	38.0±0.4
GHV (MJ/kg)		16.8	

¹ Dry ash free basis.

² Calculated by mass difference.

The biomass properties are also related to the thermogravimetric analysis (TGA) as shown in Figure 4.1. It was found that the thermal degradation could be divided into four stages. The first stage is a dehydration stage of materials in a temperature range of 35 to 190 °C. In this stage the moisture in biomass was removed with a small decrease of weight loss [84]. The second stage is an active pyrolysis at about 190 to 350 °C. During this stage, initiation of carbonization was observed and the mass loss at the end of the stage was approximately 70 wt%. The mass loss was mainly volatile matter [85]. The third stage is a passive pyrolysis in the range of 350 to 540 °C. The mass was loosed by the decomposition of lignin and fixed carbon [86]. At the final stage, the complete combustion occurred giving the ash remained about 8 wt.% at the temperature above 540 °C with the presence of air.

The result indicated that the pyrolysis-gasification of sugarcane leaves in this study was mainly considered for the steam reforming of derived volatile because of high volatile component. Therefore, the two-stage reactor was employed in this work, as mentioned in the experimental section.

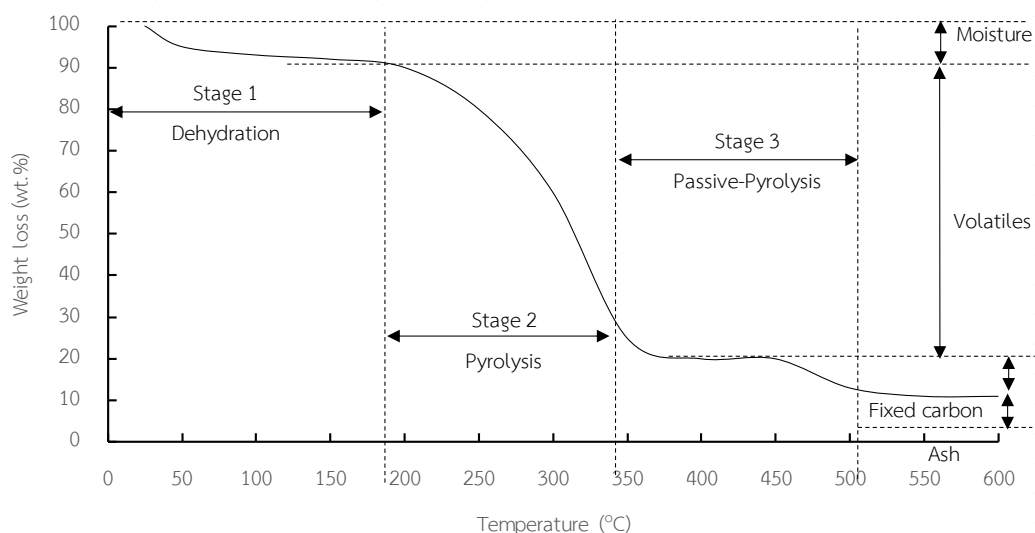


Figure 4.1 The thermogravimetric analysis of sugarcane leaves.

4.2 Catalyst/sorbents characterization.

The fresh catalyst/sorbents characterization was composed of two parts: (i) the element analysis using XRF to confirm the amount of metal loading on the surface catalyst/sorbents and (ii) the phases analysis using the XRD to expose the synthesized forms of prepared catalyst/sorbents.

4.2.1 The element analysis of prepared catalysts/sorbent using XRF

The nomenclature of the catalyst/sorbents prepared under different conditions and their total element composition analyzed using XRF technique are listed in Table 4.2. The metal content of all catalyst/sorbents was close to the desired values.

An astonishing result was found when the catalyst/sorbents were prepared using different order of metal loading, i.e. Ca5Mg5Ni10, Ni10Mg5Ca5

and Mg5NiO10Ca5. The CaO content was ranked in order of Mg5Ni10Ca5 > Ni10Mg5Ca5 > Ca5Mg5Ni10. Furthermore, the highest content of the MgO was observed in the Ni10Mg5Ca5 catalyst/sorbents up to 5.95 wt.%, which is higher than the desired value as well as the other sequential loading. In the case of NiO, the loading content was ordered from high to low value with Ca5Mg5Ni10 > Mg5Ni10Ca5 > Ca5Mg5Ni10. Although three different order of metal loading had the similar desired value of metal doping, the various of element composition was found. It might be due to that the amount of doping metal was lost during the preparation process.

4.2.2 The phases analysis of prepared catalysts/sorbent using XRD

The XRD pattern of fresh the catalyst/sorbent was discussed in this section. Figure 4.2 shows the XRD pattern of NiO/ γ -Al₂O₃ catalyst with different NiO loading content. It was found that the fresh sample of NiO/ γ -Al₂O₃ showed NiO, NiAl₂O₄ and the γ -Al₂O₃ phases at the 2θ of 37.4, 43.5 and 66.6, respectively. An increase in the NiO loading content from 3 wt.% (Ca0Mg0Ni3) to 5 wt.% (Ca0Mg0Ni5) provided higher value of the NiO intensity peak. When the NiO loading content was increased to 10 wt.% (Ca0Mg0Ni10), the complex compound phases (NiAl₂O₄) was found. The higher NiO loading content up to 15 wt.% had not gave the change in NiO intensity peak but the intensity peak of NiAl₂O₄ phase increased. The results are in good agreement with previous work [87]. The NiAl₂O₄, which is the complex compound between NiO and γ -Al₂O₃, is an inactive phase for the catalytic steam reforming. Thus, the NiO loading content loading over 10 wt.% might provide lower activity of H₂ production from pyrolysis-gasification of sugarcane leaves.

Table 4.2 Elemental analysis of prepared catalyst/sorbents using XRF with different loading contents

No	Sample Name	Desired content (wt.%)			Elemental analysis (wt%)		
		Ca	Mg	Ni	Ca	Mg	Ni
1	Ca0Mg0Ni0	-	-	-	-	-	-
2	Ca0Mg0Ni3	-	-	3	-	-	2.71
3	Ca0Mg0Ni5	-	-	5	-	-	4.86
4	Ca0Mg0Ni10	-	-	10	-	-	9.84
5	Ca0Mg0Ni15	-	-	15	-	-	13.9
6	Ca5Mg0Ni10	5	-	10	4.84	-	9.31
7	Ca5Mg3Ni10	5	3	10	4.93	2.96	9.36
8	Ca5Mg5Ni10	5	5	10	4.91	4.95	9.74
9	Ca5Mg10Ni10	5	10	10	4.82	9.46	9.41
10	Ca5Mg15Ni10	5	15	10	4.86	14.3	9.38
11	Ca0Mg5Ni10	-	5	10	-	4.91	9.69
12	Ca3Mg5Ni10	3	5	10	2.84	4.46	9.42
13	Ca5Mg5Ni10	5	5	10	4.91	4.95	9.78
14	Ca10Mg5Ni10	10	5	10	9.36	4.89	9.71
15	Ca15Mg5Ni10	15	5	10	14.1	4.92	9.69
16	Ca5Mg5Ni10	5	5	10	4.91	4.95	9.81
17	Ni10Mg5Ca5	5	5	10	5.04	5.95	8.12
18	Mg5NiO10Ca5	5	5	10	5.37	5.14	9.11

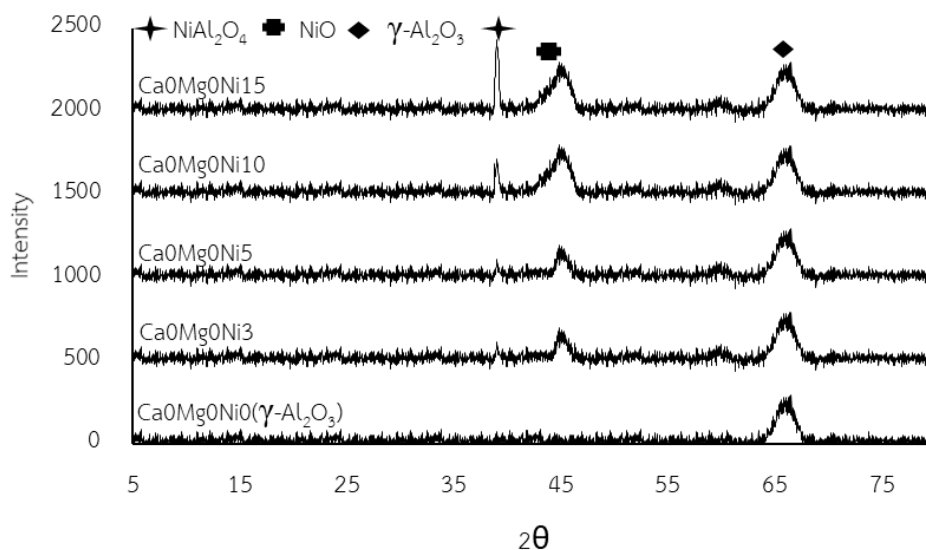


Figure 4.2 XRD pattern of fresh NiO/ γ -Al₂O₃ catalysts with different NiO loading content

The XRD pattern of CaXMg5Ni10 catalyst/sorbents with different CaO loading (X= 0 – 15 wt.%) was shown in Figure 4.3. It was observed that the fresh sample displayed the CaO, MgO, NiO, CaAl₂O₄, MgAl₂O₄ and NiAl₂O₄ phases. The intensity peak of CaO phase had direct variation with the CaO loading contents which would be the most important phases for the sorption enhanced H₂ production (SEHP). However, increasing the CaO loading content up to 5 wt.% (Ca5Mg5Ni10) showed the formation of CaAl₂O₄ phase. The further rising of the CaO loading content from 5 to 15 wt.% provided higher the intensity peak of CaAl₂O₄ phase. Therefore, the CaO loading contents over 5 wt.% might decrease the CO₂ adsorption efficiency and decrease the efficiency of SEHP.

The phases analysis of Ca5MgXNi10 catalyst/sorbents with different MgO loading content (X = 0-15 wt.%) is shown in Figure 4.4. It was found that the fresh sample of Ca5MgXNi10 catalyst/sorbents provided the CaO, MgO, NiO, CaAl₂O₄, MgAl₂O₄ and NiAl₂O₄ phases. Nonetheless, the 2θ position of NiO

phase had the close value to MgO phase in XRD pattern. The main intensity peak of NiO or MgO has remained steady because the NiO content which was fixed value at 10 wt.% on γ -Al₂O₃ had higher amount than the MgO content (3, 5 and 10 wt.%) which was the variable in this study. When the MgO content was increased from 3 to 5wt.% (Ca5Mg5Ni10), the MgAl₂O₄ phase occurred. The further rising of the MgO loading content from 5 to 15 wt.% gave higher intensity peak of the MgAl₂O₄ phase. Guo *et al.* [88] reported that the MgAl₂O₄ which was the complex compound phase between MgO and γ -Al₂O₃ had high thermal stability for the catalytic in the oxidation reaction. These indicate that the increasing of the MgO content might play a role as the effective promoter in the SEHP form pyrolysis-gasification.

The XRD patterns of fresh catalyst/sorbents with different order of metal loading are displayed in Figure 4.5. The Ni10Mg5Ca5 catalyst/sorbents had the lowest MgAl₂O₄ intensity and the highest NiAl₂O₄ intensity compared to the other two catalyst/sorbents (Mg5Ni10Ca5 and Ca5Mg5Ni10). This is because the doping of NiO before MgO onto the γ -Al₂O₃ induces the formation of the NiAl₂O₄ phase, which is less catalytic activity for gas production than the NiO phase [89]. However, doping MgO before NiO onto the γ -Al₂O₃ (Ca5Mg5Ni10 and Mg5Ni10Ca5 catalyst/sorbents) led to the formation of the MgAl₂O₄ phase and so decreased the MgO phase, which can hinder the interaction between NiO and γ -Al₂O₃ to form the NiAl₂O₄ phase. Furthermore, the intensity of the CaAl₂O₄ phase was ranked in the order Ca5Mg5Ni10 > Ni10Mg5Ca5 > Mg5Ni10Ca5 catalyst/sorbents. Huang *et al.* reported that the complex compound phase between CaO and other metals, such as Ca₂Fe₂O₅ and CaAl₂O₄, are inactive phases for CO₂ sorption because they decrease the portion

of CaO phase. [90] Thus, Mg5Ni10Ca5 catalyst/sorbents is expected to provide the best SEHP.

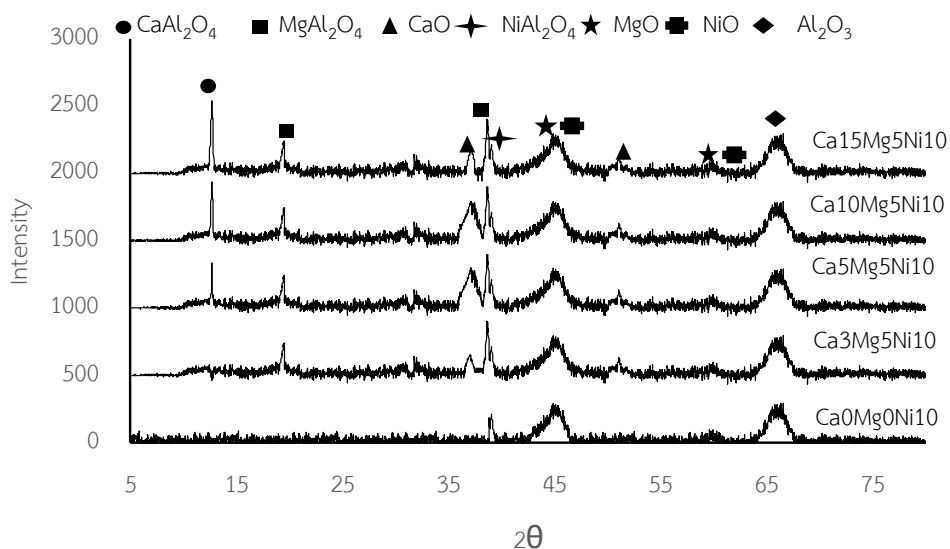


Figure 4.3 XRD pattern of fresh CaXMg5Ni10 catalyst/sorbents with different CaO (X = 0 – 15 wt.%) loading contents.

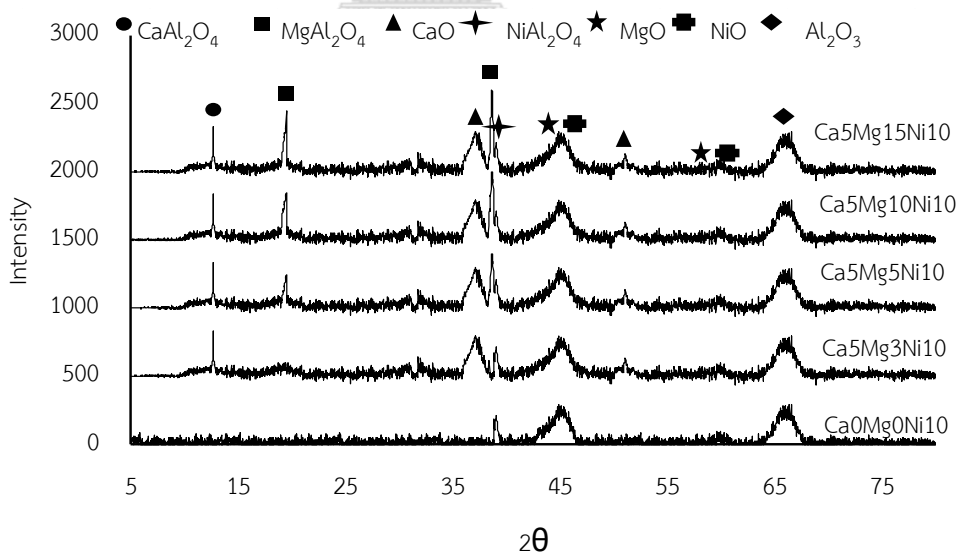


Figure 4.4 XRD pattern of fresh Ca5MgXNi10 catalyst/sorbents with different MgO (X = 0 – 15 wt.%) loading contents

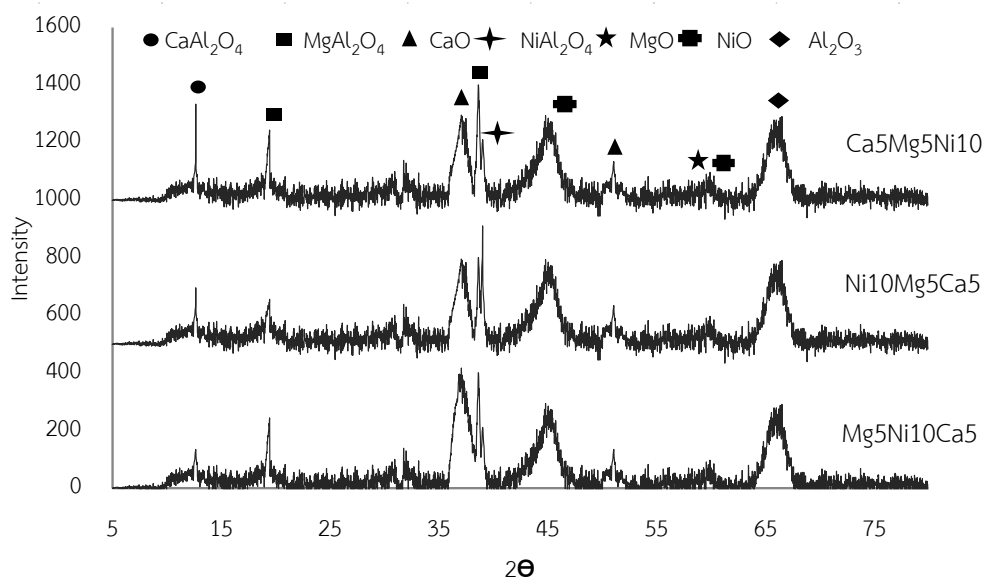


Figure 4.5 XRD pattern of fresh catalyst/sorbent with different order of metal loading.

4.3 Effects of metal loading content of metals on the H₂ production from pyrolysis-gasification of sugarcane leaves

This section focused on evaluating effects of metal loading content on gas yield and composition. Three loading metals, including NiO, MgO and CaO, were examined for the H₂ rich gas production from the pyrolysis-gasification of sugarcane leaves. Herein, the temperatures of pyrolysis and gasification zone were both fixed at 600 °C.

4.3.1 Effect of NiO loading content

The effect of the NiO loading content on γ -Al₂O₃ on the gas yield and composition is shown in Figure 4.6. The addition of NiO/ γ -Al₂O₃ catalyst increased overall gas production. Increasing the NiO loading content from 3 to 5 wt.% provided higher H₂, CO and CO₂ but gave the significant drop in CH₄ yield.

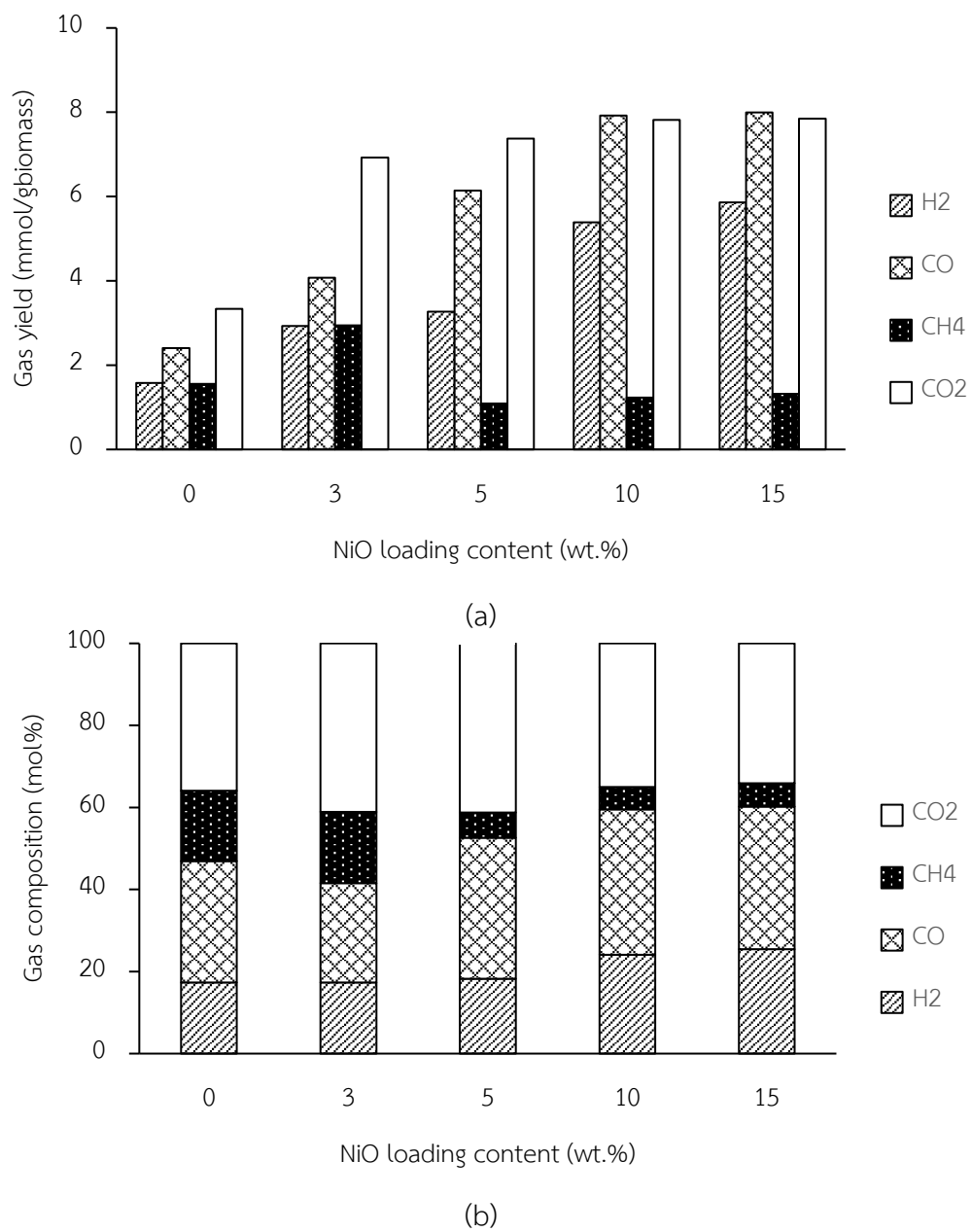


Figure 4.6 Effect of NiO loading content (CaO/MgO/NiO-15) on the (a) gas yield and (b) gas compositions from pyrolysis-gasification of sugarcane leaves.

This can be attributed that the NiO/ γ -Al₂O₃ plays a catalytic role in the steam reforming of the CH₄ to produced H₂ and CO [91-93]. The further increasing of the NiO loading content from 10 to 15 wt.% provided a slightly increase in H₂, CO and CO₂ yield. The trend of gas concentration with increasing of the NiO loading content was related to the gas yield results. This finding was related to the phases analysis of the fresh catalyst/sorbents (section 4.2.2). Increasing the NiO loading content up to 15 wt.% cannot provide higher of NiO but the NiAl₂O₄, which was the inactive phase increased. Therefore, the 10 wt.% NiO on γ -Al₂O₃ is the most suitable catalyst for the pyrolysis-gasification of the sugarcane leaves.

4.3.2 Effect of CaO loading content

The effect of the CaO loading content on the gas yield and composition are shown in Figure 4.7. It was found that the yield and concentration of H₂ were dramatically increased but the CO and CO₂ yield were decreased with the addition of CaO into the catalyst/sorbents. The increasing of CaO loading content from 3 to 5 wt.% provided higher yield and concentration of H₂ up to 20.7 mmol/g_{biomass} and 49.1 %, respectively. The lower yield and concentration of CO₂ (2.54 mmol/g_{biomass}, 9.4%) were also observed at the CaO loading content of 5wt.%. These results were agreed with the previous works [94, 95]. CaO can react with CO₂ produced during the pyrolysis-gasification of sugarcane leaves and convert into CaCO₃ through the carbonation reaction as following:



When the amount of CO₂ in the pyrolysis-gasification of sugarcane leaves decreased, it can shift the thermodynamic equilibrium of water-gas shift reaction, Eq. 4.2 to produce more yield and concentration of H₂.



However, the further increase in CaO loading content from 5 to 15 wt.% provided lower yield and concentration of H₂ while the yield and concentration of CO and CO₂ were also decreased. The catalyst/sorbents with the CaO loading content over 5 wt.% formed the CaAl₂O₄ phase which is the inactive phase for carbonation reaction as mentioned in section 4.2.2.

The CO₂ adsorption capacity of the catalyst/sorbents with different CaO loading content are listed in Table 4.3. The Ca0Mg5Ni10 catalyst/sorbent gave no CO₂ adsorption capacity. The change in the CaO loading content from 3 to 5 wt.% increased the CO₂ adsorption capacity from 7.7 to 9.8 mmol/g_{catalyst/sorbent}. The further increasing of CaO loading content over 5 wt.% showed lower CO₂ adsorption capacity. This finding is related with the gas yield and composition which were discussed above.

The XRD pattern of used catalyst/sorbents with different CaO loading content are shown in Figure 4.8. The major characteristic peak of CaCO₃ at angles 2θ of 25.7 was found in used catalyst/sorbents. Increasing the CaO loading content from 3 wt.% to 5 wt.% provided higher intensity peak of CaCO₃ phases. This result would be relevant to the CO₂ adsorption by carbonation reaction of CaO. However, the intensity of CaCO₃ became disappeared with increasing the CaO content from 5 wt.% to 15 wt.%. The high CaO loading could induce the formation of CaAl₂O₄ phase, as can be seen from the obvious peak of CaAl₂O₄ phase, reducing the CO₂ adsorption capacity.

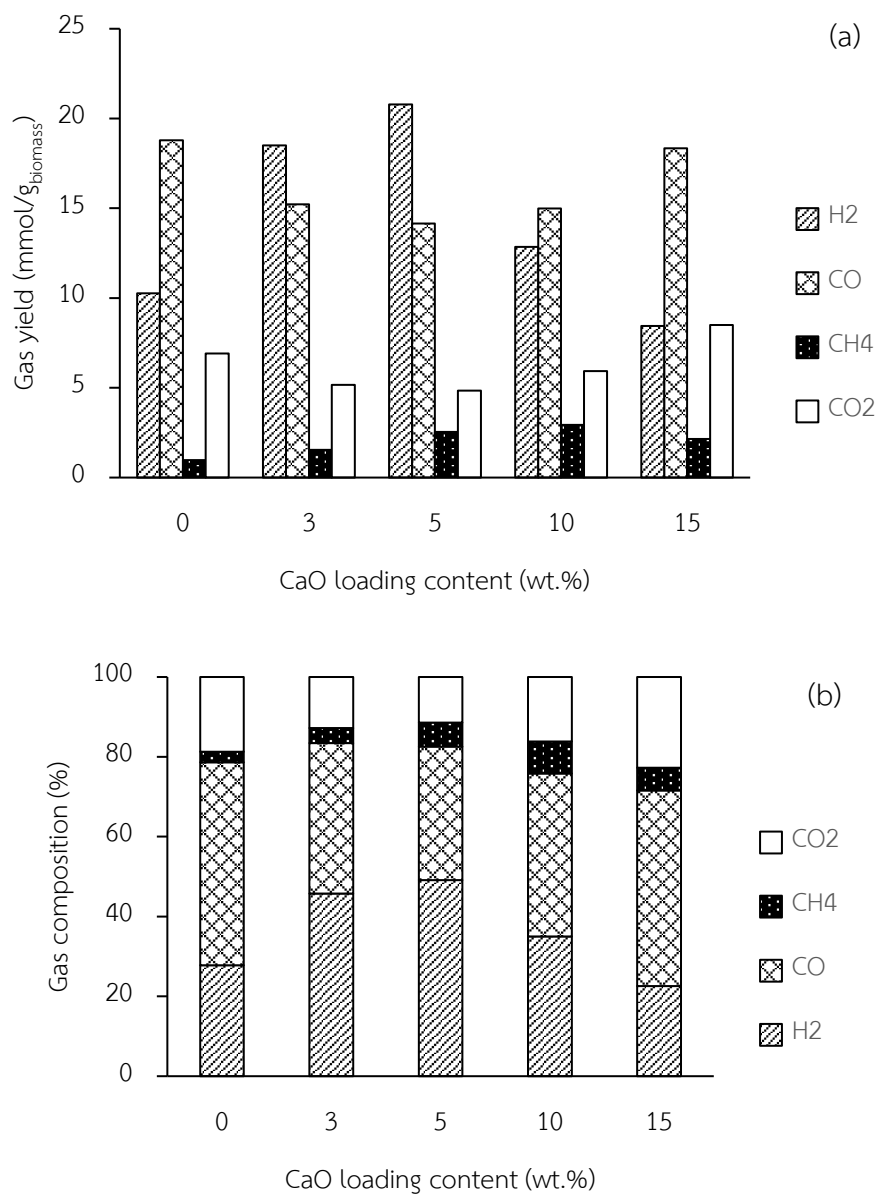


Figure 4.7 Effect of CaO loading content on the (a) gas yield and (b) gas composition from pyrolysis-gasification of sugarcane leaves.

Table 4.3 CO₂ sorption capacity of the fresh CaMgNi catalyst/sorbents with different CaO loading content

Sorption temperature (°C)	Catalyst/sorbent	CO ₂ sorption capacity (mmol·g _{catalyst} ⁻¹)
600	Ca0Mg5Ni10	0
	Ca3Mg5Ni10	7.7±0.3
	Ca5Mg5Ni10	9.8±0.1
	Ca10Mg5Ni10	6.4±0.4
	Ca15Mg5Ni10	4.3±0.3

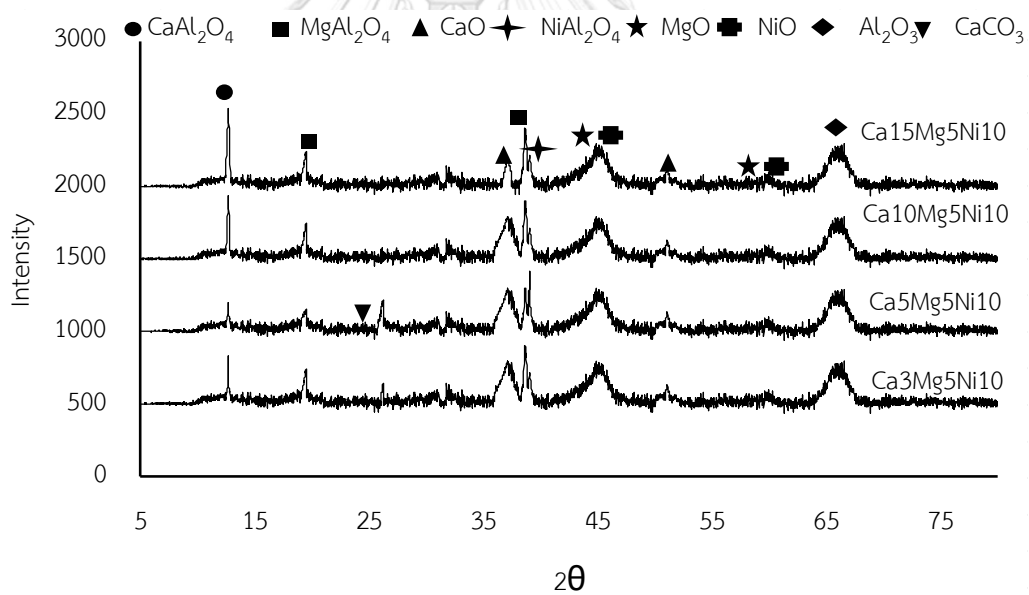


Figure 4.8 XRD pattern of used catalyst/sorbents with different CaO loading contents.

4.3.3 Effect of MgO loading content

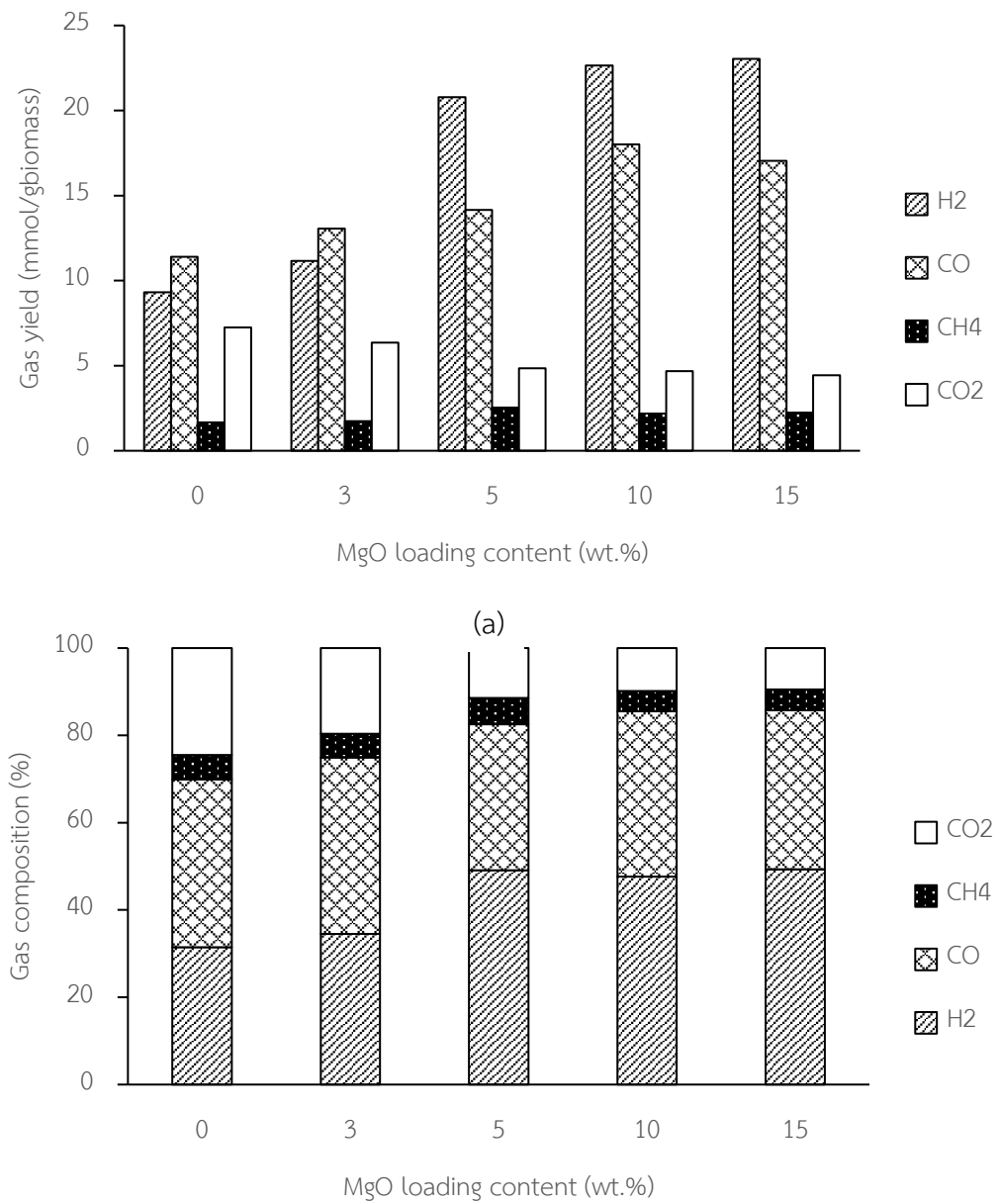
The effect of MgO loading content on the gas yield and composition are shown in Figure 4.9. The presence of 3 wt.% MgO in the Ca₅Mg₃Ni₁₀ catalyst/sorbents contributed to a slightly positive effect on gas yield and H₂ concentration. This indicated that the MgO loading content 3 wt.% might be insufficient for the catalytic pyrolysis-gasification. This is attributable to that low MgO content on catalyst has almost no influence on the gas yield [96]. The increase in MgO loading content from 3 to 5 wt.% led to the higher yield and concentration of H₂ and the lower yield and concentration of CO₂. These results were relevant to the coke deposition and tar conversion. The carbon deposition of used catalyst/sorbents was calculated by the mass difference during the combustion step in TGA analysis under air condition. The temperature range was from 200 to 650 °C with a heating rate of 20 °C/min. The calculation method for coke deposition (%C_{dep}) was provided in the section 3.3. The effect of the MgO loading content on carbon deposition of used catalyst/sorbents are shown in Figure 4.10. The results showed that the catalyst/sorbents with MgO loading content of 3 wt.% gave slightly lower carbon deposition than the catalyst/sorbents that with no MgO content. The changing of MgO loading content from 3 wt.% to 5 wt.% rendered lower percentage of carbon deposition around 28 wt.%. The further increasing of the MgO loading content over 5 wt.% made no significant reduction of the carbon deposition. Hence, this specific amount of MgO (5wt.%) might be suitable to help promote the SEHP because the MgO can hinder the deactivation of CaO species including coke formation and agglomeration [88]. Lis *et al.* reported that MgO addition causes the coke more easily oxidized, leading to an increase in the steam-carbon reaction, and consequently less carbon deposition [97]. Furthermore, tar conversion increased with increasing the MgO loading content up to 5wt.%

and the remained unchanged with raising MgO content over 5 wt.%. The addition of MgO with specific content of 5 wt.% was also effective for tar steam reforming which contributes to more H₂ yield as discussed before [98].

The further increase in MgO from 5 wt.% to 15 wt.% resulted in the slightly higher H₂ and CO yield and the rather lower yield of CO₂ (Figure 4.9). The results indicated that the addition of MgO provided the catalytic effect of the Boudouard reaction (Eq. 4.3) and water gas reaction (Eq. 4.4) to produce more H₂ and CO yield as following:



Moreover, the gas composition was remained unchanged with the addition of MgO over 5wt.%. This can be explained by that the excess MgO loading could provide an ample opportunity for the formation of MgAl₂O₄ phases. Such a complex form of MgO-Al₂O₃ can increase the thermal stability of the catalyst/sorbents but it had no significant effect on gas composition from the pyrolysis-gasification of sugarcane leaves [88].



(b)
Figure 4.9 Effect of MgO loading content on the (a) gas yield and (b) gas concentration from pyrolysis-gasification of sugarcane leaves.

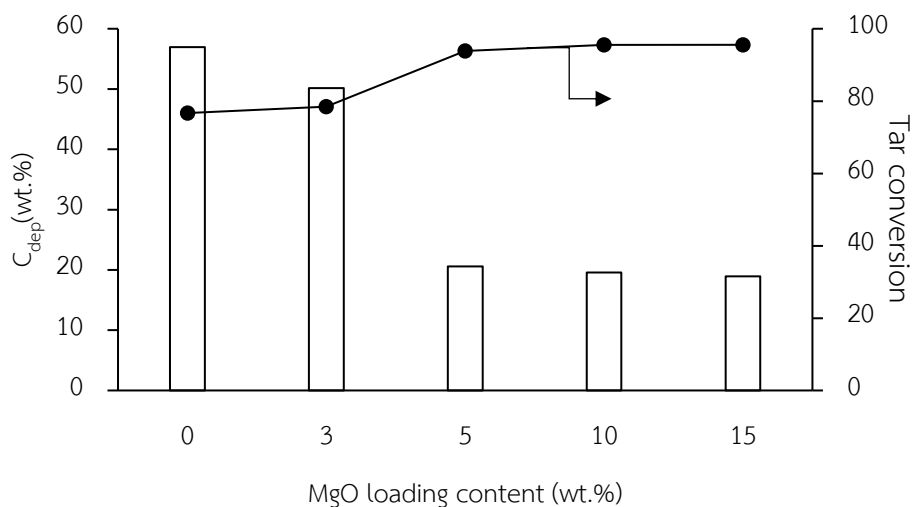


Figure 4.10 Effect of MgO loading content on the carbon deposition of used catalyst/sorbents, and tar conversion.

4.4 The order of metal loading study on H_2 production from pyrolysis-gasification of sugarcane leaves

The order of metal loading is an important factor in the performance of multi-metallic catalysts. Hence, three types of catalyst/sorbents including Ca5Mg5Ni10, Ni10Mg5Ca5 and Mg5Ni10Ca5 catalyst/sorbents, which were prepared by using excess-solution impregnation followed by calcination, were examined for the H_2 rich gas production from the pyrolysis-gasification of sugarcane leaves with two different gasification temperatures (600 and 800 °C). Here, the pyrolysis temperature remained constant at 600 °C.

4.4.1 Effect of metal loading sequence on H₂ production with catalyst/sorbent addition at low gasification temperature (600°C)

Figure 4.11 shows the gas composition and H₂ yield from the pyrolysis-steam gasification at 600 °C for the three catalyst/sorbents. It was found that the order of metal loading clearly had a significant effect on the obtained gas composition and H₂ yield. The Mg5Ni10Ca5 catalyst/sorbent gave the highest H₂ yield and concentration of 28.0 mmol/g_{biomass} and 68.7%, respectively while the yield and concentration of CO₂ were the lowest at 1.26 mmol/g_{biomass} and 5.51%, respectively. On the other hand, the Ni10Mg5Ca5 and Ca5Mg5Ni10 catalyst/sorbents gave a lower yield and concentration of H₂ but the concentration of CO₂ and CO was higher value. This is because the Mg5Ni10Ca5 catalyst/sorbents had the highest CaO phase as reported in section 4.2.2 (Figure 4.5). It contributes to the reduction in the CO₂ concentration and consequently shifts the thermodynamic equilibrium of the WGS reaction, as Eq. (4.2), leading to a higher CO conversion level and H₂ yield,

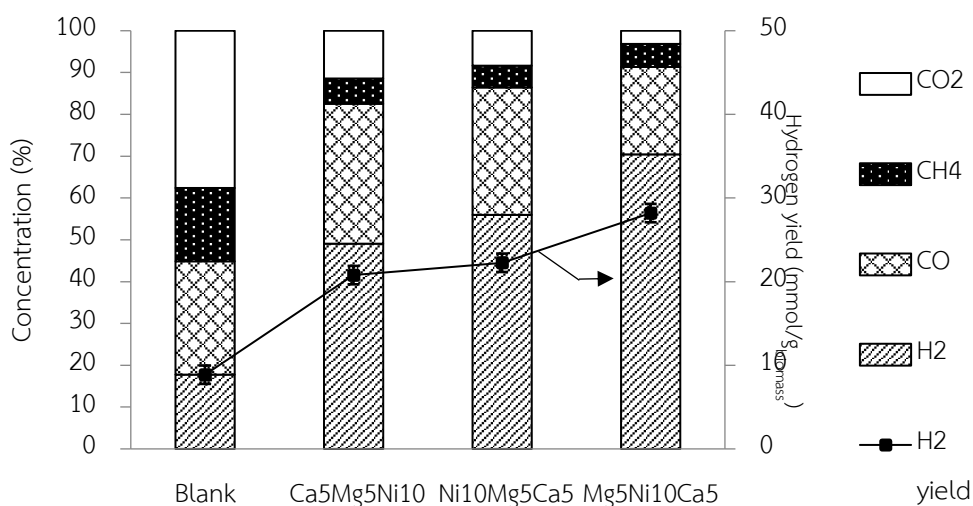


Figure 4.11 Effect of the metal salt loading sequence on the subsequent gas distribution and H₂ yield at the gasification temperature of 600 °C.

In comparing between the Ni10Mg5Ca5 and Ca5Mg5Ni10 catalyst/sorbents, the former provided a higher H₂ yield and lower CO and CO₂ concentrations than the latter, even though it had a lower MgAl₂O₄ and NiO phase, which effects the catalytic gasification (tar cracking and reforming reaction). However, more obvious CaO phase in the Ni10Mg5Ca5 catalyst/sorbents could promote SEHP, especially at the relatively low gasification temperature (600 °C). This is because both the carbonation, Eq. (4.1) and WGS reaction, (Eq. 4.2) are exothermic. Moreover, the mixed oxide between NiO and MgO had a high reduction temperature, being in the range of 638–916 °C, and the catalyst would be less reactive at the relatively low temperature of 600 °C[99]. The concentration of CH₄ did not significantly change with the different catalyst/sorbents and also the metal loading order. The variation of the CaO content due to the different order of metal loading had no significant effect on the steam reforming of CH₄. It is attributable to that CaO exhibits no obvious enhancement of the steam gasification of small molecular hydrocarbons [100].

These results are directly related to the CO₂ breakthroughs curve as shown in Figure 4.12 and the CO₂ adsorption capacity values are summarized in Table 4.4. The CO₂ adsorption capacity with different order of metal loading at the gasification temperature of 600 °C showed clearly different value. The Mg5Ni10Ca5 catalyst/sorbents which had the highest of the intensity peak of CaO phases showed the highest CO₂ sorption capacity up to 12.7 mmol/g_{sorbent} and the lowest of CO₂ sorption capacity down to 9.8 mmol/g_{sorbent} was observed at the Ca5Mg5Ni10 catalyst/sorbents. The results indicated that the catalyst/sorbents with high CO₂ adsorption capacity could provide high efficiency for SEHP from pyrolysis-gasification of sugarcane leaves.

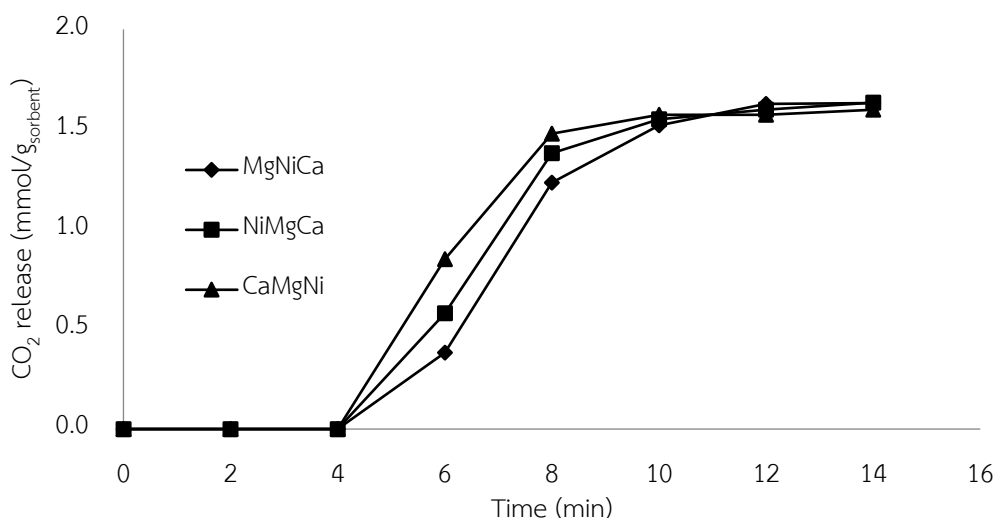


Figure 4.12 Breakthrough curves of the different fresh catalyst/sorbents at a gasification reaction temperature of 600 °C.

Table 4.4 CO₂ sorption capacity of the fresh catalyst/sorbents.

Sorption temperature (°C)	Catalyst/sorbent	CO ₂ sorption capacity (mmol/g _{catalyst})
600	CaMgNi	9.8±0.3
	NiMgCa	11.0±0.2
	MgNiCa	12.7±0.1

The SEHP in pyrolysis-gasification of sugarcane leaves with catalyst/sorbents were confirmed by using the XRD pattern of used catalyst/sorbents after gasification at 600 °C as illustrated in Figure 4.13. The intensity of the CaCO₃ phase, shown at 2θ of 26.2 and 33.2, became prominent in the used Mg₅Ni₁₀Ca₅ catalyst/sorbents, which gave the highest H₂ yield. Therefore, it surmises that the CaO phase in the prepared catalyst/sorbents is the important factor for shifting thermodynamic equilibrium of the WGS reaction associated with the carbonation reaction to enhance H₂ production.

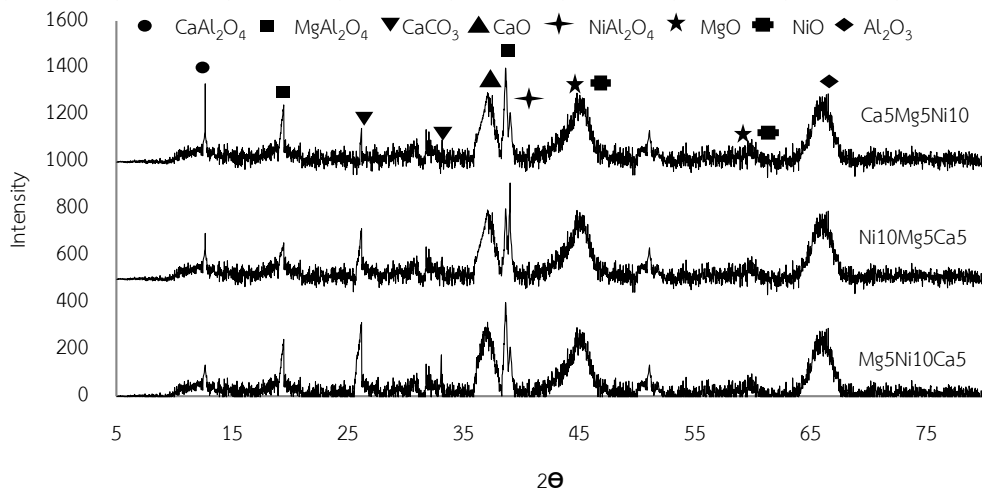


Figure 4.13 XRD patterns of the used catalyst/sorbent (a) Ca₅Mg₅Ni₁₀, (b) Ni₁₀Mg₅Ca₅ (c) Mg₅Ni₁₀Ca₅ at the gasification temperature of 600 °C.

The schematic for SEHP in pyrolysis-gasification of the sugarcane leaves using Mg₅Ni₁₀Ca₅ catalyst/sorbents mechanism is shown in Figure 4.14. Firstly, the volatile from the pyrolysis stage of sugarcane leaves was introduced into the gasification stage, where the reaction with steam in Mg₅Ni₁₀Ca₅ catalyst/sorbents occurs. The NiO phase catalyzes the gasification of the sugarcane leaves producing the gaseous product including H₂, CO, CO₂ and CH₄. The produced CO can be reacted with H₂O producing H₂ and CO₂ by the WGS reaction Eq. (4.2). The produced CO₂ can be adsorbed by CaO and converted into CaCO₃. Consequently, the thermodynamic equilibrium of WGS reaction to produce more H₂.

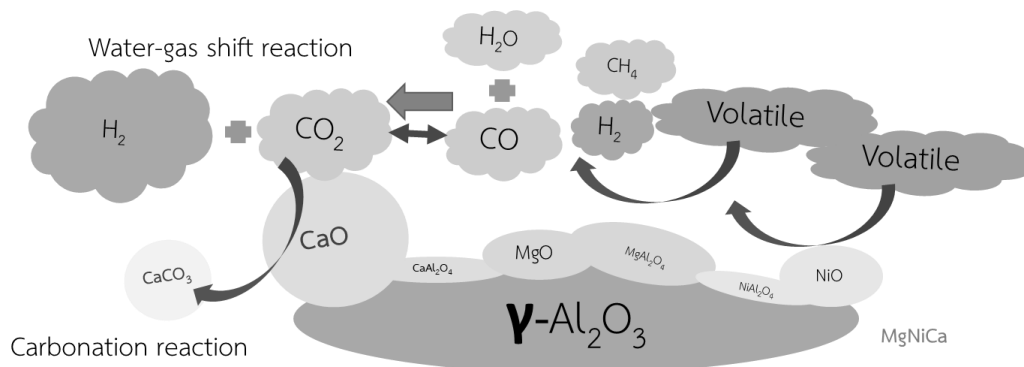
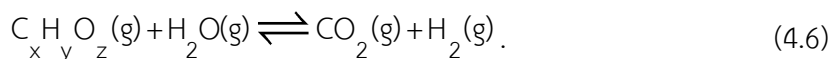
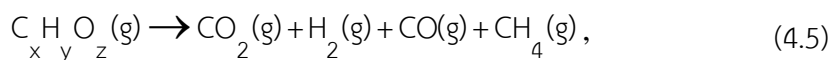


Figure 4.14 The schematic of the catalyst/sorbent mechanism for SEHP in pyrolysis-gasification of sugarcane leaves.

4.4.2 Effect of metal loading sequence on H₂ production with catalyst/sorbent addition at low gasification temperature (800°C)

The gasification temperature was found to have a significant effect on the SEHP during pyrolysis-gasification of sugarcane leaves using Mg5Ni10Ca5 catalyst/sorbent as shown in Figure 4.15. The higher temperature increased all the gas yields (H₂, CO, CH₄ and CO₂). This was similar to the results reported in the previous work [101]. It is due to enhancement of thermal cracking and steam gasification of the volatiles, Eqs. (4.5) and (4.6), to which the high temperature is favorable.



Moreover, the gasification temperature predominantly affected the thermodynamic equilibrium of the carbonation reaction within the temperature range of 600–800 °C. The yield of CO₂ increased with increasing gasification temperature. An explanation for this is that the carbonation reaction is exothermic. Thus, the increase in temperature rather promotes that of CaCO₃ calcination, resulting in a higher CO₂ yield in the product gas [102].

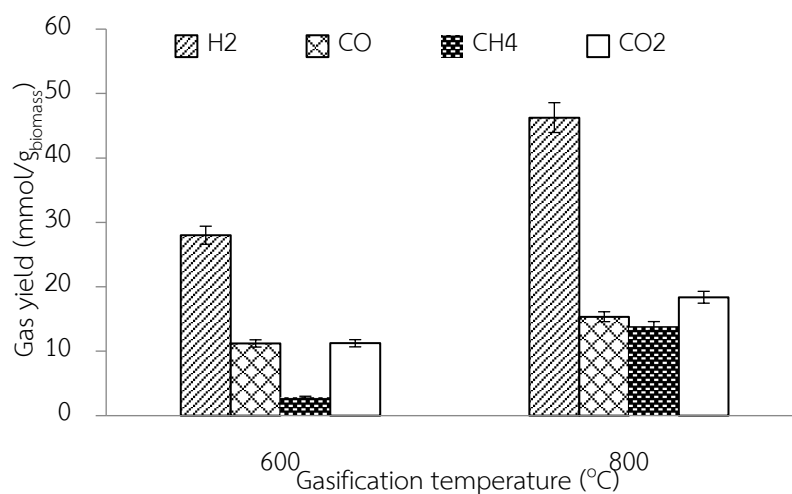


Figure 4.15 Effect of the gasification temperature on the gas yield with the Mg₅Ni₁₀Ca₅ catalyst/sorbents.

Effect of the metal salt loading sequence on the subsequent gas distribution and H₂ yield at the gasification temperature of 800 °C are displayed in Figure 4.16. The order of metal loading showed a minor effect on the obtained gas composition and H₂ yield. The Ca₅Mg₅Ni₁₀ catalyst/sorbents gave the highest H₂ yield (up to 46.3 mmol/g_{biomass}), while that for the Mg₅Ni₁₀Ca₅ and Ni₁₀Mg₅Ca₅ catalyst/sorbents were around 45.0 and 41.3 mmol/g_{biomass}, respectively. No significant change was found in the gas composition with the three different catalyst/sorbents. It is anticipated that the SEHP could not play an important role at such a high temperature, i.e. 800 °C.

These results are associated with the CO₂ adsorption capacity and BET surface area of the fresh and used catalyst/sorbents. The CO₂ adsorption capacity is summarized in Table 4.5. Although the amount of CaO for catalyst/sorbents were different, no significant change in CO₂ adsorption capacity was observed. A reason would be that the carbonation reaction has less contribution at a high gasification temperature of 800 °C [103].

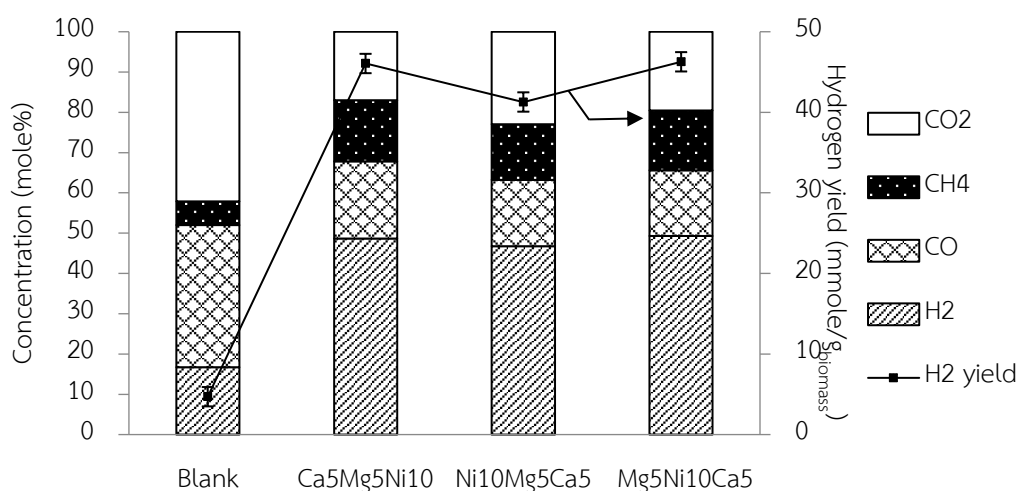


Figure 4.16 Effect of the metal salt loading sequence on the subsequent gas distribution and H₂ yield at the gasification temperature of 800 °C

Table 4.5 CO₂ sorption capacity of the fresh catalyst/sorbents with the temperature of 800 °C.

Sorption temperature (°C)	Catalyst/sorbent	CO ₂ sorption capacity (mmol/g _{sorbent})
800	CaMgNi	7.3±0.3
	NiMgCa	7.5±0.2
	MgNiCa	7.9±0.2

The textural properties of the different order of metal loading catalyst/sorbents are summarized in Table 4.6. The BET surface area of fresh catalyst/sorbents ranged from a high to a low value for the Ca5Mg5Ni10 > Ni10Mg5Ca5 > Mg5Ni10Ca5 catalyst/sorbents, respectively. In this point, the BET surface area could be the key point that leads to the higher H₂ production [104]. The Ca5Mg5Ni10 catalyst/sorbents had the highest magnitude of BET surface area reduction between the (101.2 m²/g) and used catalyst/sorbents (77.3 m²/g) up to 23.6%, while that for the Mg5Ni10Ca5 and Ni10Mg5Ca5 catalyst/sorbents were around 13.0% and 6.59%, respectively, after use at a gasification temperature of 800 °C. However, when used at a gasification temperature of 600 °C the catalyst/sorbents showed a slightly reduction in their BET surface area. The reduction in the BET surface area might indicate the active surface usage of the catalyst/sorbents [105,106], where a high magnitude of BET surface area reduction between the fresh and used catalyst/sorbents would imply to a high performance for the catalytic gasification. Moreover, the XRD analysis of the fresh catalyst/sorbents (Figure 4.4) showed the highest intensity NiAl₂O₄ peak in the Ni10Mg5Ca5 catalyst/sorbents. The NiAl₂O₄ component on the surface catalyst has lower reactivity than NiO [107] and the Ni10Mg5Ca5 catalyst/sorbent gave the lowest catalytic activity for the steam gasification process, including tar cracking and reforming, as shown in Eqs. (4.5) and (4.6), respectively.

Table 4.6 Textural properties of the used catalyst/sorbents with different gasification temperature.

Catalyst/sorbent	Gasification temperature (°C)	BET surface area (m ² /g)	
		Fresh	Used
Ca5Mg5Ni10	600	101.2	92.1
	800		77.3
Ni10Mg5Ca5	600	80.4	80.4
	800		75.1
Mg5Ni10Ca5	600	93.5	89.8
	800		81.3

The role of SEHP at a high gasification temperature of 800°C was supported by using the XRD pattern of used catalyst/sorbents as shown in Figure 4.17. The peak intensity of CaCO₃ was very small in all three catalyst/sorbents and the pattern was only slightly changed in comparison with the fresh catalyst/sorbents. The result confirmed that SEHP does not play an important role at high temperature.

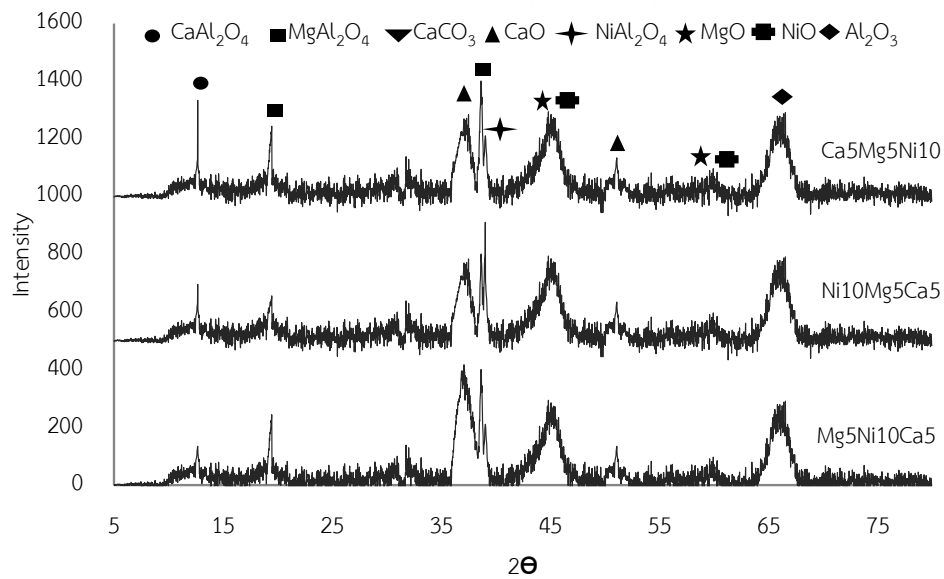


Figure 4.17 XRD patterns of the used catalyst/sorbent (a) Ca5Mg5Ni10, (b) Ni10Mg5Ca5 (c) Mg5Ni10Ca5 at the gasification temperature of 800 °C.

4.5 The optimal condition of catalyst/sorbent on H₂ production from pyrolysis-gasification of sugarcane leaves

The condition including the catalyst/sorbents to biomass mass ratio and the regeneration of catalyst/sorbents were investigated with Mg5Ni10Ca5 catalyst/sorbents. The reaction temperature of both pyrolysis and gasification zone were maintained at 600 °C. This section focused on appraising the optimal condition of catalyst/sorbents on gas yield and H₂ concentration.

4.5.1 Effect of the Mg5Ni10Ca5 catalyst/sorbent to biomass mass ratio

Figure. 4.18 shows the effect of the catalyst/sorbents: biomass mass ratio on the obtained gas composition and H₂ yield from the pyrolysis-gasification process at 600 °C. The H₂ concentration and yield initially increased dramatically as the mass ratio increased from 4 to 8, but further increasing the mass ratio to 12 did not cause any further change in the yield and concentration of H₂. Therefore, optimum catalyst/sorbents: biomass mass ratio

in this case was 8, which gave a maximum H₂ concentration and yield of 70.4 % and 28.1 mmol/g_{biomass} respectively. The CH₄ concentration did not significantly changed with increasing catalyst/sorbents: biomass mass ratio, but the CO and CO₂ concentrations decreased, which is in accord with a previous report [108]. These results can be explained by the increased number of available adsorption sites as the catalyst/sorbents: biomass mass ratio increased until it cannot adsorb more CO₂, when the number of adsorption sites was no longer the rate limiting step for the carbonation reaction Eq. (4.1) and WGS reactions Eq. (4.2).

4.5.2 The regeneration of Mg5Ni10Ca5 catalyst/sorbent on H₂ yield and gas concentration

The regeneration study is one of the important point for the sustainable catalyst/sorbents. Figure 4.19 shows the regeneration cycle of used Mg5Ni10Ca5 catalyst/sorbents in pyrolysis-steam gasification of sugarcane leaves. The used Mg5Ni10Ca5 catalyst/sorbent was regenerated with the calcination at 850 °C which is a suitable temperature to decompose the CaCO₃ to CaO phase [109]. It can be seen that yield and concentration of H₂ were decreased with the regeneration cycles. After the second cycle, the yield and concentration of H₂ significantly dropped to 15.1 mmol/g_{biomass} and 31.1 %, respectively. On the other hand, the CO and CO₂ contents were increased with increasing the regeneration cycles. It can be explained by that the deactivation of catalyst/sorbents could lead to decrease the performance of the WGS reaction Eq. (4.2) and other H₂ production reactions.

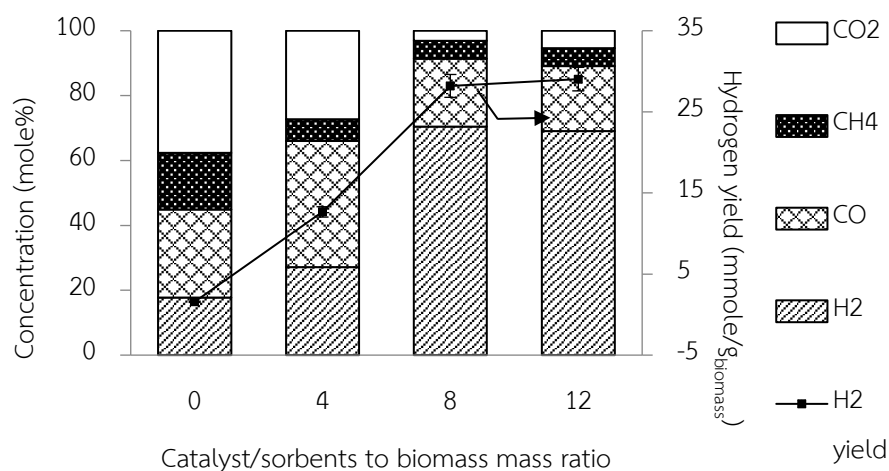


Figure 4.18 Effect of the catalyst/sorbents: biomass mass ratio on the gas distribution and H₂ yield at a low gasification temperature (600°C).

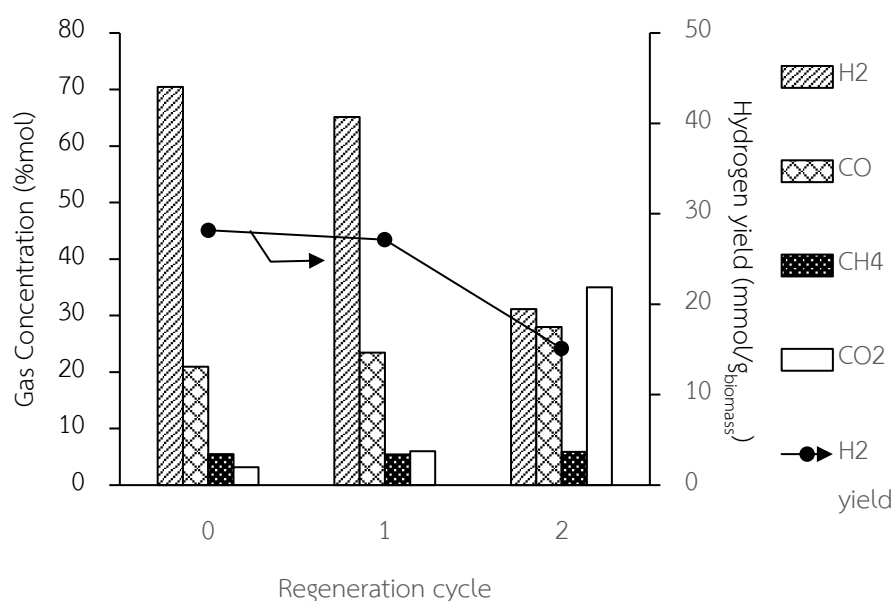


Figure 4.19 The regeneration cycle of Mg₅Ni₁₀Ca₅ catalyst/sorbents.

(Gasification temperature of 600 °C , the catalyst/sorbent to biomass mass ratio = 8)

The SEM images of the catalyst/sorbents after cyclic used are shown in Figure 4.20. It indicated that after the second regeneration of used Mg₅Ni₁₀Ca₅ catalyst/sorbents (Figure 4.20c), there showed clearly some sintering and agglomeration in Mg₅Ni₁₀Ca₅ catalyst/sorbents when compare with 0 and 1 regeneration cycles (Figure 4.20a and

4.20b). Therefore, Mg₅Ni₁₀Ca₅ catalyst/sorbents is suitable for one regeneration cycles. The improvement of regeneration cycles of Mg₅Ni₁₀Ca₅ catalyst/sorbents would be an important issue for the future works.

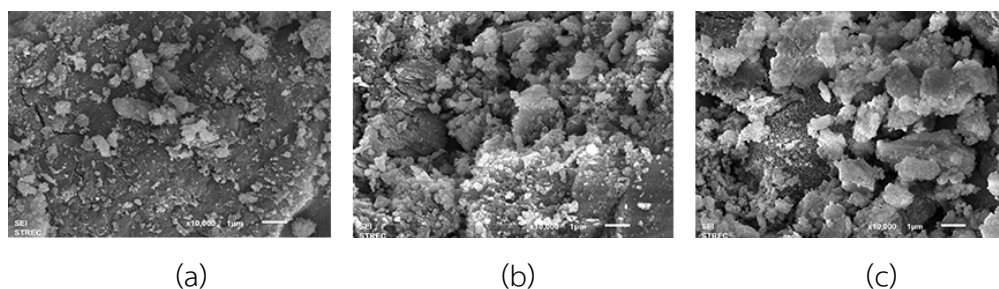


Figure 4.20 SEM images of sorbent (a) 0 cycle, (b) 1 cycle, (c) 2 cycle.

4.6 Role of MgO and CaO study on γ -Al₂O₃ with different gasification temperature on the H₂ production from pyrolysis-gasification of sugarcane leaves.

In this part, the role of MgO and CaO for SEHP was clarified by using the gasification temperature results. Thus, the effects of gasification temperature on H₂ yield with the presence of MgO/ γ -Al₂O₃, CaO/ γ -Al₂O₃ and CaO-MgO/ γ -Al₂O₃ sorbents which were prepared with 5 wt.% of each metal salt doping by the excess solution impregnation method were examined in pyrolysis-gasification of sugarcane leaves.

4.6.1 Effect of the gasification temperature on gas yield with MgO/ γ -Al₂O₃

Figure 4.21 shows the effect of gasification temperature (300 – 600 °C) with the MgO/ γ -Al₂O₃ sorbent. The addition of MgO/ γ -Al₂O₃ into the pyrolysis gasification of sugarcane leaves provided higher the H₂ yield from 0.93 mmol/g_{biomass} to 3.23 mmol/g_{biomass} and lower the CO₂ yield from 5.50 mmol/g_{biomass} to 3.23 mmol/g_{biomass} at the gasification temperature of 300 °C in comparison with the blank condition (No sorbent). Xiao *et al.* reported that the MgO sorbent has high reactivity and good capacity toward CO₂ sorption in

the temperature range of 300 – 450 °C [110]. Nonetheless, increasing the gasification contributed higher H₂ yield and also greater CO₂ yield. The highest H₂ yield (13.6 mmol/g_{biomass}) was observed at the gasification temperature of 600°C. This result indicated that higher yield of all produced gases was improved by the catalytic properties of MgO at elevated temperature (400 – 800 °C) [111]. Therefore, at 300 °C is the suitable gasification temperature for sorption-enhanced H₂ production of MgO/ γ -Al₂O₃ sorbent.

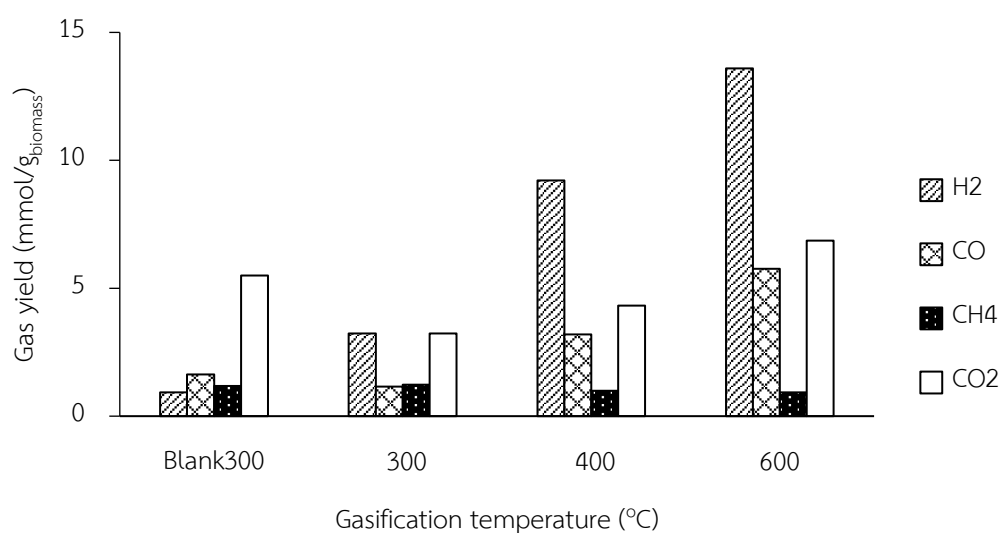


Figure 4.21 Effect of the gasification temperature on gas yield with 5 wt.% of MgO on γ -Al₂O₃.

4.6.2 Effect of the gasification temperature on gas yield with CaO/ γ -Al₂O₃

The effect of gasification temperature on gas yield with CaO/ γ -Al₂O₃ is displayed in Figure 4.22. The results divided into two temperature ranges, 400 – 600 °C and 600 – 800 °C. Raising the gasification temperature from 400 to 600 °C provided higher of the H₂ yield and lower CO₂ yield. The decreasing of CO₂ caused the shift of the thermodynamic equilibrium of WGS reaction to produce more H₂ as mention before (Eq. 4.2). When the gasification

temperature was applied from 600 °C to 800 °C, the H₂ yield increased and the CO₂ yield also increased. This can be explained by two reasons: Firstly, CaO can play role as the catalyst for the gasification of biomass. It might catalyze water gas reaction, thermal cracking and steam gasification of the volatiles as shown in Eqs. (4.4), (4.5) and (4.6) respectively. Secondary, some CO₂ was produced by the decomposition of CaCO₃ at gasification temperature of 800°C. This leads to higher the CO₂ yield with increasing the gasification temperature up to 800 °C.

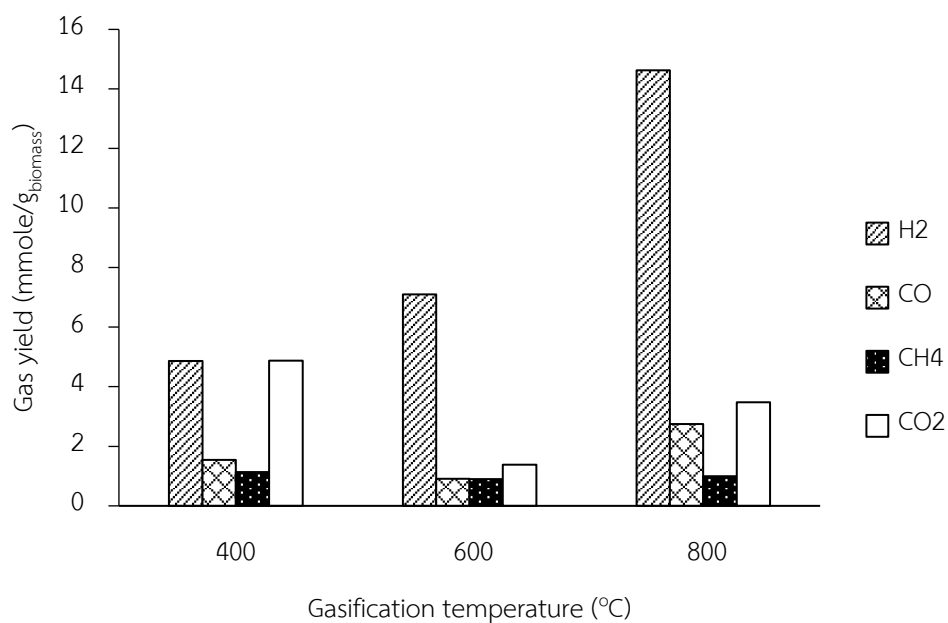


Figure 4.22 Effect of the gasification temperature on gas yield with 5 wt.% of CaO on γ -Al₂O₃.

4.6.3 Effect of the gasification temperature on gas yield with CaO-MgO/ γ - Al_2O_3

The effect of the gasification temperature on gas yield with CaO-MgO/ γ - Al_2O_3 is demonstrated in Figure 4.23. Increasing the gasification temperature from 300 °C to 500 °C afforded higher of H_2 yield and lower CO_2 yield. When increased the gasification temperature further from 500 °C to 700 °C, H_2 , CO and CO_2 yield increased. These results can be explained by using the XRD pattern of used CaO-MgO/ γ - Al_2O_3 as shown in Figure 4.24. The CaO, MgO, CaCO_3 , MgCO_3 and Al_2O_3 phases were found in all used sorbents. The CaCO_3 phase is the product from the CO_2 adsorption of CaO Eq. (4.1) and the MgCO_3 phase is produced by the CO_2 adsorption of MgO phase Eq. (4.7) as shown below.



The highest intensity peak of MgCO_3 phase and the lowest intensity peak of CaCO_3 phase were noticed at the gasification temperature of 400 °C. This result showed that the MgO phase can play more considerable role for CO_2 adsorption at low gasification temperature (400°C) than the CaO phase [110]. In case of the gasification temperature of 500 °C, high CaCO_3 and MgCO_3 phases occurred. It could indicate that both CaO and MgO can adsorb with CO_2 to produce more H_2 yield. Moreover, the highest intensity peak of CaCO_3 phase and the lowest MgCO_3 phase intensity were found at the gasification temperature of 600 °C. Although the highest H_2 yield was not observed at the gasification temperature of 600 °C, the lowest CO_2 yield occurred. It implied that the CaO has high potential for SEHP and the MgO is suitable metal oxide to use as promoter for SEHP.

4.6.4 Regeneration process of CaO-MgO/ γ -Al₂O₃ sorbent

Figure 4.25 shows the pyrolysis-gasification performance of the cyclic used CaO-MgO/ γ -Al₂O₃. H₂ yield decreased while the CO₂ yield increased with increasing the regeneration cycles. At the third cycle, H₂ yield decreased and both CO and CO₂ yield significantly increased whereas the CH₄ were almost constant. Zhang *et al.* indicated that after the regeneration cycle, the sintering and agglomeration of CaO/MgO was observed [98]. Hence, the sorbent activity might be reduced with the number of regeneration cycle.

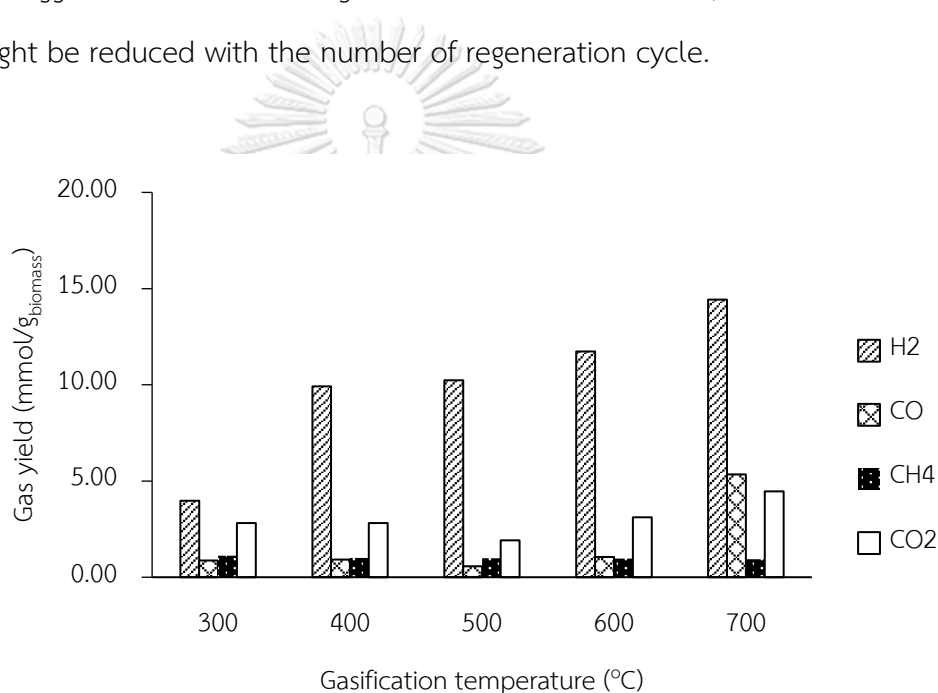


Figure 4.23 Effect of the gasification temperature on gas yield with CaO-MgO/ γ -Al₂O₃.

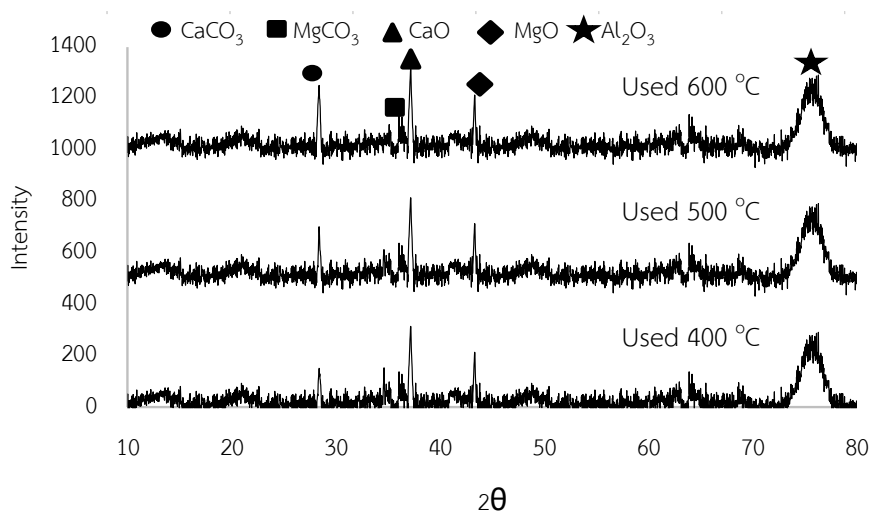


Figure 4.24 XRD pattern of used sorbent (CaO-MgO/ γ -Al₂O₃) for pyrolysis-gasification of sugarcane leaves.

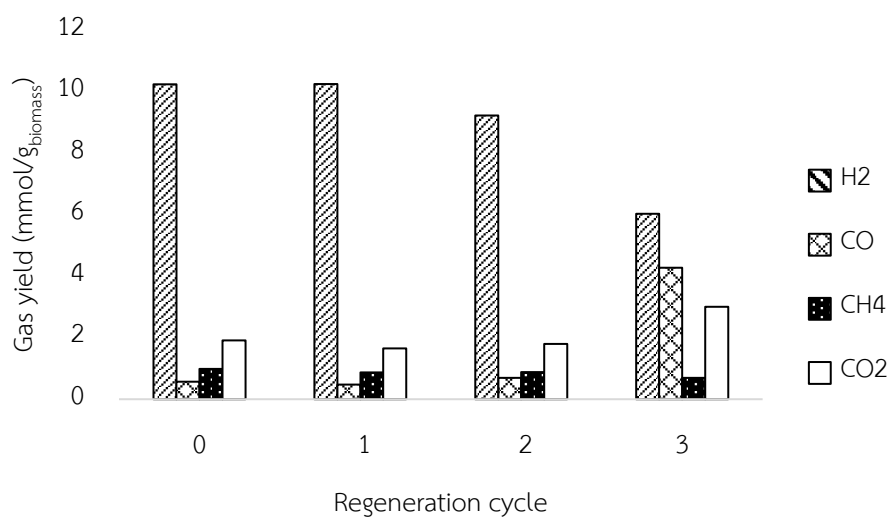


Figure 4.25 The regeneration cycle of CaO-MgO on γ -Al₂O₃ for biomass pyrolysis gasification on gas yield.

CHAPTER 5

Ni/CaO-MgO CATALYTS/SORBENTS STUDY ON H₂ PRODUCTION DURING THE PYROLYSIS-STEAM GASIFICATION OF SUGARCANE LEAVES

In this chapter, the pyrolysis-steam gasification of sugarcane leaves was investigated with the Ni/CaO-MgO which was prepared using the excess solution impregnation method. The experimental was carried out in a drop-tube two-stages fixed bed reactor as described in Chapter 3. The results are divided into three aspects; (I) the preparation of supported CaO-MgO, (II) The metal loading (NiO) on prepared support and (III) Comparison of Mg₅Ni₁₀Ca₅ and NiO/CaO-MgO catalyst/sorbents. In section 5.1, the effect of the CaO to MgO molar ratio, the supported preparation methods, the devolatilization temperature and gasification temperature were discussed. In the section 5.2, effect of NiO loading content and the regeneration of catalyst/sorbents were reported. In the last section (section 5.3), the comparison between Mg₅Ni₁₀Ca₅ and NiO₅/WM(2:1) catalyst/sorbents were reported in the point of gas production and operating parameters.

5.1 The preparation of supported CaO-MgO on H₂ production

Two alkaline earth metals including CaO and MgO were examined for the H₂ rich gas production from the pyrolysis-gasification of sugarcane leaves. The several parameters including, the CaO:MgO ratio, the preparation methods were investigated. Moreover, the reaction temperature of pyrolysis and gasification zone were studied on gas yield and composition. The corresponding name of prepared support was shown in Table 5.1.

5.1.1 Effect of the CaO:MgO molar ratio on the gas yield and composition.

The gas composition from the pyrolysis-gasification of sugarcane leaves with CaO/MgO sorbents of different CaO:MgO molar ratios was examined at 600 °C for both the pyrolysis and gasification zones, with the results are shown in Figure 5.1.

Table 5.1 Corresponding name of prepared support

No.	Name	Preparation method	Molar ratio	
			CaO	MgO
1	CaO	Commercial	1	-
2	MgO	Commercial	-	1
3	DM (2:1)	Dry mixing	2	1
4	DM (1:1)	Dry mixing	1	1
5	DM (1:2)	Dry mixing	1	2
6	WM (2:1)	Wet mixing	2	1
7	WM (1:1)	Wet mixing	1	1
8	WM (1:2)	Wet mixing	1	2

Pure CaO provided a H₂ concentration (54.4%) that was about five-fold higher than that without a sorbent (8.7%), while the CO₂ concentration was about three-fold lower. These results were attributed to the role that CaO plays as an effective CO₂ sorbent to promote the SEHP [112]. In contrast, pure MgO gave a 1.8-fold lower H₂ concentration than pure CaO (but still higher than that with no sorbent), reflecting its weaker CO₂ adsorption capacity. However, the mixing of MgO and CaO rendered a positive effect on the H₂ production, where the highest H₂ concentration (75.1%) and lowest CO₂ concentration (7.7%) were

observed with the DM 2:1 sorbent. Increasing the molar ratio of MgO in the mixed CaO/MgO sorbent above 0.33 to 0.5 and 0.67 (DM 1:1 and DM 1:2) decreased the obtained H₂ concentration (1.4-fold) and increased that of CO(1.4-fold).

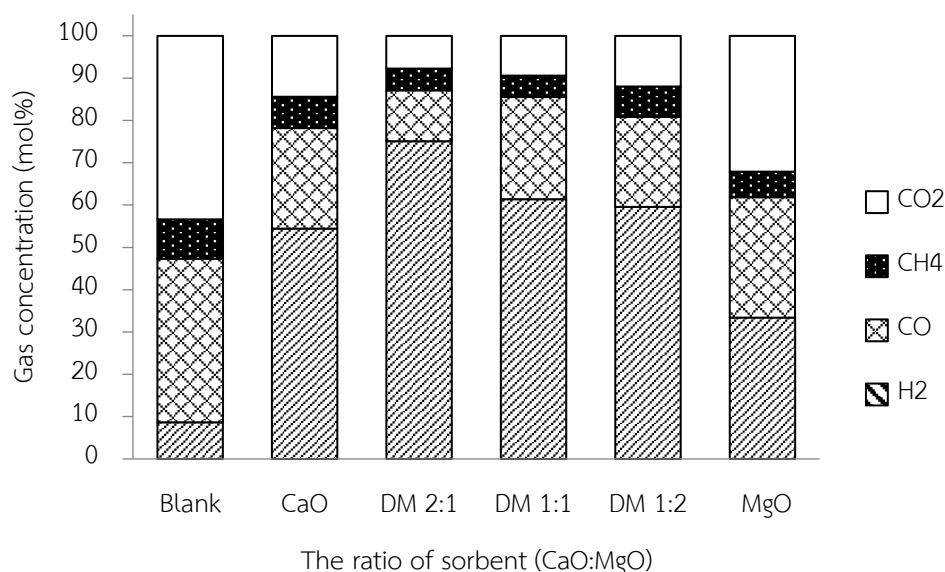


Figure 5.1 Gas concentration from pyrolysis-gasification with the dry mixed CaO: MgO sorbents at different molar ratios.

For the synergistic study, the experimental yields have to compare with the theoretical yield. The predicted yield ($Y_{\text{predicted}}$) was obtained by the equation as shown in Chapter 3.

The Figure 5.2 shows a comparison of the experimentally derived and the theoretically predicted values of the H₂ and CO₂ yields with different MgO to CaO molar ratios. All three CaO: MgO ratios exhibited higher experimental H₂ yields and lower CO₂ yields compared with the predicted values. This finding supports the synergy of the mixed CaO/MgO sorbents during the SEHP in the pyrolysis-gasification of sugarcane leaves.

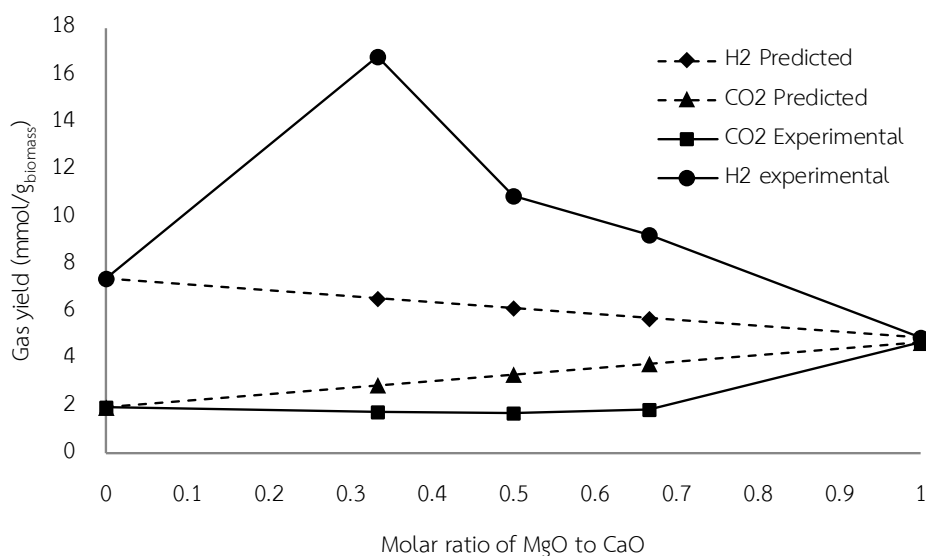


Figure 5.2 Gas yield obtained from pyrolysis-gasification (600 °C pyrolysis and gasification) of sugarcane leaves with the dry mixed CaO: MgO sorbents at different molar ratios.

The CO₂ adsorption capacity was deduced from the breakthrough curves at a reaction temperature of 600 °C (Figure 5.3). For the pure MgO, the amount of CO₂ released increased rapidly from an adsorption time between 0 and 8 min, which can be attributed to the fact that the MgO provided the lowest CO₂ adsorption capacity. Although MgO can promote CO₂ adsorption, the suitable temperature range for this is typically low (70–350 °C) [112]. Pure CaO and the mixed CaO/MgO sorbents showed no detectable CO₂ release from an adsorption time between 0–4 min and then rapidly increased from 8–10 min with all the sorbents reaching equilibrium at around 12–14 min. The highest CO₂ adsorption capacity (12.6 mmol/g_{sorbent}) was observed with the DM 2:1 sorbent and increasing the molar MgO fraction above 0.33 (DM 2:1) reduced the CO₂ adsorption capacity. Therefore, it can be concluded that the CO₂ adsorption capacity of the mixed CaO/MgO sorbent is proportional to the amount of CaO in the mixed sorbent.

The presence of MgO in place of CaO in the mixed DM 2:1 sorbent provided a higher CO₂ adsorption capacity than the pure CaO sorbent, indicating that there is a synergistic effect between CaO and MgO in the mixed sorbent. Although the MgO does not play a major role in CO₂ adsorption itself at the reaction temperature over 500 °C, it could prevent sintering of CaO during the carbonation and calcination cycles in the gasification process [113]. However, increasing the MgO proportion in the mixed sorbent above a 0.33 molar ratio (DM 2:1) reduced the yield and concentration of H₂ due to the reduced amount of CaO available for CO₂ adsorption to promote the SEHP.

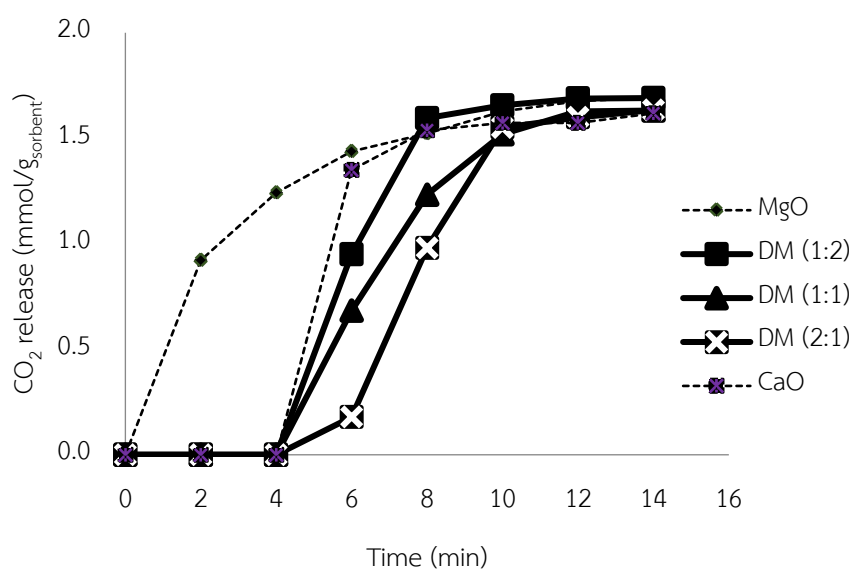


Figure 5.3 Breakthrough curves of the different fresh (unused) dry mixed CaO/MgO sorbents at different molar ratios (pyrolysis and gasification at 600 °C).

5.1.2 Effect of the sorbent preparation method on the gas yield and composition.

Figure 5.4 shows the gas yield obtained with the dry and wet mixed CaO/MgO sorbents in the pyrolysis-gasification of sugar cane leaves at a pyrolysis and gasification zone temperature of 600 °C. The wet-mixed sorbents provided a higher H₂ and lower CO₂ yield than the dry-mixed sorbents at the same CaO: MgO ratio for both evaluated ratios (2:1 and 1:1), suggesting a higher efficiency of the wet mixing for the SEHP than dry mixing. Thus, the WM 2:1 sorbent also showed the highest H₂ yield and the lowest CO₂ yield.

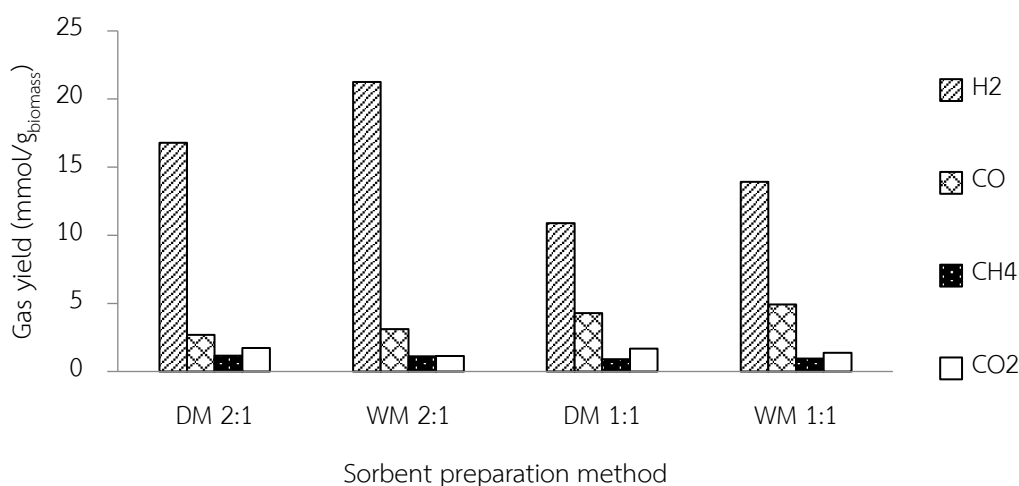


Figure 5.4 Gas yields obtained from the pyrolysis-gasification (600 °C pyrolysis and gasification) of sugarcane leaves with the dry and wet mixed CaO/MgO sorbents at different molar ratios.

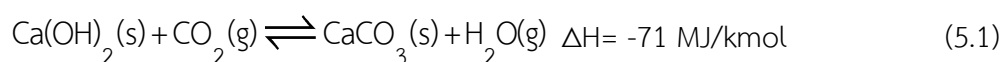
Table 5.2 shows the CO₂ adsorption capacity for the fresh CaO/MgO sorbents at 600 °C. The highest CO₂ adsorption capacity was observed with the WM 2:1 sorbent (15.1 mmol/g_{sorbent}) and both WM sorbents showed a higher CO₂ adsorption capacity than the corresponding DM ones. This correlates to the gas yield results and indicated that the higher H₂ yield production from

pyrolysis-gasification of sugarcane leaves with the CaO/MgO sorbents was caused by the CO₂ adsorption shifting the thermodynamic equilibriums of the WGS reaction.

Table 5.2 CO₂ adsorption capacity of the fresh mixed CaO/MgO sorbents.

Sorbent	CO ₂ adsorption capacity (mmol /g _{sorbent})
DM 2:1	12.6±0.6
DM 1:1	11.0±0.4
WM 2:1	15.1±0.4
WM 1:1	12.8±0.5

The main reason that could explain the difference between the wet and dry mixing methods comes from the phase analysis. Figure 5.5a shows the XRD patterns of the as-prepared fresh WM and DM mixed sorbents before being used in the pyrolysis-gasification reaction. All the fresh CaO/MgO sorbents showed both CaO and MgO peaks, but at different intensities. The intensity of the CaO and MgO peaks depended on the CaO: MgO molar ratio. However, all the samples produced by wet mixing were found to display peaks for the Ca(OH)₂ phase, which has a higher reactivity in the gas-solid carbonation of Ca(OH)₂ for CO₂ adsorption, shown in reaction 5.1, than the carbonation reaction of CaO at a high temperature (400–800 °C).



This is because the simultaneous expelling of the produced water during the gas-solid carbonation of Ca(OH)₂ significantly enhanced the CO₂ transfer from the gas phases towards the unreacted Ca(OH)₂ surface. The wet

mixed CaO/MgO sorbents consisted of both CaO and Ca(OH)₂, which then promoted CO₂ adsorption and SEHP.

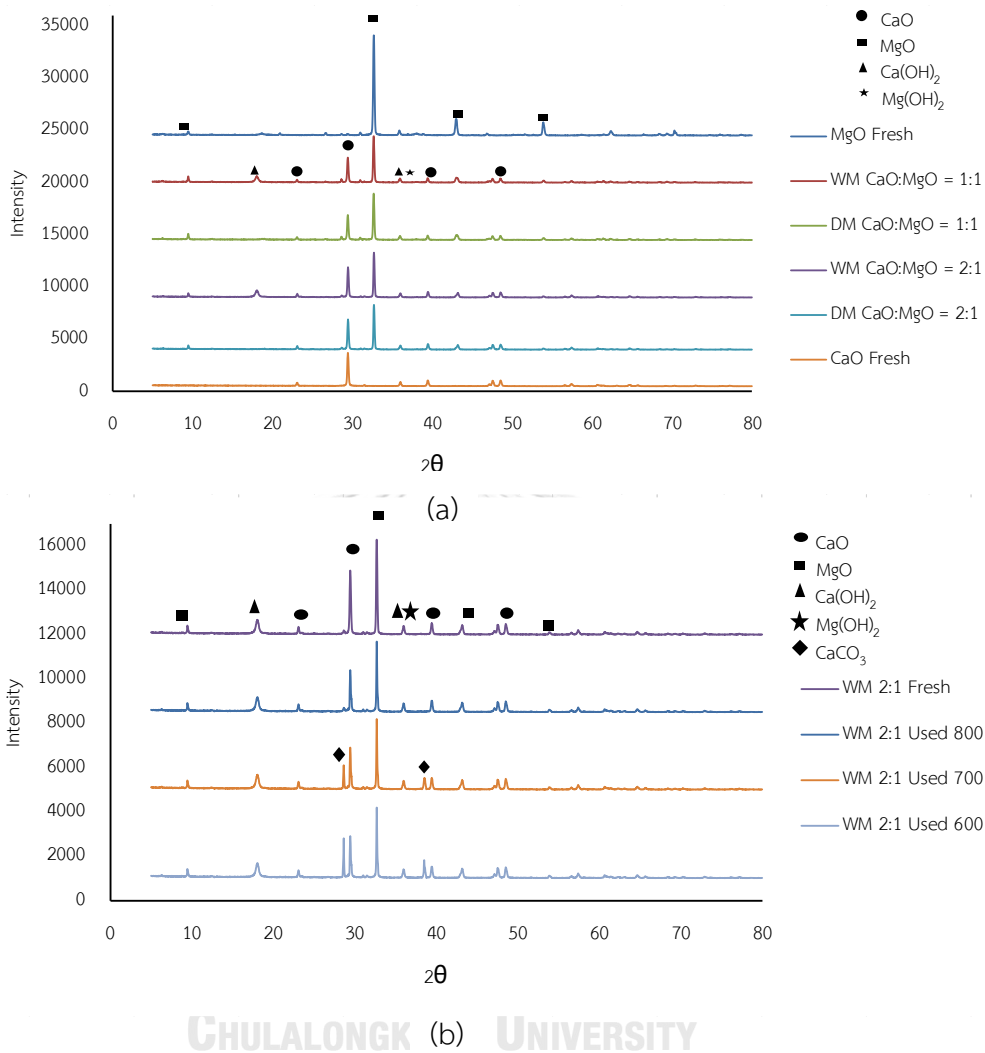


Figure 5.5 Representative XRD pattern of the (a) fresh (before pyrolysis-gasification) wet and dry mixed CaO/MgO sorbents and (b) WM 2:1 before and after pyrolysis-gasification at different gasification temperatures.

Table 5.3 shows the textural properties of the CaO, MgO and the different CaO/MgO mixed sorbents. The mixed sorbents showed a higher BET surface area than either the pure CaO or MgO ones. The highest BET surface area (30.6 m²/g), as well as the largest pore volume and size, was observed in the WM 2:1 sorbent. Increasing the molar fraction of MgO up to 0.5 (WM 1:1) reduced the BET surface area (1.18-fold) and pore volume (1.08-fold). These results correlate to the CO₂ adsorption of the sorbents as well as to the H₂ production in the pyrolysis-gasification of sugarcane leaves. Thus, the BET surface area is likely to be an important factor in the higher H₂ production activity.

Table 5.3 Textural properties of the fresh (as-prepared) sorbents.

Sorbent	BET surface area (m ² /g)	Pore volume (cm ³ /g)	Pore size (cm ³ /g)
CaO	9.75	0.0088	36.1
MgO	23.8	0.1885	31.6
DM 2:1	28.1	0.0262	37.4
DM 1:1	24.1	0.0175	29.1
WM 2:1	30.6	0.0356	46.7
WM 1:1	26.0	0.0329	50.7

5.2.3 Effect of the devolatilization temperature on the gas yield.

The devolatilization temperature (the first stage of pyrolysis) has an important effect on the production of volatile components from the raw biomass. Figure 5.6 shows the gas concentration and H₂ yield obtained from the pyrolysis-gasification of sugarcane leaves with the WM 2:1 sorbent at

devolatilization temperatures of 400, 600 and 800 °C. Increasing the devolatilization temperature from 400 °C to 600 °C provided a higher H₂ and lower CO₂ yield. However, the H₂ yield was reduced with increasing the devolatilization temperature from 600 °C to 800 °C.

This can be explained by the product distribution from the pyrolysis of sugarcane leaves with no sorbent (Figure 5.7). At a pyrolysis temperature of 400 °C, the condensable volatile and gas products were the lowest, which might be the main factor that decreased the gas product in the pyrolysis-gasification of sugarcane leaves with a sorbent. A devolatilization temperature of 800 °C showed a higher gas product level than at 600 °C, while the pyrolysis-gasification of sugarcane leaves with the sorbent showed the best result at a devolatilization temperature of 600 °C. While there was no significant difference in the condensable volatile content obtained at a pyrolysis temperature of 600 °C and 800 °C, the composition of these volatiles was examined since it was reported that the condensable component is one of the most effective factors in the catalytic pyrolysis-gasification process [114].

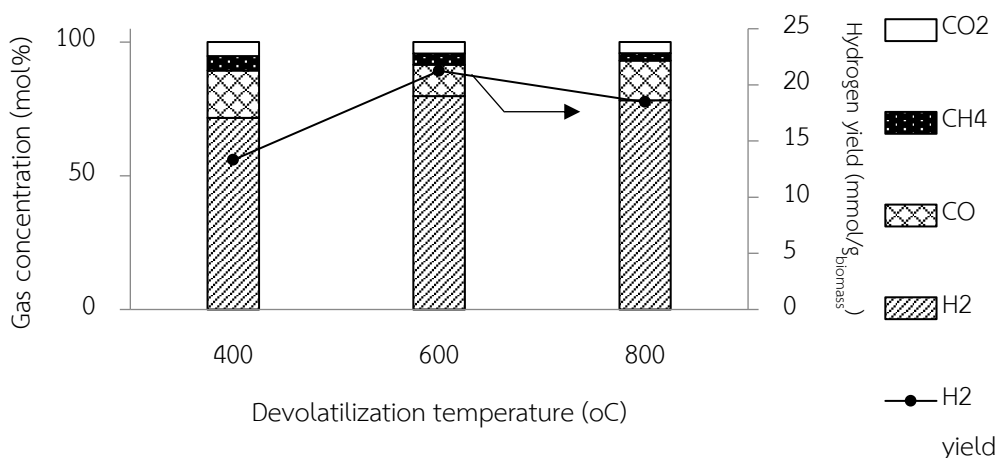


Figure 5.6 Gas concentration and H₂ yield obtained from the pyrolysis-gasification with WM 2:1 sorbent.

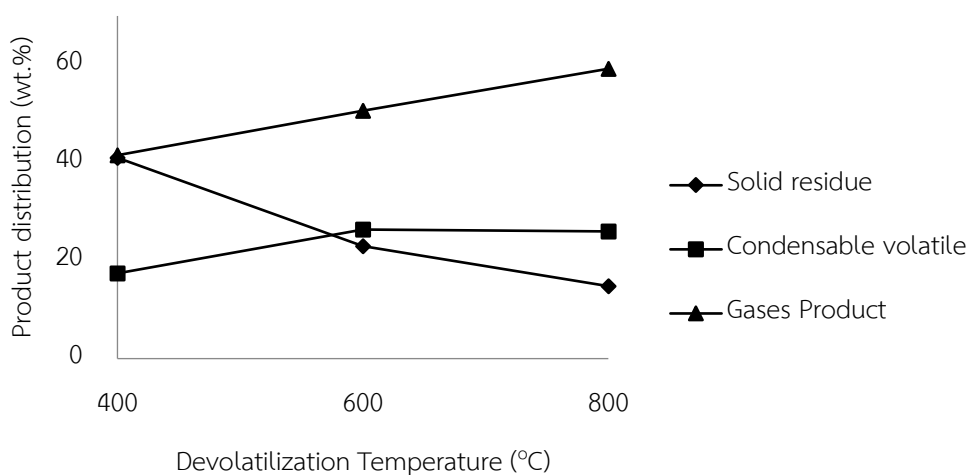


Figure 5.7 The product distribution obtained from the pyrolysis of sugarcane leaves without any sorbent at different devolatilization (pyrolysis) temperatures.

Figure 5.8 shows the GC-MS analysis of the condensable volatiles from the pyrolysis of sugarcane leaves at different devolatilization temperatures of 600 °C and 800 °C. At 600 °C (Figure 5.8a), the condensable volatiles mainly consisted of oxygenated compounds (ketones), alcohols and phenols. These compounds are the major volatile components derived from the decomposition of cellulose and hemicelluloses at 600 °C [115]. Increasing the

devolatilization temperature to 800 °C (Figure 5.8b) provided higher heavy aromatic compounds, such as naphthalene. Likewise, the tar derived from pine wood pyrolysis at devolatilization temperatures above 700 °C was also reported to mostly contain heavy aromatic compounds (anthracene and fluorine) [116].

The oxygenate compound in volatiles derived at the devolatilization temperature of 600 °C could more preferentially react with steam and decompose over the WM 2:1 sorbent than the heavy aromatic compounds, resulting in the higher H₂ yield.



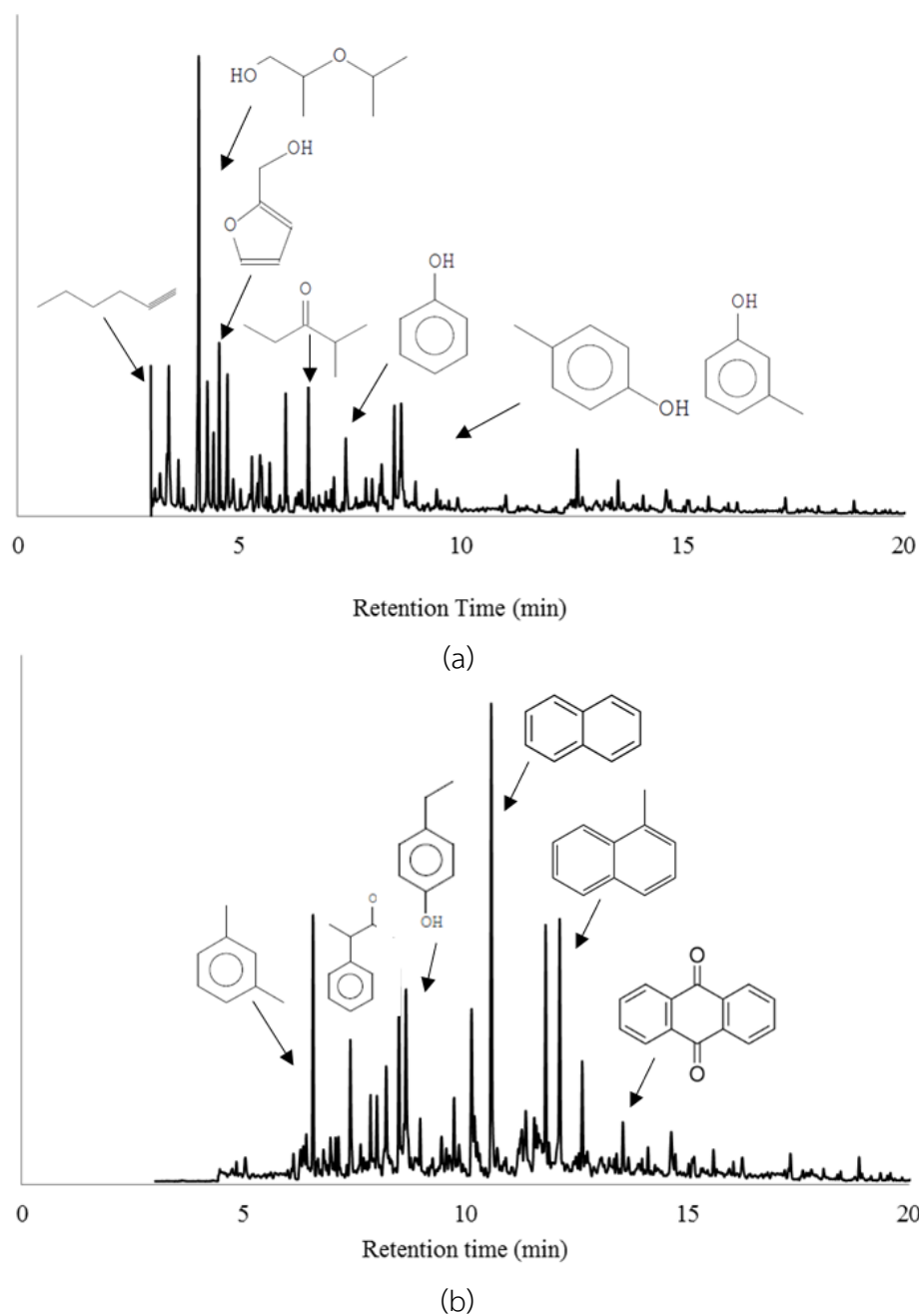


Figure 5.8 Effect of the devolatilization temperature on the GC-MS patterns of the volatiles obtained from the pyrolysis-gasification of sugarcane leaves at (a) 600 °C and (b) 800 °C without any sorbent.

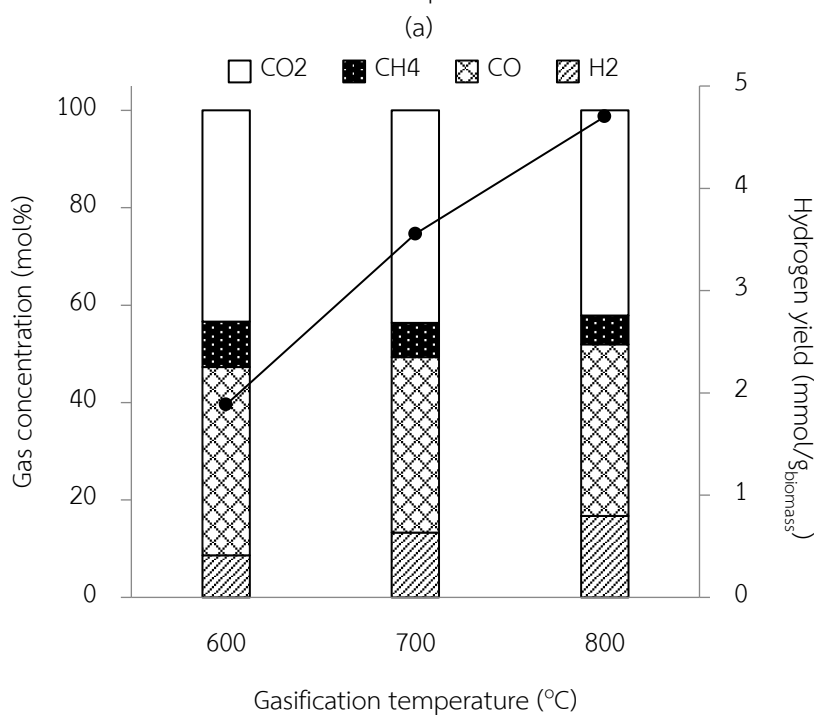
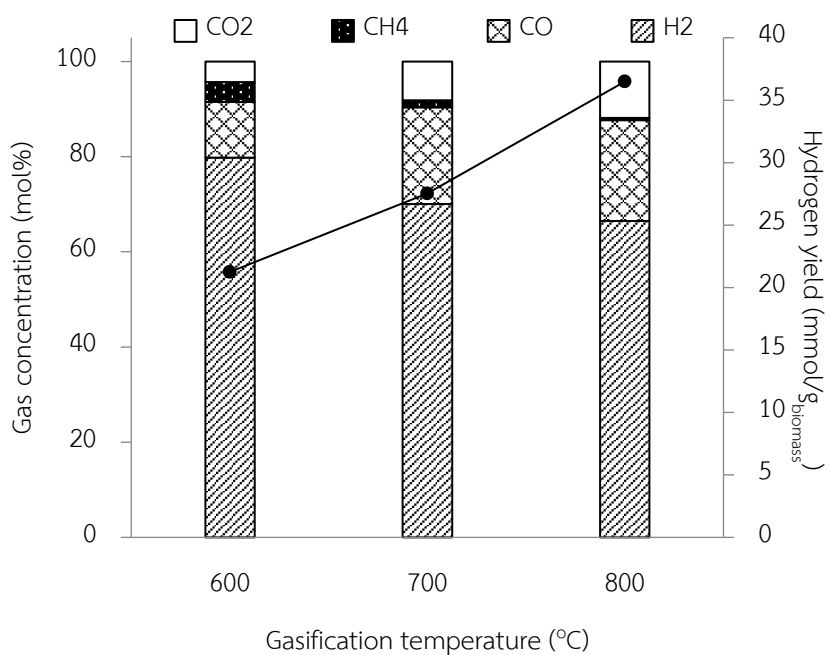
Figure 5.9a shows the H₂ yield and gas composition from the SEHP in the pyrolysis-gasification of sugarcane leaves at different gasification temperatures with the WM 2:1 sorbent. When the gasification temperature was increased from 600 °C to 800 °C, the yield of H₂ increased. However, the highest H₂ concentration and the lowest CO₂ concentration were observed at a gasification temperature of 600 °C.

Different trends were observed without a sorbent (Figure 5.9b), where both the yield and concentration of H₂ were increased with increased gasification temperatures above 600 °C. This is because almost all the reactions which produced H₂ (Eqs. (5.2), (5.3) and (5.4)) are endothermic.



Accordingly, the higher H₂ concentration and lower CO₂ concentration obtained with WM 2:1 at the low gasification temperature (600 °C) might be because the SEHP that exhibited a more dominant effect than the thermodynamic equilibrium at a low gasification temperature [117].

Comparison of the XRD patterns between the fresh and used WM 2:1 sorbent is shown in Figure 5.5b, where CaCO₃ peaks were found in all the used samples. This confirmed that the CaO carbonation reaction took place during the pyrolysis-gasification of sugarcane leaves, and so was likely to contribute to the SEHP effect on the pyrolysis-gasification via shifting the WGS equilibrium. Increasing the gasification temperature reduced the CaCO₃ intensity peaks, supporting that the SEHP was mainly effective at a low temperature (600 °C) because of its exothermic nature.



(b)

Figure 5.9 The H₂ yield and gas concentration obtained from the pyrolysis-gasification of sugarcane leaves at different gasification temperatures (pyrolysis at 600 °C) in the presence of (a) WM 2:1 or (b) no sorbent.

5.2 The Metal loading study with the prepared CaO-MgO on H₂ production

In this section, the NiO metal loading content from 3 to 15 wt.% were loaded on the WM (2:1) by using the excess solution impregnation method and the regeneration of catalyst/sorbents was also investigated on gas yield and composition. The pyrolysis and gasification temperature were maintained at 600 °C which was the suitable reaction temperature for SEHP in pyrolysis-gasification of sugarcane leaves. NiOX/WM(2:1) is the corresponding name of catalyst/sorbent in this part, where X is the NiO metal loading content (wt.%) on the WM (2:1) support.

5.2.1 Effect of NiO loading content of H₂ production from pyrolysis-gasification of sugarcane leaves.

The effect of the NiO loading content on WM (2:1) on the gas yield and composition are shown in Figure 5.10. For the gas yield (Figure 5.10a), the addition of NiO increased all gaseous product yield. Increasing NiO loading content from 3 to 5 wt.% showed positive effect on H₂ production. It can increase the H₂ yield from 24.4 to 30.3 mmol/g_{biomass}. The CO₂ yield was dramatically increased with increasing the NiO loading content from 5 to 10 wt.%. The highest H₂ yield was found with the NiO loading content of 15 wt.%. These results can be explained into two ways: firstly, increasing the NiO loading content can catalyze the water gas reaction Eq (5.2) and methane steam reforming Eq (5.4) [104-106]. Secondly, high CO₂ yield with the NiO loading content over 5 wt.% was caused by the covering of NiO on the WM (2:1) prepared support which could decrease the CO₂ adsorption efficiency.

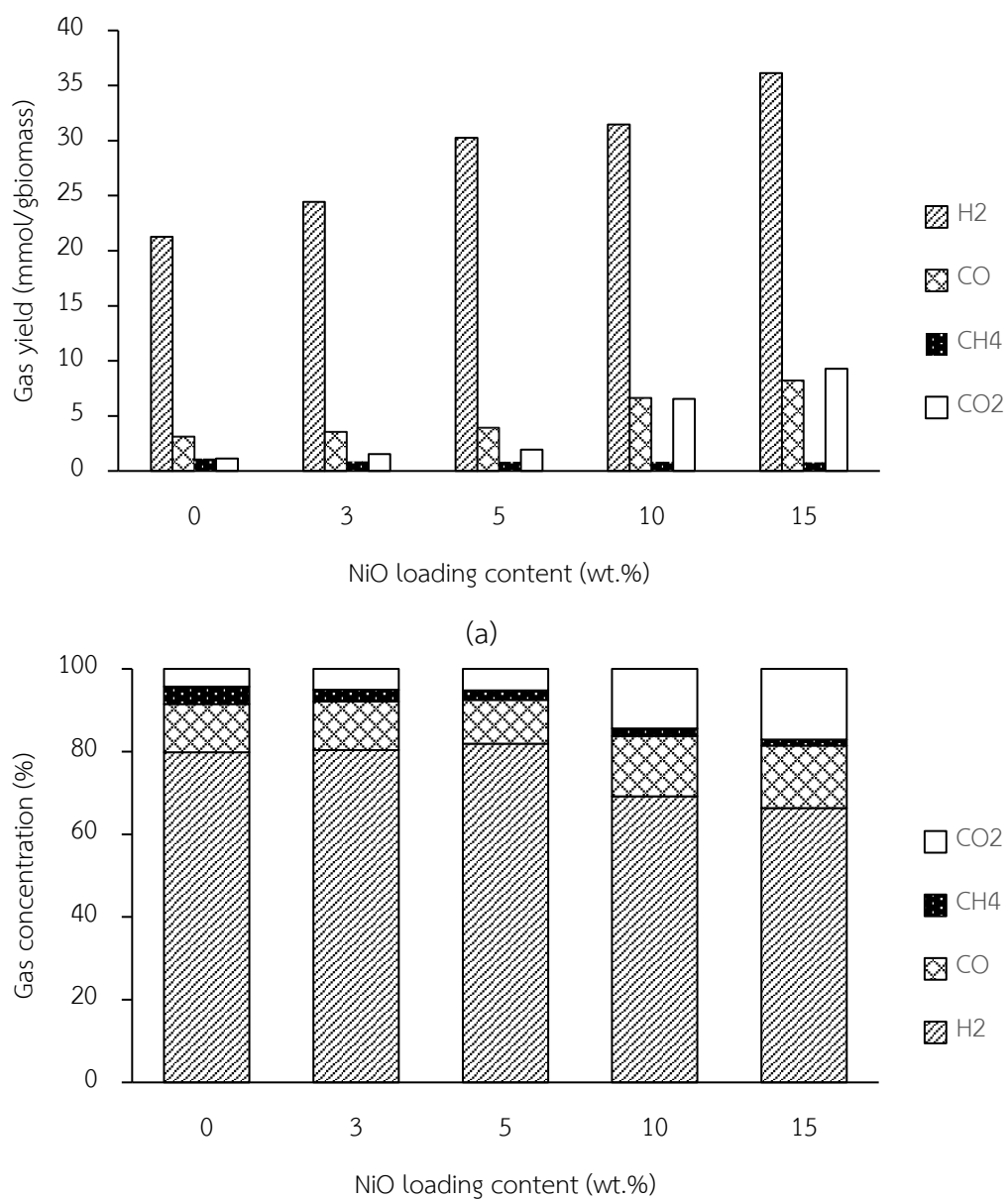


Figure 5.10 Effect of NiO5/WM (wt.%) loading content on (a) gas yield and (b) gas concentration from pyrolysis-gasification of sugarcane leaves.

The gas composition from pyrolysis-gasification with different NiO loading is shown in Figure 5.10b. No significant change of H₂ concentration was observed with increasing the NiO loading content from 3 to 5 wt.%. This can be attributed to that the addition of NiO on WM (2:1) could not be the main effect on the SEHP which the important factor could control the H₂ concentration. The highest H₂ concentration up to 81.8 % was obtained with the NiO loading content up to 5 wt.%. The concentration of H₂ decreased from 81.8% to 6.4 % but the CO₂ concentration was increased from 5.4% up to 17.1 % with increasing the NiO loading content from 5 to 15 wt%. The gas composition results were related with the catalyst/sorbents characterization. Figure 5.11 shows the CO₂ adsorption breakthrough curve of catalyst/sorbents and the CO₂ adsorption capacity are summarized in Table 5.4. For the 15 wt.% of NiO loading content, the amount of CO₂ released increased rapidly from an adsorption time between 2 and 10 min, which can be interpreted that the 15 wt.% of NiO showed the lowest of CO₂ adsorption capacity. Pure WM (2:1) and the NiO loading content from 3 to 10 wt.% showed no detectable CO₂ release from an adsorption time between 0–4 min and then rapidly increased from 6–10 min with all the sorbents reaching equilibrium at around 12–14 min. The highest CO₂ adsorption capacity (12.6 mmol/g_{sorbent}) was observed with no NiO loading sorbent and increasing the molar NiO loading content could reduce the CO₂ adsorption capacity. The results might be concluded that the NiO loading content over 5 wt.% cannot promote the CO₂ adsorption which is related to the gas yield and composition above.

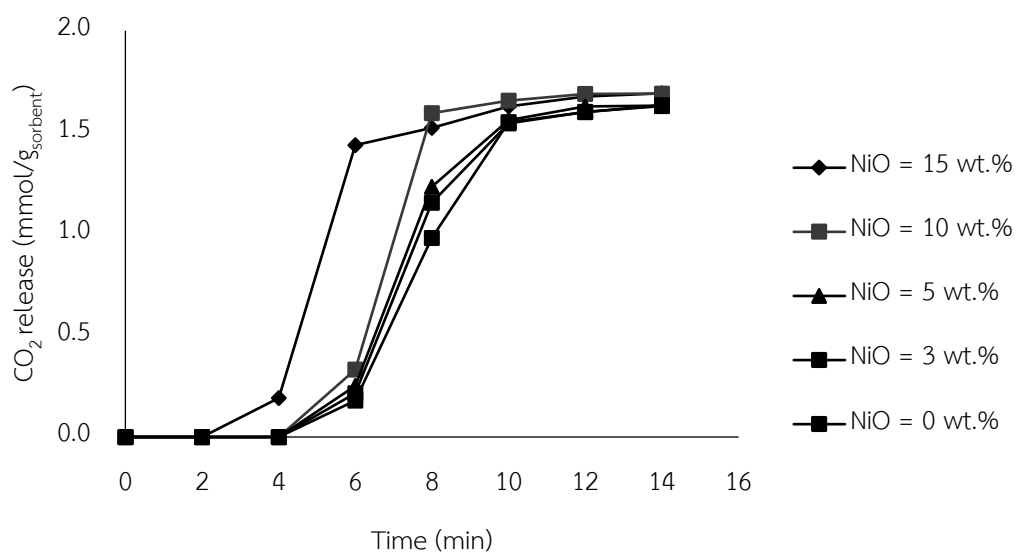


Figure 5.11 Breakthrough curves of the different NiO loading content of fresh catalyst/sorbents at a gasification reaction temperature of 600 °C.

Table 5.4 CO₂ adsorption capacity with different NiO loading content at 600 °C

Sorption temperature (°C)	NiO loading (wt.%)	CO ₂ sorption capacity (mmol/g _{Catalyst})
600	0	12.6
	3	12.1
	5	11.8
	10	11.4
	15	9.0

These examinations were confirmed by using the XRD pattern with different NiO loading content on WM (2:1) as shown in Figure 5.12. It was found that fresh catalyst/sorbents (Figure 5.12a) observed that increasing the NiO loading content increased the intensity peak at the 2θ of 32.7° which is close to the intensity peak of MgO (32.3°). The intensity peak of CaO around the 2θ of 29.5° was decreased with increasing the NiO loading content. These findings indicated that some particles of NiO could cover the active site of CaO which is the important phase for SEHP. Figure 5.12b shows the XRD pattern of used catalyst/sorbents with different NiO loading content. It was found that the CaCO_3 phase which is produced from the CO_2 absorption of CaO increased with increasing the NiO loading content from 3 to 5 wt.%. It could be explained that rising the NiO loading content can promote the steam reforming of methane (reaction 5.4) which provided higher CO_2 yield. The NiO5/WM(2:1) catalyst/sorbents could adsorb more CO_2 using the CaO carbonation reaction and it provided higher CaCO_3 phases on the surface of catalyst/sorbents. For further increasing the NiO loading content from 5 wt.% to 15 wt.% the intensity peaks of CaCO_3 were lower. It might be concluded that increasing NiO loading content can hinder the CaO phases in catalyst/sorbents. It could lead to decrease the CO_2 adsorption capacity of the catalyst/sorbent. Therefore, NiO5/WM(2:1) is the best catalyst/sorbent for SEHP from the pyrolysis-gasification of sugarcane leaves.

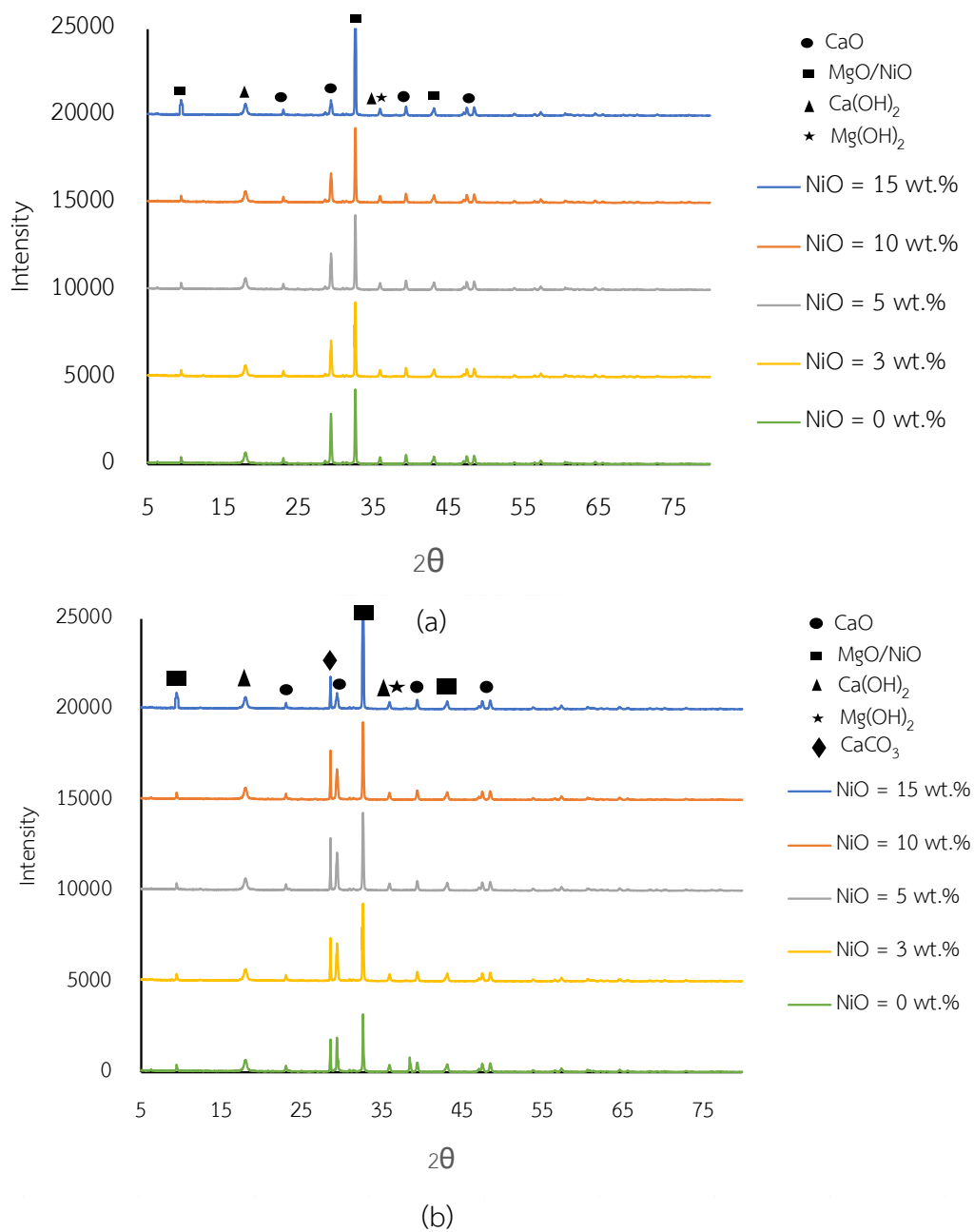


Figure 5.12 XRD pattern of (a) fresh and (b) used catalyst/sorbent with different NiO loading content on WM (2:1).

5.2.2 The regeneration process of NiO₅/WM(2:1) catalyst/sorbent

Figure 5.13 shows the pyrolysis-gasification performance of the cyclic used NiO₅/WM(2:1) catalyst/sorbents. All gas composition could remain constant and the H₂ yield was slightly decreased with increasing the regeneration cycle up to third cycle. At the fourth cycle, the H₂ yield was dramatically decreased and both CO and CO₂ concentration significantly increased whereas the CH₄ were almost constant. Bang *et al.* indicated that after several regeneration cycle of NiO on the support Al₂O₃ catalyst could produce more carbon coke and the regeneration cycle, other deactivation of catalyst including the sintering and agglomeration was involved [118]. Therefore, the prepared NiO₅/WM(2:1) catalyst/sorbent had the suitable regeneration cycle of three.

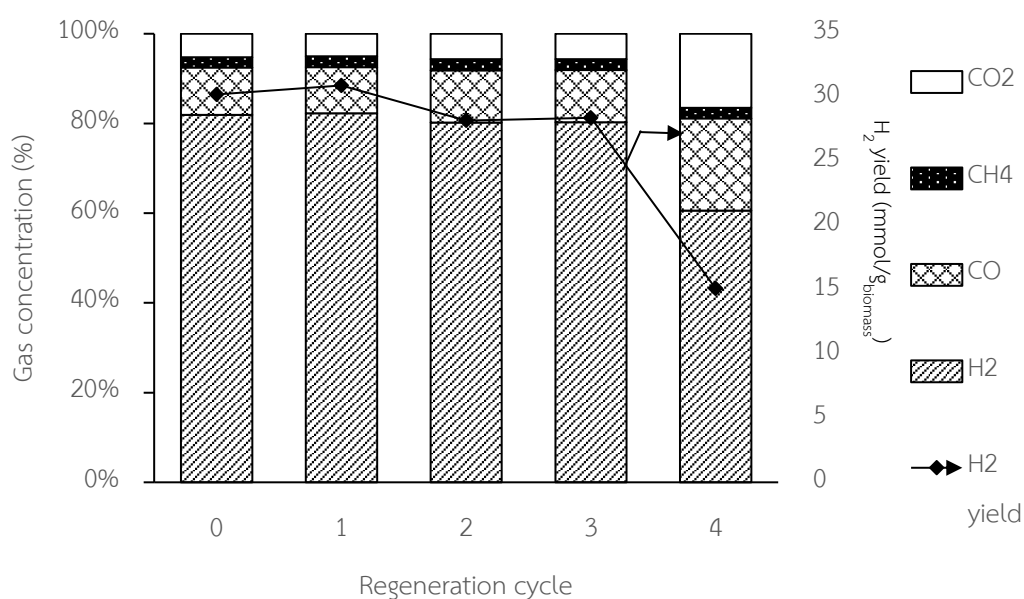


Figure 5.13 The regeneration cycle of NiO₅/CaO-MgO catalyst/sorbent.

5.3 Comparison of Mg5Ni10Ca5 catalyst/sorbent and NiO5/WM(2:1) on H₂ production.

The comparison between Mg5Ni10Ca5 and NiO5/WM(2:1) catalyst/sorbents on SEHP of biomass pyrolysis-gasification are summarized in Table 5.4. The NiO5/WM(2:1) had slightly higher yield and concentration of H₂ but it had dramatically lower yield and concentration of CO₂ at the pyrolysis and gasification temperature of 600 °C. It could indicate that the NiO5/WM(2:1) which had higher CaO and MgO content showed more effective for SEHP than Mg5Ni10Ca5 catalyst/sorbents. For the regeneration of catalyst/sorbents, the NiO5/WM(2:1) had higher regeneration cycle (3 cycles) than Mg5Ni10Ca5 catalyst/sorbent (1 cycles). This result is supported by the previous work reported that the multi-metal loadings on the support catalysts are easily deactivated than the single metal doping [119]. From the comparison, it interpreted that the NiO5/WM(2:1) showed the best catalyst/sorbents for EEHP from pyrolysis-gasification of sugarcane leaves.

Table 5.5 Comparison of gas production from Mg5Ni10Ca5 catalyst/sorbent and NiO/CaO-MgO.

Lists	catalyst/sorbent		
	Blank	Mg5Ni10Ca5	NiO5/WM(2:1)
Catalyst/sorbent	Blank	Mg5Ni10Ca5	NiO5/WM(2:1)
Amount of catalyst (g)	-	1	1
Support	-	γ -Al ₂ O ₃	CaO-MgO
Metal content			
γ -Al ₂ O ₃ content (g)	-	1.00	-
NiO content (g)	-	0.10	0.05
MgO content (g)	-	0.05	0.26
CaO content (g)	-	0.05	0.74
Pyrolysis and gasification temperature = 600 °C			
Gas yield (mmol/g _{biomass})			
H ₂	1.6	28.0	30.3
CO	2.4	8.4	3.6
CH ₄	1.6	2.2	0.9
CO ₂	3.3	2.3	1.9
Gas concentration (%)			
H ₂	17.8	68.7	81.9
CO	27.1	20.4	10.6
CH ₄	17.5	5.3	2.3
CO ₂	37.6	5.6	5.2
Regeneration cycle	-	1	3

CHAPTER 6

CONCLUSIONS AND RECOMMENDATIONS

6.1 Conclusions

1. NiMgCa/ γ -Al₂O₃ catalyst/sorbents study during the pyrolysis- steam gasification of sugarcane leaves

The study on NiMgCa/ γ -Al₂O₃ catalyst/sorbents during the pyrolysis- steam gasification of sugarcane leaves was carried out in a two-stages fixed bed reactor. The results showed that by increasing NiO content loading content up to 10 wt.%, the H₂, CO and CO₂ yield were increased. The further increasing of the NiO loading content over 10 wt.%, the NiAl₂O₄ phases was formed. It provided a slightly increasing of the H₂, CO and CO₂ yield. Increasing CaO content up to 5 wt.% (Ca5Mg5Ni10 catalyst/sorbent), H₂ yields was improved to 20.7 mmol/g_{biomass} (H₂ yield = 1.57 mmole/g_{biomass} with no catalyst/sorbent) The CaAl₂O₄ phase was formed at CaO loading over 10 wt.%, lowering the activity of the catalyst. The addition of MgO can promote the H₂ production by obstruction of the deactivation of catalyst/sorbents. Therefore, Ca5Mg5Ni10 catalyst/sorbents is the suitable metal content loading for sorption enhanced H₂ production (SEHP).

The order of metal loading was also studied with the same metal loading content. Four principal conclusions could be drawn as follows: (1) doping Mg before Ni and Ca increased the proportion of active NiO and CaO phases, because of the reduction in the less-active NiAl₂O₄ and CaAl₂O₄ phases, (2) the sorption of CO₂ plays a predominant role at the lower temperature (600 °C) leading to the highest H₂ concentration (up to 52.5%) and lowest CO₂ concentration (down to 21.0%) with the Mg5Ni10Ca5 catalyst/sorbent, (3) at a higher temperature (800 °C), no significant change

in the gas concentration was observed but the H_2 yield likely depended on the BET surface area. The proper order of metal loading for catalyst/sorbents was that MgO was firstly loaded, then NiO, and eventually CaO.

In addition, the optimal condition of catalyst/sorbents including catalyst/sorbents to biomass mass ratio and the regeneration cycle were investigated. Concentration and yield of H_2 increased when the catalyst/sorbents: biomass mass ratio was increased from 4 to 8, and then became unvarying with the further increases from 8 to 12. For the regeneration cycle, the sintering and aggregation of Mg5Ni10Ca5 catalyst/sorbent were observed at the second regeneration cycle.

Roles of MgO and CaO were also examined at the different gasification temperature. The addition of the MgO/ γ - Al_2O_3 provided higher H_2 yield and lower CO_2 yield at low gasification temperature ($300^\circ C$). The role of MgO/ γ - Al_2O_3 as catalyst could become more predominant rather than the role as sorbent at the high gasification temperature. The CaO/ γ - Al_2O_3 seems to be a better CO_2 sorbent at higher temperature, leading to more H_2 yield. Both CaO and MgO on γ - Al_2O_3 can promote the CO_2 adsorption together at the gasification temperature of $500^\circ C$. The higher H_2 yield and was observed at the gasification temperature of $600^\circ C$ because the CaO shows the good performance for CO_2 adsorption. MgO could perform as the good promoter, enhancing the sorbent activity of CaO/ γ - Al_2O_3 . Increasing the gasification temperature over $600^\circ C$, CaO and MgO play a inferior role as the CO_2 adsorption but they act as catalysts in pyrolysis-gasification of sugarcane leaves.

2. NiO/CaO-MgO catalyst/sorbent study on H_2 production during the pyrolysis- steam gasification of sugarcane leaves

Mixed CaO/MgO sorbents prepared by wet and dry physical mixing at different CaO: MgO molar ratios were studied in the pyrolysis-gasification of sugarcane leaves

for H₂-rich gas production. A synergistic effect between CaO and MgO was observed at all molar ratios of the CaO/MgO mixed sorbents, and the highest H₂ concentration (75.1%) and yield (21.3 mmol/g_{biomass}), and the lowest CO₂ concentration (7.73%), was found with the DM 2:1 sorbent. The wet mixing method showed a higher H₂ production yield than the dry mixing method because the Ca(OH)₂ phases in the wet-mixed sorbents induced the sorption enhanced H₂ production. Moreover, it was found that the different compositions in volatiles obviously influenced the sorption enhanced H₂ production. The devolatilization temperature of 600 °C that produced the volatiles consisting mainly of oxygenated compounds gave the highest H₂ yield. In addition, increasing the gasification temperature over 600 °C was not preferable in terms of H₂ concentration although the H₂ yield becomes higher.

The effect of NiO loading content on WM(2:1) was also examined for the H₂ production. Increasing the NiO up to 5 wt.% on WM (2:1) improved the H₂ yield up to 30.3 mmol/g_{biomass}. Increasing the NiO over 10 wt.% could lead to higher CO₂ yield and lower of the H₂ because of NiO covering on the WM (2:1) prepared support which could lead to decreased the CO₂ adsorption efficiency. The CO₂ adsorption capacity and XRD pattern of fresh and used catalyst/sorbent were supported the assumption as discussed before. The regenerability of NiO 5 wt.% on WM (2:1) was around three times.

Comparison of Mg₅Ni₁₀Ca₅ and NiO₅/WM(2:1) catalyst/sorbents on H₂ production was also discussed. It can be concluded that NiO₅/WM(2:1) catalyst/sorbents gave higher performance of sorption enhanced H₂ production and the higher regeneration cycle than Mg₅Ni₁₀Ca₅ catalyst/sorbents.

6.2 Recommendations and future works

Although the comprehensive results can be obtained from this study, some recommendation were proposed for further investigation about catalyst/sorbent on sorption enhanced H₂ production from pyrolysis-gasification of biomass as followed.

1. The complex compound phases including CaAl_2O_4 , MgAl_2O_4 and NiAl_2O_4 were found. Some complex compound phase such as the MgAl_2O_4 which had high thermal stability provided the positive effect for the H_2 rich production with CO_2 adsorption. Therefore, the further study could be concerned about the catalyst/sorbents preparation which can produced MgAl_2O_4 phase including co-precipitation method to confirm the role of MgAl_2O_4 phase for sorption enhanced H_2 production [120].

2. The biomass feedstock in this study had only one type which is the sugarcane leaves. Type of biomass contributes to variation of chemical compositions which could lead to the different volatile component from the pyrolysis zone of biomass. It could provide the different gas production from the biomass pyrolysis-gasification. Therefore, the various types of biomass could be examined for H_2 rich gas production.

3. The $\text{Mg}_5\text{Ni}_{10}\text{Ca}_5$ and $\text{NiO}_5/\text{WM}(2:1)$ catalyst/sorbent had the typically low of the regeneration cycle. The addition of some promoter such as CeO_2 and ZrO_2 and varying the support preparation method such as the co-precipitation would be explored in a further study to help increase the regeneration cycle of catalyst/sorbent [121].

4. Although the $\text{NiO}_5/\text{WM}(2:1)$ with the NiO of 5 wt.% had high efficiency to enhance H_2 production from pyrolysis-gasification of biomass, these metal loading was not the novel catalyst/sorbent. Therefore, the novel catalyst/sorbent such as LiSiO_4 might be examined for H_2 production of biomass gasification.

5. The study of suitable conditions for regeneration and the *instu*-regeneration cycles have been concerned for future research. The catalyst/sorbent have been regenerated inside the two stages fixed bed reactor by introducing of O_2 and Ar gas into the system and the metallic size should investigate in future work. It can be used by the calculation from XRD pattern and SEM image for the explanation in catalyst/sorbents deactivation.

6. The laboratory scale of biomass gasification with catalyst/sorbent was widely explored. Therefore, a future work should employ a macro scale of biomass pyrolysis-gasification with catalyst and sorbent.



REFERENCES

- [1] Payormhorm, J., Kangvansaichol, K., Reubroycharoen, P., Kuchonthara, P., and Hinchiranan N., Pt/Al₂O₃-catalytic deoxygenation for upgrading of *Leucaena leucocephala*-pyrolysis oil. Bioresource Technology 139 (2013) :128-135.
- [2] Kirkels, A., and Verbong, G., Biomass gasification: still promising? A 30 year global overview. Renewable & Sustainable Energy Reviews 15 (2011): 471-481.
- [3] Guan, J., Wang, Q., Li, X., LuO, Z., and Cen, K., Thermodynamic analysis of a biomass anaerobic gasification process for hydrogen production with sufficient CaO, Renewable Energy 32 (2007): 2502-2515.
- [4] Kumar, A., Jones, D., and Hanna, M., Thermochemical biomass gasification: a review of the current status of the technology. Energies (Basel, Switz) 3 (2009): 556-581.
- [5] Li, X., Tao, L., Jian, G., Xue, F., Xia, W., and Yuan, J., Effect of moisture content in sewage sludge on air gasification. Fuel Chemistry and Technology 38 (2010): 615-620.
- [6] Rapagna, S., Jand, N., Kienneman, A., and Foscolo, P., Steam-gasification of biomass in a fluidized bed the of olivine particle. Biomass and Bioenergy 19 (2000): 2110-2120.
- [7] Huang, B., Chen, H., Chuang, K., Yang, R., and Wey, M., Catalytic steam reforming of biomass tar at low-temperature. International Journal of Hydrogen Energy 37 (2012): 6511-6520.
- [8] Asadullah, M., Ito, S., Kunimori, K., Yamada, M., and Tomishige, K., Sustainable processing of waste plastics to produce high yield hydrogen rich synthesis gas and high-quality carbon nanotubes. Environmental Science and Technology 36 (2002): 4476-4481.

- [9] Onwudili, J., and Williams, P., Biomass conversion to H₂ with substantially suppressed CO₂ formation in the presence of Group I and Group II hydroxides and a Ni/ZrO₂ catalyst. Applied Catalysis B: Environmental 132 (2013): 70-79.
- [10] Czernik, S., and French, R., Hydrogen Production via Steam Reforming of the Aqueous Phase of Bio-Oil in a Fixed Bed Reactor. Energy & Fuels 20 (2006): 754-758.
- [11] Florin, N., and Harris, A., Enhanced hydrogen production from biomass with in situ carbon dioxide capture using calcium oxide sorbent. Chemical Engineering Science 63 (2008): 287-316.
- [12] Hufton, J., Mayorga, S., and Sircar, S., Sorption-enhanced reaction process for hydrogen production. AIChE Journal 45 (1999): 248-256.
- [13] Satrio, J., Shank, B., and Wheelock, T., A combined catalyst and sorbent for enhancing hydrogen production from coal or biomass. Energy & Fuels 21 (2007): 322-326.
- [14] Harrison, D., Sorption-enhanced hydrogen production: a review. Industrial & Engineering Chemistry Research 47 (2008): 6486-6501.
- [15] Fujimoto, S., Hanaoka, T., Taniguchi, H., Kuramoto, K., Matsumura, Y., and Lin S., A kinetic study of the decomposition of CaCO₃ at high CO₂ partial pressure for the regeneration of a CO₂ sorbent. Journal of Chemical Engineering of Japan 39 (2006): 1191-1194.
- [16] Shogo, K., Jon, A., Paula, H., Chunfei, W., Toshiaki, Y., Martin, O., and Paul, T., Novel Ni-Mg-Al-Ca catalyst for enhanced hydrogen production for the pyrolysis-gasification of a biomass/plastic mixture. Journal of Analytical and Applied pyrolysis 113 (2015): 15-21.
- [17] Boerrigter, H., and Rauch, R. Review of applications of gases from biomass gasification. The Biomass Technology Group (BTG), Syngas production and utilization, pp.7-14. Netherlands: ECN Research, 2006.

- [18] Goetsch, D. Types of Gasifiers. SynGas Technology, Inc [Online]. 2010. Available from: http://www.syngastechnology.com/gasification_2.html [2018, May 14].
- [19] Sadaka, S. Department of Agricultural and Biosystems Engineering Iowa State University, USA [Online] Gasification Available from <http://bioweb.sungrant.org/NR/rdonlyres/F4AE220B-0D98-442C-899F-177CFD725ADD/0/Gasification.pdf> [2018, May, 14].
- [20] Demirbas, A., Biomass resource facilities and biomass conversion processing for fuel and chemicals. Energy Conversion and Management 42 (2001):1357–1378.
- [21] Barakat, A., de Vries, H., and Rouau, X., Dry fractionation process as an important step in current and future lignocellulose biorefineries: a review. Bioresource Technology 134 (2013): 362-373.
- [22] Morais, S., Morag, E., Barak, Y., Goldman, D., Hadar, Y., Lamed, R., Shoham, Y., Wilson, D. B. and Bayer, A., Deconstruction of lignocellulose into soluble sugars by native and designer cellulosomes. mBio 3 (2012): 508-512.
- [23] Agbor, B., Cicek, N., Sparling, R., Berlin, A., and Levin, B., Biomass pretreatment: fundamentals toward application. Biotechnology Advances 29 (2011): 675-685.
- [24] Zhou, H., Xia, X., Lin, X., Tong, S. and Beltramini, J., Catalytic conversion of lignocellulosic biomass to fine chemicals and fuels. Chemical Society Reviews 40 (2011): 5588-5617.
- [25] Somerville, C., Youngs, H., Taylor, C., Davis, C., and Long, P., Feedstocks for lignocellulosic biofuels. Science 329 (2010): 790-792.
- [26] Rubin, M., Genomics of cellulosic biofuels. Nature 454 (2008): 841-845.
- [27] Hamid, M., Solbiati, O. and Cann, K., Insights into lignin degradation and its potential industrial applications. Advances in Applied Microbiology 82 (2013): 1-28.

- [28] Menon, V., and Rao, M., Trends in bioconversion of lignocellulose: Biofuels, platform chemicals & biorefinery concept. Progress in Energy and Combustion Science 38 (2012): 522-550.
- [29] Mohan, D., Pittman, U., and Steele, J., Pyrolysis of wood/biomass for bio-oil: A critical review. Energy & Fuels 20 (2006): 848-889.
- [30] Chungsangunsit, A., Shabbir, T., Gheewala, H., and Patumsawad, S., Environmental Assessment of Electricity Production from Rice Husk: A Case Study in Thailand. International Energy Journal 6 (2005): 47-53.
- [31] Ngaemngam, S., Tezuka, T., Thailand Biomass-Based Power Generation and Cogeneration within Small Rural Industries. Final Report, Supported by National Energy Policy Office. Black & Veatch (Thailand) Co., Ltd., Bangkok, 2000.
- [32] Cluskey, J., and Jason, A., Pre-empting Public Regulation with Private Quality Standards. European Review of Agricultural Economics 36 (2009): 525-539.
- [33] Department of Alternative Energy Development and Efficiency. Oil Palm. Momostry of Energy, Bangkok. 2003 (Thai Version).
- [34] Reimert, R., and Schaub, G., Gas production. In, Ullmaan's Encyclopedia of Industrial chemistry, pp. 215. VCH Verlagsgesellschaft Weinherm, 1989.
- [35] Higman, C., and Burgt, M., Gasification. Elsevier. Massachusetts, USA, 2008.
- [36] Whiting, J., Solid waste gasification perspectives. Paper presented at Waste Gasification Seminar (S594) (1998).
- [37] Smooth, D., and Smith, J., Coal combustion and gasification Plenum, New York, US, 1985.
- [38] Somorjai, A. Introduction to Surface Chemistry and Catalysis Wiley, New York, 1994.

- [39] Mudge, K., Baker, G, Mitchell, H., and Brown, D., Catalytic steam gasification of biomass for methanol and methane production. Journal of Solar Energy Engineering107 (1985): 88-92.
- [40] Jong, P., Synthesis of solid catalysts Wiley –VCH, 2009.
- [41] Richardson, T., Principle of catalysts development Plenum Press, 1989.
- [42] Ertl, G., Weitkamp, H., Handbook of Heterogeneous Catalysis Wiley – VCH, 1997
- [43] Farrauto, J. and Bartholomew H., Fundamentals of Industrial Catalytic Processes Blackie Academic & Professional, 1997.
- [44] Richardson, T., Fundamental of catalysss, Plenum Press, New York, 1999.
- [45] Dekmon, B. New trends in catalyst preparation. Solid state ionics 16 (1985): 243-249.
- [46] Yoe, J., Treatise on Analytical Chemistry. Part I. Theory and Practice. Journal of the American Chemical Society 86 (1964): 3182-3182.
- [47] Twigg, U., Catalyst Handbook, Wolfe Ltd., 1989.
- [48] Patnaik, P., Dean's Analytical Chemistry Handbook Mc Graw-Hill, 2004.
- [49] Kelleher, B., and Ross, J., Review of literature on catalysts for biomass gasification. Fuel Processing Technology 73 (2001): 155–173.
- [50] Aznar, P., Corella, J. Gill, J., Martin, A., Caballero, A., Olivares, A., and Frances, E., Proceedings of Conference on Developments in Thermochemical Biomass Conversion, Banff, Canada, (1996): 1117-1121.
- [51] Lammers, G., and Beenackers, A., Proceedings of Conference on Developments in Thermochemical Biomass Conversion, Banff, Canada, (1996): 1179-1185.
- [52] Ekstrom, C., Lindman, N., and Pettersson, R. Proceedings of Conference on Developments in Thermochemical Biomass Conversion, Banff, Canada, (1996): 601-625.

- [53] Colby, L., Dauenhauer, J., and Schmidt, D., Millisecond autothermal steam reforming of cellulose for synthetic biofuels by reactive flash volatilization. Green Chemistry 10 (2008): 773–783.
- [54] Baker, G., Mudge, K., and Brown, MD., Steam gasification of biomass with nickel secondary catalysts. Industrial & Engineering Chemistry Research 26 (1987): 1335–1339.
- [55] Li, T., Grace, R., Lim, J., Watkinson, P., Chen, P., and Kim, R., Biomass gasification in a circulating fluidized bed. Biomass & Bioenergy 26 (2004):171–193.
- [56] Sehested, J., Four challenges for nickel steam-reforming catalysts. Catalysis Today 111 (2006): 103–110.
- [57] Caballero, A., Aznar, P., Gil, J., Martin, A., Frances, E., and Corella, J., Commercial steam reforming catalysts to improve biomass gasification with steam–oxygen mixtures. Industrial & Engineering Chemistry Research 36 (1997): 5227–5239.
- [58] Aznar, P., Caballero, A., Gil, J., Martin, A., and Corella, J., Commercial steam reforming catalysts to improve biomass gasification with steam–oxygen mixtures: Catalytic tar removal. Industrial & Engineering Chemistry Research 37 (1998): 2668–2680.
- [59] Pfeifer, C., Development of catalytic tar decomposition downstream from a dual fluidized bed biomass steam gasifier. Powder Technology 180 (2008): 9–16.
- [60] Kinoshita, M., Wang, Y., and Zhou, J., Effect of reformer conditions on catalytic reforming of biomass-gasification tars. Industrial & Engineering Chemistry Research 34 (1995): 2949–2954.
- [61] Garcia, L., French, R., Czernik, S., and Chornet, E., Catalytic steam reforming of bio-oils for the production of hydrogen: effects of catalyst composition. Applied Catalysis A 201 (2000): 225–239.

- [62] Leung, C., Yin, L., Wu, Z., A review on the development and commercialization of biomass gasification technologies in China. Renewable and Sustainable Energy Reviews 8 (2004): 565–580.
- [63] Essaki, K., Muramatsu, T., and Kato, M., Effect of equilibrium shift by using lithium silicate pellets in methane steam reforming. International Journal of Hydrogen Energy 33 (2008): 4555–4559.
- [64] Balasubramanian, B., Ortiz, L., Kaytakouglu, S., and Harrison, P., Hydrogen from methane in a single-step process. Chemical Engineering Science 54 (1999): 3543–3552.
- [65] Li, S., and Cai, S., Modeling of multiple cycles for sorption-enhanced steam methane reforming and sorbent regeneration in fixed bed reactor. Energy & Fuels 21 (2007): 2909–2918.
- [66] Harrison, P., Sorption-enhanced hydrogen production: a review. Industrial & Engineering Chemistry Research 47 (2008): 6486–6501.
- [67] Iliuta, I., Radfarnia, R., and Iliuta, C., Hydrogen production by sorption-enhanced steam glycerol reforming: sorption kinetics and reactor simulation. AIChE Journal 59 (2013): 2015–2118.
- [68] He, L., Parra, S., Blekkan, A., and Chen, D., Towards efficient hydrogen production from glycerol by sorption enhanced steam reforming. Energy & Environmental Science 3 (2010): 1046–1056.
- [69] Li, S., Sun, M., and Cai, S., Rate equation theory for the carbonation reaction of CaO with CO₂. Energy & Fuels 26 (2012): 4607–4616.
- [70] Li, S., Fang, F., Tang, Y., and Cai, S., Effect of temperature on the carbonation reaction of CaO with CO₂. Energy & Fuels 26 (2012): 2473–2482.
- [71] Li, Z., Liu, Y., and Cai, N., Understanding the enhancement effect of high-temperature steam on the carbonation reaction of CaO with CO₂. Fuel 127 (2014): 88–93.

- [72] Bhatia, K., and Perlmutter, D., Effect of the product layer on the kinetics of the CO₂-lime reaction. *AIChE Journal* 29 (1983): 79–86.
- [73] Montes, G., Chiriac, R., Toche, F., and Renard, F., Gas–solid carbonation of Ca(OH)₂ and CaO particles under non-isothermal and isothermal conditions by using a thermogravimetric analyzer: Implications for CO₂ capture. *International Journal of Greenhouse Gas Control* 11 (2012): 172–180.
- [74] Qin, C., Liu, W., An, H., Yin, J., and Feng, B., Fabrication of CaO-based sorbents for CO₂ capture by a mixing method. *Environmental Science & Technology* 46 (2012): 1932–1939.
- [75] Wu, F., Li, H., Kim, N., and Yi, B., Properties of a nano CaO/Al₂O₃ CO₂ sorbent. *Industrial & Engineering Chemistry Research* 47 (2008):180–184.
- [76] Bhagiyalakshimi, M., Lee, Y., and Jang, T., Synthesis of mesoporous magnesium oxide: its application to CO₂ chemisorption. *International Journal of Greenhouse Gas Control* 4 (2010): 51–56.
- [77] Ho, K., and Lee H., Sorption capacity and stability of mesoporous magnesium oxide in post-combustion CO₂ capture. *Materials Chemistry and Physics* 198 (2017): 51–56.
- [78] Li, L., Wen, X., Fu, X., Wang, F., Zhao, N., Xiao, F., Wei, W., and Sun, Y., MgO/Al₂O₃ sorbent for CO₂ capture. *Energy & Fuels* 24 (2010): 5773–5780.
- [79] Han, J., Bang, Y., Kwon, J., Lee, C., Hiremath, V., Song, K., and Seo, G., Elevated temperature CO₂ capture on nano-structured MgO–Al₂O₃ aerogel: effect of Mg/Al molar ratio. *Chemical Engineering Journal* 242 (2014): 357–363.
- [80] Mostafavi, E., Mahinpey, N., and Manovic, V., A novel development of mixed catalyst-sorbent opellets for steam gasification of coal chars with in situ CO₂ capture, *Catalysis Today* 237 (2014): 111-117.
- [81] Shogo, K., Jon, A., Paula, H., Chunfei, W., Toshiaki, Y., Martin, O., and Paul, T., Novel Ni-Mg-Al-Ca catalyst for enhanced hydrogen production for the pyrolysis-

- gasification of a biomass/plastic mixture, Journal of Analytical and Applied pyrolysis 113 (2015): 15-21.
- [82] Zamboni, I., Courson, C., and Kiennemann, A., Sythesis of Fe/CaO active for CO₂ absorption and tar removal in biomass gasification, Catalysis Today 176 (2011): 197-201.
- [83] Sinha, S., Jhalani, A., Ravi, R., and Ray, A., Modelling of pyrolysis in Wood A review. Journal of the Solar Energy Society of India 10 (2000): 41-62.
- [84] Yu, H., Kim, D., Lee, M., and Lee, H., Kinetic studies of dehydration, pyrolysis and combustion of paper sludge. Energy 27 (2002): 457-469.
- [85] Ounas, A., Pyrolysis of olive residue and sugar cane bagasse: non-isothermal thermogravimetric kinetic analysis. Bioresource technology 102 (2011): 11234-11238.
- [86] Fernandes, E., Thermochemical characterization of banana leaves as a potential energy source. Energy conversion and management 75 (2013): 603-608.
- [87] Vizcaino, J., Arena, P., Baronetti, G., Carrero, A., Calles, A., and Laborde, A., Ethanol steam reforming on Ni/Al₂O₃ catalysts: effect of Mg addition. International Journal of Hydrogen Energy 33 (2008): 3489–3492.
- [88] Guo, L., Liu, L., Zhu, X., Zhang, Q., and Li, C., Effect of Mg/Al molar ratios on NO reduction activity of CO using Ce-La/MgAl₂O_{4-x} catalysts, Journal of Fuel Chemistry and Technology, 45 (2017): 723–730.
- [89] Koo, K., Roh, H., Seo, Y., Seo, D., Yoon, W., and Park, S., A highly effective and stable nano-sized Ni/MgO–Al₂O₃ catalyst for gas to liquids (GTL) process. International Journal of Hydrogen Energy 33 (2008): 2036-2043.
- [90] Huang, B., Chen, H., Chuang, K., Yang, R., and Wey, M., Hydrogen production by biomass gasification in a fluidized bed reactor promoted by an Fe/CaO catalyst, International Journal of Hydrogen Energy 37 (2012): 6511-6518.

- [91] Kaydouh, N., Hassan, E., Davidson, A., Casale, S., Zakhem, E., and Massiani, P., Effect of the order of Ni and Ce addition in SBA-15 on the activity in dry reforming of methane. Comptes Rendus Chimie 18 (2015): 293–301.
- [92] Kumar, P., Sun, Y., and Idem, O., Nickel-based ceria, zirconia, and ceria–zirconia catalytic systems for low-temperature carbon dioxide reforming of methane, Energy & Fuel 21 (2007): 3113–3123.
- [93] Lemonidou, A., and Vasalos, A., Carbon dioxide reforming of methane over 5 wt.% Ni/CaO-Al₂O₃ catalyst. Applied Catalysis A: General 228 (2002): 227–235.
- [94] Zhang, B., Zhang, L., Yang, Z., Yan Y., Pu G. and GuO, M., Hydrogen-Rich Gas Production from Wet Biomass Steam Gasification with CaO/MgO. International Journal of Hydrogen Energy. 40 (2015): 8816-8823.
- [95] Kumagai, S., Alvarez, J., Blanco, H., Wu, C., Yoshioka, T., Olazer, M. and Williams, T., Novel Ni-Mg-Al-Ca Catalyst for Enhanced Hydrogen Production For The Pyrolysis-Gasification Of A Biomass/Plastic Mixture. Journal of Analytical and Applied Pyrolysis 113 (2015): 15-21.
- [96] Vizcaí no, J., Arena, P., Baronetti, G., Carrero, A., Calles, J., Laborde, A., and Amadeo, N., Ethanol steam reforming on Ni/Al₂O₃ catalysts: Effect of Mg addition. International journal of hydrogen energy 33 (2008): 3489 – 3492.
- [97] Lisboa, S., Santos, M., Passos, B., and Noronha, B., Influence of the addition of promoters to steam reforming catalysts. Catalysis Today 101 (2005): 15–21.
- [98] Aupretre, F., Descorme, C., Duprez, D., Casanave D, and Uzio D. Ethanol steam reforming over Mg_xNi_{1-x}Al₂O₃ spinel oxide supported Rh catalysts. Journal of Catalysis 233 (2005): 464–477.

- [99] Requies, J., Cabrero, M., Barrio, V., Cambra, J., and Guemez, M., Nickel/alumina catalysts modified by basic oxides for the production of synthesis gas by methane partial oxidation. Catalysis Today 116 (2006): 304-312.
- [100] Bretado, M., Vigil, M., Gutierrez, J., Ortiz, A., and Martinez, V., Hydrogen production by absorption enhanced water gas shift (AEWGS) International Journal of Hydrogen Energy 35 (2009): 12083-12090.
- [101] Wei, L., Yang, H., Li, B., Wei, X., Chen, L., Shao, J., and Chen, H., Absorption-enhanced steam gasification of biomass hydrogen production: Effect of calcium oxide addition on steam gasification of pyrolytic volatiles. International Journal of Hydrogen Energy 39 (2014): 15416-15423.
- [102] Han, L., Wang, Q., Yang, Y., Yu, C., Fang, M., and Luo, Z., Hydrogen production via CaO sorption enhanced anaerobic gasification of sawdust in a bubbling fluidized bed, International Journal of Hydrogen Energy 36 (2011): 4820-4829.
- [103] Xu, G., Murakami, T., Suda, T., Kusuma, S., and Fujimori, T., Distinctive Effects of CaO Additive on Atmospheric Gasification of Biomass at Different Temperatures, Industrial & Engineering Chemistry Research 44 (2005): 5864-5856.
- [104] Thomas, J., and Thomas, W., Principles and practice of Heterogeneous Catalysis; VCH Verlagsgesellschaft mbH, Weinheim, Germany, 1997.
- [105] Maneewan, K., Kerkkaiwan, S., Sunphorka, S., Vitidsant, T., and Kuchonthara, P. Catalytic effect of biomass pyrolyzed char on the atmospheric pressure hydrogasification of Giant Leucaena (*Leucaena leucocephala*) wood. Industrial & Engineering Chemistry Research 53 (2014): 11913-11919.
- [106] Klinghoffer, B., Castaldi, J., and Nzihou, A., Catalyst properties and catalytic performance of char from biomass gasification. Industrial & Engineering Chemistry Research 51 (2012): 13113-13122.

- [107] Cheng, Z., Wu, Q., Li, J., and Zhu, Q., Effects of promoters and preparation procedures on reforming of methane with carbon dioxide over Ni/Al₂O₃ catalyst. Catalysis Today 30 (1996): 147-155.
- [108] German, R., and Munir, Z., Surface area reduction during isothermal sintering. Journal of the American Ceramic Society 59 (1976): 379-383.
- [109] Borgwardt, H., Calcium oxide sintering in atmospheres containing water and carbon dioxide. Industrial & Engineering Chemistry Research 28 (1989): 493-500.
- [110] Xiao, G., Singh, R., Chaffee, A., and Webley, P. Advanced adsorbents based on MgO and K₂CO₃ for capture of CO₂ at elevated temperatures. International Journal of Greenhouse Gas Control 5(2011): 634-639.
- [111] Wu, S., Li, Q., Kim, J., and Yi, K. Properties of a nano CaO/Al₂O₃ CO₂ sorbent. Industrial & Engineering Chemistry Research 47 (2008): 180-184.
- [112] Blamey, J., Lu, Y., Fennell, S., and Anthony, E., Reactivation of CaO-based sorbents for CO₂ capture: Mechanism for the carbonation of Ca(OH)₂. Industrial & Engineering Chemistry Research 50 (2011) 10329-10334.
- [113] Lopez, A., and Harrison, P., Hydrogen production using sorption-enhanced reaction. Industrial & Engineering Chemistry Research 40 (2001): 5102-5109.
- [114] Kerkkaiwan, S., Tsutsumi, A., and Kuchonthara, P., 2013. Biomass derived tar decomposition over coal char bed. Science Asia 39 (2013): 511-519.
- [115] Shi, L., Yu, S., Wang, C., and Wand, J., Pyrolytic characteristics of rice straw and its constituents catalyzed by internal alkali and alkali earth metal. Fuel 87 (2012): 586-594.
- [116] Sun, Q., Yu, S., Wang, C., and Wand, J., Decomposition and gasification of pyrolysis volatile from pine wood through a bed of hot char. Fuel 90 (2011): 1041-1048.

- [117] Wei, L., Yang, H., Wei, X., Chen, L., Shao, J., and Chen, H., Absorption-enhanced steam gasification of biomass for hydrogen production: Effect of calcium oxide addition on steam gasification of pyrolytic volatiles, International Journal of Hydrogen Energy 39 (2014): 15416-15423.
- [118] Bang, Y., Park, S., Han, S., Yoo, J., Song, J., Choi, J., Kang, K., and Song, I., Hydrogen production by steam reforming of liquefied natural gas (LNG) over mesoporous Ni/Al₂O₃ catalyst prepared by an EDTA-assisted impregnation method. Applied Catalysis B 180 (2016): 179-188.
- [119] John, B., and Petersen, B., Regeneration of coked particle., Activation, Deactivation, and Poisoning of Catalyst, pp.321-343. England: Elsevier Inc., 1988.
- [120] Mullen, A., and Boateng, A., Chemical Composition of bio-oils produced by fast pyrolysis of two energy crops. Energy & Fuels 22 (2008): 2104–2109.
- [121] Liu, Q., Liao, L., Liu, Z., and Dong, X., Hydrogen production by glycerol reforming in supercritical water over Ni/MgO-ZrO₂ catalyst. Journal of Energy Chemistry 2 (2013): 665-670.

REFERENCES



จุฬาลงกรณ์มหาวิทยาลัย
CHULALONGKORN UNIVERSITY



APPENDIX

จุฬาลงกรณ์มหาวิทยาลัย
CHULALONGKORN UNIVERSITY

APPENDIX A

THE PHYSICAL PROPERTIES OF BIOMASS METHODS.

A1 Moisture Content: ASTM D3173

Methodology

1. The aluminum plate was dried at the temperature of 104-110 oC for 30 min. Then, the dried plate is kept in the desiccator for 15 min and weighed the plate before moisture test.
2. 1 g of biomass sample contained in the dried aluminum plate and recorded the total weigh (Plate and biomass)
3. The sample and aluminum plate were dried at the temperature of 104-110 °C for 1 hr or the weight of sample was stable.
4. The sample and aluminum plate were placed into the desiccator for 15 min and weighed the plate after drying process.

Calculation

$$M = \frac{W_1 - W_2}{W} \times 100$$

Where,

M = Percentage moisture contains

W_1 = The weight of aluminum plate and sample before testing (g)

W_2 = The weight of aluminum plate and sample after testing (g)

W = The weight of sample (g)

A2 Volatile matter: ASTM D3175

Methodology

1. The crucible was burned with the cover plate at the temperature of 950 °C for 30 min.
2. 1 g of biomass sample contained in the crucible.
3. The crucible which contained the sample was burned at the top of tubular furnace at the temperature of 300 °C for 3 min.
4. The crucible was moved in to the center of the tubular furnace at the temperature of 600 °C for 3 min.
5. The crucible was moved in to the bottom of the tubular furnace at the temperature of 950 °C for 6 min.
6. The crucible was placed into the desiccator for 15 min and weighed the sample and crucible.

Calculation

$$V = \frac{W_3 - W_4}{W} \times 100 - M$$

Where,

V = Percentage volatile matter

W_3 = The weight of crucible with the cover plate and the sample before burning (g)

W_4 = The weight of crucible with the cover plate and the sample after burning (g)

W = The weight of sample (g)

M = Percentage moisture contains

A3 Ash content: ASTM D3174

Methodology

1. The crucible was burned with the cover plate at the temperature of 750 °C for 1 h. and recorded the weight of crucible and cover plate.
2. 1 g of biomass sample contained in the crucible.
3. The crucible which contained the sample was burned at the top of muffle furnace at the temperature of 750 °C for 3 h.
4. The crucible was placed into the desiccator for 15 min and weighed the sample and crucible.

Calculation

$$A = \frac{W_5 - W_6}{W} \times 100$$

Where,

A = Percentage of ash

W_5 = The weight of crucible with the cover plate and the sample before burning (g)

W_6 = The weight of crucible with the cover plate and the sample after burning (g)

W = The weight of sample (g)

A4 Fixed carbon content

Calculation

$$F = 100 - M - V - A$$

Where, F = Percentage of fixed carbon

A = Percentage of ash

M = Percentage of moisture contains

V = Percentage of volatile matter



APPENDIX B
GAS YIELD AND COMPOSITION CALCULATION

Raw data

Weight of biomass	0.1211 g
Pyrolysis temperature	600 °C
Gasification temperature	600 °C
Total gas flow	100 ml/min
Interval time to keep the gas product	5 min
The volume of gas bag	1100 ml

Table B1 The concentration of standard gas

Component	GC area	%Balanced in N ₂
H ₂	42121	1.0
CO	2389	1.0
CH ₄	8777	1.0
CO ₂	2706	1.0

Table B2 The concentration of gas product1st gas bag (5 min)

Gas	GC area	%Std (%)	Volume of gas (ml)	Mole of gas (mol) PV=nRT
H ₂	16442	$\frac{16442}{42121} = 0.39$	$0.39 \times \frac{1100}{100} = 4.29$	$\frac{4.29}{0.082 \times 298} = 0.18$
CO	2958	$\frac{2958}{2389} = 1.23$	$1.23 \times \frac{1100}{100} = 13.5$	$\frac{13.5}{0.082 \times 298} = 0.56$
CH ₄	3500	$\frac{3500}{8777} = 0.39$	$0.39 \times \frac{1100}{100} = 4.29$	$\frac{4.29}{0.082 \times 298} = 0.18$
CO ₂	1268	$\frac{1268}{2706} = 0.47$	$0.47 \times \frac{1100}{100} = 5.17$	$\frac{5.17}{0.082 \times 298} = 0.21$

1st gas bag (5 min)

Gas	Mole of gas (mol)	Gas yield (mmol/g _{biomass})	Gas composition (%)
H ₂	0.18	$\frac{0.18}{0.1211} = 1.48$	$\frac{1.48}{9.31} \times 100 = 15.9$
CO	0.56	$\frac{0.56}{0.1211} = 4.62$	$\frac{4.62}{9.31} \times 100 = 49.6$
CH ₄	0.18	$\frac{0.18}{0.1211} = 1.48$	$\frac{1.48}{9.31} \times 100 = 15.9$
CO ₂	0.21	$\frac{0.21}{0.1211} = 1.73$	$\frac{1.73}{9.31} \times 100 = 18.6$
Total	1.13	9.31	100

VITA

Mr. Teerayut Bunma was born on February 4th, 1992 at Udon Thani, Thailand. He received the Bachelor of Science in field of fuel technology (Chemical technology), Chulalongkorn University. Mr. Bunma joined the Department of Chemical Technology, Chulalongkorn University, as a doctoral student in 2014. He has received the 100th anniversary Chulalongkorn University scholarships (2014-2018)

During the graduate study, Mr. Bunma spent 4 years for doing research in Fuel laboratory at department of Chemical Technology. He had three publications as following:

1. Hydrogen production from steam pyrolysis-gasification of sugarcane leaves with sorbent-catalyst has been accepted for publication in Jurnal Teknologi
2. Effect of temperature on sorption-enhanced hydrogen production from biomass gasification using alkaline earth sorbents has been accepted for publication in Advanced Science letters.
3. Synergistic study between CaO and MgO sorbents for hydrogen rich gas production from the pyrolysis-gasification of sugarcane leaves has been accepted for publication process safety environmental protection.

He also presented his work in three international conferences as following:

1. 2015 Advancement in Petroleum and Chemical Engineering Technology and Applications International Conference at Krabi, Thailand.
2. 2017 Asian Pacific community of chemical and process engineers and industrial chemists at Hongkong.
3. 2017 Renewable Energy and Green Technology International Conference at Malaysia.



จุฬาลงกรณ์มหาวิทยาลัย
CHULALONGKORN UNIVERSITY